Targeted Delivery of BMP4-siRNA to Hepatic Stellate Cells for Treatment of Liver Fibrosis

by

Refaat Omar

A Thesis submitted to the Faculty of Graduate Studies of

The University of Manitoba

in partial fulfilment of the requirements of the degree of

MASTER OF SCIENCE

College of Pharmacy, Faculty of Health Sciences

University of Manitoba

Winnipeg

ABSTRACT

Hepatic fibrosis is a serious health problem in many parts of the world. However, its treatment remains severely limited because of inadequate target specificity. HSC are the largest reservoir of vitamin A in the body. They are also the principal players responsible for the pathogenesis of liver fibrosis. Targeting HSC is an effective strategy for treatment of liver fibrosis. The specific association of BMP4 with various liver diseases including liver fibrosis makes it an ideal candidate for targeting HSC cells using siRNA. The objective of this study is to develop and characterize vitamin A (VA)-coupled liposomes for the targeted delivery of BMP4-siRNA to cultured HSC. DOTAP/DOPE liposomes surfaces were prepared by thin film hydration and their surfaces were decorated with VA (1:2 mol/mol). Particle size and zeta potential were determined using ZetaPALS. In addition, the siRNA binding efficiency was determined by ultra-centrifugation and fluorescence assays. The cytotoxicity of VA-conjugated liposomes was evaluated by the WST-1 cytotoxicity assay. Inhibition of BMP4 and α-SMA was determined by real time PCR and ELISA. Their average particle size was in the range of 100-120 nm and they exhibited zeta potential around +45 mV. VA-coated liposomes were mixed with BMP4-siRNA, forming lipoplexes with particle sizes less than 200 nm and zeta potential around +25 mV. The presence of VA did not alter the siRNA binding efficiency, it also had no effect on cytotoxicity, but resulted in enhanced cellular uptake of siRNA as shown by flow cytometry. There was a significant reduction in BMP4 mRNA with VA-coupled liposomes carrying BMP4-siRNA. Moreover, BMP4 gene silencing was accompanied by a significantly reduced the expression of the potent fibrinogenic α-SMA at mRNA and protein levels. In conclusion, VA-coated liposomes were successfully able to target and deliver BMP4-siRNA to HSC. This could offer an interesting perspective for the treatment of liver fibrosis.

ACKNOWLEDGEMENTS

I would like to acknowledge my esteemed supervisors, Dr. Yuewen Gong and Dr. Frank J Burczynski for their guidance, patience, encouragement, and supervision during the completion of my thesis. Thank you for trusting me and provide me the chance to join your research group, for your understanding and making time to advise me, especially during the stressful times. Your kindness, support and valuable time kept me going easily throughout the progress of my work.

I am also grateful to Dr. Gerald Y Minuk for serving on my advisory committee and for his valuable time and insightful comments and suggestions in the annual review meetings.

I would like to thank all my friends and colleagues., Dr. Khaled al-Taweel, Dr. Ousama Rachid, Dr. Jijin Gu, Yannick Traoré, Jiaqi Yang, Samaa Alrushaid, Nour Eissa and Tyson Le for their the kind support and encouragement.

I am grateful to the University of Manitoba for the financial support during my studies. Such a project would not have been possible to contemplate without their financial support.

My deepest gratitude goes to my family especially my parents for their love, constant inspiration and encouragement. To them I dedicate this thesis.

TABLE OF CONTENTS

LIST OF TABLES

LIST OF FIGURES

ABBREVIATIONS

%	Percent
°C	Degrees Celsius
µg	Microgram
µL	Microliter
ALK	Activin receptor-like kinase
ALR	Augmentation of liver regeneration
AMD	Age-related macular degeneration
BDL	Bile duct ligation
BE	Binding Efficiency
BMP	Bone morphogenetic protein
CCR5	Chemokine receptor type 5
CDK1	Cyclin-dependent kinase inhibitor protein
CINC	Cytokine-induced neutrophil chemoattractant
CTGF	Connective tissue growth factor
ddH_2O	Double distilled water
DLPC	Dilinoleoylphosphatidylcholine

DMEM	Dulbecco's Modified Eagle Medium
DMN	Dimethylnitrosamine
DMSO	Dimethyl sulfoxide
DOPC	1,2-dioleoyl-sn-glycero-3-phosphatidylcholine
DOPE	1,2-Dioleoyl-sn-Glycero-3-Phosphoethanolamine
DOTAP	1,2-dioleoyl-3-trimethylammonium-propane
DOTMA	N-[1-(2,3-dioleoyloxy)propyl]-N,N,N-trimethyl-ammonium methyl sulfate
dsRNAs	Double-stranded RNAs
ECM	Extracellular matrix
ECs	Endothelial cells
EE	Encapsulation Efficiency
EMT	Epithelial to Mesenchymal transition
ET-1	Endothelin-1
FACS	Fluorescence-activated cell sorting
FAM	Fluorescein amidite
FBS	Fetal bovine serum
GDFs	Growth differentiation factors

gp 46	Collagen specific chaperone
h	Hours
HA	Hyaluronic acid
HCC	Hepatocellular carcinoma
HGF	Hepatocyte growth factor
HPCs	Hepatic progenitor cells
HRP	Horseradish peroxidase
HSC	Hepatic stellate cells
ICAM-1	Intercellular adhesion molecule type 1
IGF-1	Insulin-like growth factor 1
IL-6	Interleukin type 6
KCs	Kupffer cells
LPL	Lipoprotein lipase
LPS	Lipopolysaccharide
M6P-HAS	Human serum albumin and mannose-6-phosphate
MAPK	Mitogen-activated protein kinase
MCP-1	Monocyte chemoattractant protein-1

M-CSF	Macrophage colony-stimulating factor
min	Minutes
MIPs	Macrophage inflammatory proteins
miRNAs	MicroRNAs
MMPs	Matrix metalloproteinases
NASH	Non-alcoholic steatohepatitis
NDMA	N-nitrosodimethylamine
NGFR	Nerve growth factor receptor
NK	Natural killer cells
NO	Nitric oxide
PBS	Phosphate buffer saline
PCR	Polymerase chain reaction
PDGF	Platelet-derived growth factor
PEG	Polyethylene glycol
PEI	Polyethyleneimine
rAAV	Recombinant adeno-associated viruses
RANTES	Regulated and normal T cell expressed and secreted

RBP	Retinol binding protein
RES	Reticuloendothelial system
rhapo A-I	Recombinant human apolipoprotein A-I
RHD	Renal hypodysplasia
RISC	RNA-induced silencing complex
RNAi	RNA interference
ROS	Reactive oxygen species
RP-HPLC	Reverse Phase High-Performance Liquid Chromatography
RT	Room Temperature
sec	Seconds
shRNA	Short-hairpin RNA
siRNAs	Small interfering RNAs
SNALP	Stable nucleic acid lipid particle
TGF-β	Transforming growth factor-β
TIMPs	Tissue inhibitors of matrix metalloproteinase
TLRs	Toll-like receptors
TMB	Tetramethylbenzidine

TNF-α	Tumor necrosis factor alpha
VA	Vitamin A
VCAM-1	Vascular adhesion molecule type 1
VEGF	Vascular endothelial growth factor
α-SMA	Smooth muscle alpha actin

Chapter 1: Introduction

Liver is considered the second largest organ after the skin in the human body. In addition, the liver forms the largest internal glandular organ that is located on the right side of the belly. It weighs about three pounds representing approximately 2% of the adult body weight. The liver is composed of four lobes, including two major large lobes (left, right) and two small ones (caudate and quadrate). The liver is connected to a double blood supply; the first is the portal vein that provides nutrient-rich blood from the gastrointestinal system and the second is the hepatic artery that brings oxygen-rich blood from the aorta. The blood passes inside the liver thorough micro-vessels called sinusoids, which ultimately deliver blood to hepatic lobules; each lobule consists of millions of metabolic hepatic cells. Blood then flows into the central vein of each lobule. Finally, these veins drain the de-oxygenated blood into the inferior vena cava (1-3).

The liver has numerous functions in the body. In addition to the metabolism of proteins, carbohydrates and lipids; the liver also secretes bile and synthesizes important proteins, such as coagulation factors, hormones and plasma proteins (*e.g*. albumin and globulin). Moreover, it detoxifies chemicals, drugs and other xenobiotic compounds, which are eliminated through the bile and urine afterwards. The hepatic lobules are the building units of the liver; they are made of parenchymal cells (hepatocytes) and non-parenchymal cells, including Kupffer cells (KCs), endothelial cells (ECs), and hepatic stellate cells (HSC) (3, 4).

Hepatocytes are the major cells in the liver accounting about 78% of the total cellular makeup and occupying more than 90% of its volume. They are responsible for most of the metabolic functions of the liver, including the urea cycle. The outer membrane surfaces of hepatocytes are characterized by various domains, such as sinusoidal, contiguous, and canalicular domains, each

exhibiting a different function. For example, the canalicular domain is responsible for the transport of bile salt, lipids, bilirubin and xenobiotics into the bile, whereas, the sinusoidal domain contains the sodium pump that plays an important role in the transport of organic ions and drugs. In addition, hepatocytes are the primary sites of glycogen storage and glucose release, which maintains normal blood glucose levels (1, 2)

Liver endothelial cells represent 2.8% of the liver volume. ECs possess several small pores (50-170 nm in size), that are referred to as fenestrations. These fenestrations act as selective filters or sieves, which regulate the passage of specific small molecules from blood through the perisinusoidal space to the liver hepatocyte (5). Fenestrations also help in filtering the blood from different macromolecular metabolic waste products. In addition, ECs produce inflammatory cytokines, such as tumor necrosis factor alpha (TNF-α) and interleukin type 6 (IL-6). Morever, they secrete adhesion molecules, including intercellular adhesion molecule type 1 (ICAM-1) and vascular adhesion molecule type 1 (VCAM-1). In a normal liver, ECs synthesize both type IV collagen and laminin which are components of the extracellular matrix (ECM) (1, 2, 6, 7).

Kuppfer cells (KCs) constitute approximately 2.1 % of the total liver volume and represent 80–90 % of all the liver macrophages (8). KCs are part of the reticuloendothelial system (RES) and are known for their high phagocytic activity that allows them to protect the liver and the body from harmful microorganisms and detoxify their toxic products. KCs also aid in removing immune complexes, dead cells and other materials absorbed from the gastrointestinal tract that are present in the blood (3). The immune-regulatory function of KCs involves their activation in response to external stimuli, such as alcohol or bacterial endotoxin. Activation of KCs is followed by the production of inflammatory cytokines such as TNF-α, IL-1 and IL-6 (8) in addition to reactive oxygen species (ROS), proteases and eicosanoids. These products promote

phagocytic activity of KCs and also activate the surrounding parenchymal and other sinusoidal lining cells (1-3).

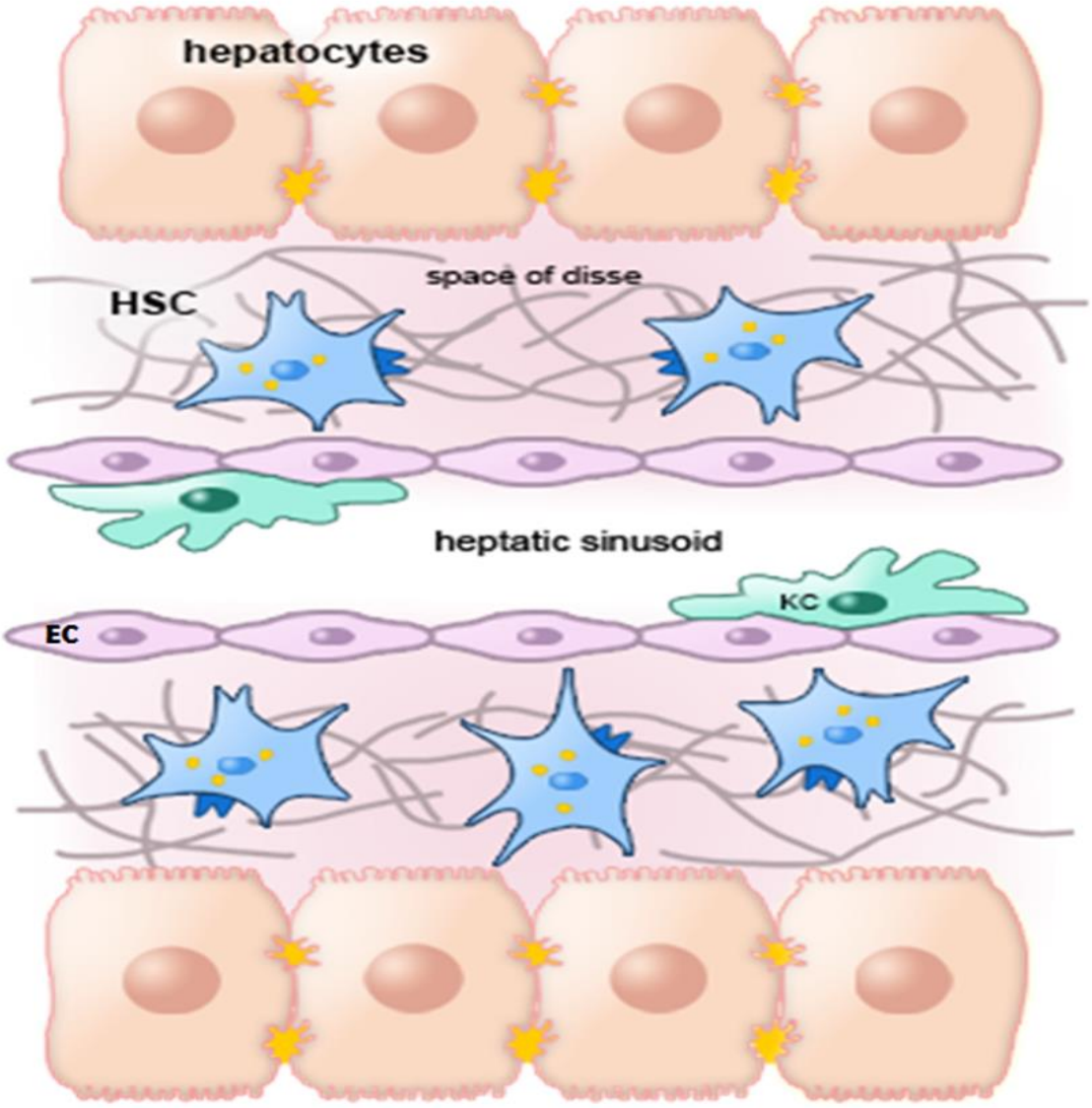

Figure 1: Schematic representation of liver. KCs are found in sinusoids. HSC are sited in the space of Disse between ECs and Hepatocytes. ECs feature the walls of sinusoids and possess fenestrations that act as a selective sieve, which regulate the passage of molecules from the blood through the perisinusoidal space to the liver hepatocyte.

(Figure was created by Ms Jiaqi Yang).

Hepatic stellate cells (HSC)

Hepatic stellate cells (HSC) are also referred to as vitamin A-storing cells, fat storing cells, lipocytes and Ito cells. HSC are non-parenchymal cells of the liver, representing 1.4 % of total liver volume and 5 to 8 % of the total liver cells. HSC are located in the perisinusoidal space (space of Disse) between hepatocytes and sinusoidal endothelial cells. This anatomical position of HSC provides physical contact to the sinusoidal endothelial cells and to the hepatocytes (9, 10). HSC display two different phenotypes that exhibit various structures and behaviors: the quiescent phenotype in the normal liver, and the activated myofibroblast-like phenotype in the injured liver.

Functions of HSC in the normal and in the injured liver

Storage of Vitamin A

The primary function of quiescent HSC is the storage of retinoid (vitamin A). The liver stores around 70% of the total retinoid found in the body. HSC store about 90-95 % of hepatic retinoid in their lipid droplets as retinyl esters complexed via retinol binding protein (RBP). Therefore, HSC are considered the largest reservoir of retinoid in the body (11).

Dietary retinol in the gastrointestinal tract is esterified and incorporated into chylomicrons which enter the systemic circulation through the lymphatic system (12). The retinol-containing chylomicrons are hydrolyzed by lipoprotein lipase (LPL) resulting in the formation of chylomicron remnants (13). Hepatocytes take up 75% of chylomicron remnants from the blood stream as esters and convert them to free retinol via hydrolysis (14). Retinol binds to RBP before being transferred to HSC for storage (15). Moreover, RBP-bound retinoid can pass directly from the circulation to HSC (16, 17). Retinoid is stored in HSC bound to RBP as a retinyl ester, which

can be released again into the plasma. The process of storage and transport of vitamin A is controlled by the availability of vitamin A in the animal body. In the case of vitamin A deficiency, retinoid stored in the HSC is transported to the circulation. Also, dietary retinoid stored in hepatocytes in a RBP-bound form can be released back to the circulation without transfer to HSC (14, 17, 18).

ECM synthesis and degradation

HSC are mainly responsible for the production of ECM in the liver and for the synthesis of enzymes that regulate ECM degradation (6). Consequently, HSC are the major players in the development of liver fibrosis. Generally, quiescent HSC in the normal liver secrete adequate amounts of ECM proteins. In addition, HSC secrete several degrading enzymes called matrix metalloproteinases (MMPs), such as MMP-1, MMP-8 and MMP-13, which promote ECM degradation. HSC also produce inhibitors called tissue inhibitors of matrix metalloproteinase (TIMPs), such as TIMP-1 and TIMP-2. The balance between MMPs and TIMPs regulates the ECM degradation processes. The extra cellular membrane protein synthesis also contribute to ECM homeostasis (19, 20).

Liver Development and Regeneration

Due to their anatomical position, HSC play an important role in liver growth and regeneration. HSC surround sinusoids in a cylindrical manner that enables them to control blood flow through those sinusoids and regulate the sinusoidal tone. In addition, they secrete vasoactive proteins, such as substance P, neuropeptide Y and somatostatin (21).

Furthermore, HSC express epimorphin, which is a mesenchymal morphogenetic protein that regulates liver regeneration especially after partial hepatectomy. In addition, HSC produce

morphogenetic proteins, such as hepatocyte growth factor (HGF) (22) and pleiotrophin (23), which stimulate hepatocyte proliferation and regeneration respectively. HSC also express vascular endothelial growth factor (VEGF) that stimulates the growth of both sinusoidal and vascular endothelial cells (24). Moreover, HSC secrete various molecules that regulate homeostasis process within the liver, such as endothelin-1 (25), transforming growth factor-β (TGF-β) (26) and erythropoietin (27).

Immunoregulatory Function

When liver injury takes place, HSC along with other cell types, release inflammatory cytokines, such as platelet-derived growth factor (PDGF), which is the most potent mitogen and chemotactic mediator (17, 28). Another key cytokine that is released is TGF-β1 that plays a significant role in liver fibrosis development (17).

In addition, HSC secrete chemokines that enable their interactaction with Gram-negative bacterial-derived lipopolysaccharides (LPS); these are exemplified by the chemotactic monocyte chemoattractant protein-1 (MCP-1) (29). They also secrete and express macrophage inflammatory proteins (MIPs), Toll-like receptors (TLRs) and chemokine receptors, including CCR5 and CXCR7 (17, 30-35).

The involvement of HSC in developing inflammatory response to alcoholic liver disease is attributed to their ability to produce complement protein 4 and neutrophil chemoattractants, such as MCP-1and macrophage colony-stimulating factor (M-CSF) (17, 35-39).

The contribution of HSC in developing antiviral inflammatory responses has been evaluated (17, 40). HSC can act as antigen presenting cells and modulate lymphocyte behavior (41, 42).The interaction between HSC and lymphocytes has been established (33, 40). Studies showed that

there is not only direct adhesion between lymphocytes and HSC (43), but also that diseased lymphocytes are ingested by HSC in hepatic fibrosis resulting in activation of HSC (40). In addition, the capacity of HSC to present antigen leads to stimulation of lymphocyte proliferation (42).

HSC and Liver Fibrosis

Fibrosis of the liver is a reversible response following liver injury (44). Although fibrosis is an attempt to minimize liver injury, liver function is significantly impaired. The major causes of liver injury include; chronic viral infection by hepatitis B and C viruses (HBV and HCV), excessive alcohol consumption, non-alcoholic steatohepatitis (NASH), iron overload, autoimmune disorders like primary biliary cirrhosis and autoimmune hepatitis, drug-related toxicity, cholestasis, and inherited metabolic diseases such as hematochromatosis as well as Wilson's disease and Alfa 1- antitrypsin deficiency (1, 45, 46).

Hepatic fibrosis is characterized by increased deposition and decreased degradation of ECM (47, 48). Decreased degradation of ECM is due to an imbalance between MMPs TIMPs that regulate the ECM degradation processes (19, 20). After liver injury, TIMP-1 is over expressed, resulting in decreased removal of ECM (48).

Accumulation of ECM leads to formation of fibrous scars, development of nodules and cirrhosis (49). Cirrhosis increases the portal hypertension and leads to liver failure (10).

There are several cells involved in the development of liver fibrosis. However, HSC are still the major player in the development of liver fibrosis as they are the main source of the excessive production of ECM in an injured liver (6, 50). When the liver is injured, HSC receive signals

from immune cells and from damaged hepatocytes resulting in HSC activation. HSC activation is a complex process that involves the interaction of various cells and inflammatory mediators. HSC activation is divided into two major phases: initiation and perpetuation. These may be followed by a resolution phase when liver injury resolves (51).

The initiation stage (also called the pre-inflammatory stage) refers to the early changes in gene expression and phenotype, which subsequently render the cells responsive to certain cytokines and other stimuli shortly after the occurrence of liver injury. The perpetuation is the stage at which the effect of these stimuli on maintaining HSC activated and development of fibrosis take place (44, 52). Resolution occurs when fibrotic HSC undergo apoptosis or revert to a normal, quiescent phenotype (52).

The initial paracrine stimulation that leads to HSC activation and changes in ECM includes signals received from immune cells, damaged hepatocytes, KCs and from ECs, as well as exposure to lipid peroxides (17, 46).

The activation of HSC involves migration, proliferation, contraction and morphological transformation from a quiescent (retinoid- rich phenotype) to a myofibroblast-like phenotype (9). In contrast to quiescent HSC, their activated counterparts express more smooth muscle alpha actin (α-SMA) protein and produce greater amounts of ECM proteins, such as collagen type I, III and laminin (48). In addition, activated HSC are characterized by loss of retinoid droplets (17, 53-62).

Despite the contribution of KCs and ECs to the production of TGF-β, HSC remain the main source of production of this growth factor in the fibrotic liver (26).

TGF-β is a very important cytokine in the development of liver fibrosis. TGF-β1 is a key factor in the regulation of HSC proliferation (63).

Another important cytokine is the Platelet-derived growth factor (PDGF), which is over expressed in liver injury. PDGF is mainly produced by HSC, KCs and ECs (64). It is considered the most potent stimulus for HSC activation (38, 65, 66), in particular for HSC proliferation (28). In an injured liver, HSC display elevated levels of PDGF and up-regulation of its receptor (67, 68). In order to understand the role of PDGF in the development of liver fibrosis, a previous study showed that treatment with PDGF-C induces fibrosis, as well as results in the development of hepatocellular carcinoma (HCC) in a mouse model (17, 69).

Bone morphogenetic protein-7 (BMP7) may also play an important role in liver fibrinogenesis. Although, BMP7 has a protective role in renal fibrosis by inhibiting TGF-β-mediated effects (70, 71), recent studies indicated that BMP7 is over expressed in fibrotic and cirrhotic liver (72). The profibrinogenic role of BMP7 results from its activity on HSC transdifferentiation (73). In addition, BMP7 stimulates HSC to produce collagen and fibronectin (72).

However, a different study reported that treatment with rhBMP7 has an antifibrotic effect in liver in agreement with its antifibrotic protective role in renal fibrosis (74). This antifibrotic effect is attributed to inhibiting TGF-β1-induced EMT (Epithelial to Mesenchymal transition) (70, 71). Treatment with rhBMP7 was also associated with reduced expression of collagen type I and-III by HSC (74).

Activated HSC play a significant role in the development of inflammatory responses during liver injury as they tend to migrate and accumulate around damaged areas in response to chemotactic factors, such as MCP-1 (35, 39) and M-CSF (38). MCP-1 attracts activated HSC

and promotes recruitment of monocytes and leukocytes (75), while M-CSF regulates macrophage accumulation and growth (38). Other cytokines released by HSC include PDGF, which stimulates M-CSF synthesis (38). PDGF is also the most potent chemotactic mediator that induces migration for the activated HSC but not for the quiescent ones (76, 77). Moreover HSC release cytokine-induced neutrophil chemoattractant (CINC)/IL-8 (36) and adhesion molecules such as ICAM-1 and VCAM-1 (44, 78).

Contractility of the activated HSC is common following liver injury. HSC contraction has been identified as a major cause of increased intrahepatic resistance to blood flow and portal hypertension through constricting sinusoids (17, 79, 80). HSC contraction is mainly regulated by two HSC-derived compounds; endothelin-1 (ET-1) and nitric oxide (NO) (81). ET-1 is referred to as the contraction stimulus to HSC (82, 83) while NO is the antagonist to ET-1 (84). Activated HSC also produce excessive contractile filament such as α-SMA (85, 86).

Bone morphogenetic protein-4

Bone morphogenetic protein 4 (BMP4) is a member of the BMPs family that is a part of the TGF-β superfamily. BMPs are the major subgroup of this superfamily as there are 15 BMPs and four growth differentiation factors (GDFs). Because BMPs members share some similarities with each other, they are categorized into four subclasses according to their sequence similarity. For example, the chemical structure and biological activity of BMP4 and BMP2 are very similar therefore they fall into the same subclass (87, 88).

In general, the biologically active BMPs are 30–38 kDa homodimers that are initially synthesized as a large precursor composed of 400–525 amino acids (89, 90). Subsequently, the large precursor is cleaved into the active BMPs, each consisting of 50-100 amino acids. The

BMP structure contains seven cysteine residues, six of which form three intra-molecular disulphide bonds (cysteine knots). The remaining cysteine is used for the dimerization of two BMP monomers through forming a covalent disulphide bond to make the biologically active mature BMP dimer (91-93).

The biologically active BMP dimer binds to membrane receptors type I BMPRIA (or activin receptor-like kinase 3 (ALK3)), BMPRIB (ALK6), and type II receptor-BMPRII (88, 90). When a BMP dimer binds to a type I receptor and type II receptor, the type II receptor is phosphorylated resulting in the activation of the type I receptor. Activation of type I receptor phosphorylates R-SMAD proteins (Smad1, Smad5, Smad8), or mitogen-activated protein kinase (MAPK). The phosphorylated R-SMADs and MAPK associate with smad4 and form a complex. This complex enters and accumulates in the nucleus, consequently interacting with specific DNA sequences, leading to transcription regulation of target genes (89, 90, 93).

BMPs were originally discovered based on their role in bone and cartilage formation (94). However, recent studies demonstrated that BMPs have significant functions in regulating the vertebrate development through interlinked regulation of cellular proliferation and differentiation (93, 95). BMPs play fundamental roles during the embryonic stage, and have been shown to regulate processes such as hematopoiesis, differentiation of the left and right side of the body, engineering of the skeleton and nervous tissues, and formation of body organs and limbs (93, 95-97). Not only that, but the vitality of BMPs extend beyond embryonic development and birth. This is because they maintain the health of cartilage and bone mass through regulating the differentiation of bone marrow cells and healing bone fractures. Additionally, they repair spinal cord defects (97, 98).

BMP4 together with BMP2 like other BMPs are required for the early stages of development, such as specification of the dorsal-ventral axis and formation of the appendages (99). The vital role of BMP4 and other BMPs during embryonic development has been analyzed. Animal studies showed that knocking out BMP4 leads to early death of mice embryos accompanied by a defect in mesoderm development. This finding reveals the contribution of BMP4 in mesoderm formation (100). Another study showed that BMP4 inhibition has led to inhibition of blood formation in hematopoietic stem cells. This evidence highlights the critical role of BMP4 in the development of the hematopoietic system and its function as a hematopoietic growth factor (101). There is evidence that BMP4 is involved in the regulation of other organ, such as the kidney. Mutations in the BMP4 gene have been observed in patients with renal hypodysplasia (RHD) (102). In addition, BMP4 is expressed in several tumors, such as gastric (103), hepatocellular (104), melanoma (105), colorectal (106), ovarian cancer (107) and renal carcinomas (108). The role of BMP4 in different tumors is attributed to its activity on cellular behaviour, including regulation of cell growth, differentiation migration, invasion, apoptosis, and angiogenesis (93). Reports on the effect of BMP4 on the growth of cancer cells are contradictory. For instance, treatment with BMP4 led to inhibition of cell growth in basal cell carcinomas, myeloma (109), breast (110), gastric (103, 111), lung (112) and pancreatic cancers (113). In contrast, other cancer cells, such as melanoma, colon cancer, ovarian cancer, and retinoblastoma cells, showed no effect in terms of cell growth after treatment with BMP4 (105, 106, 114-116).

Similarly, one study reported that the inhibition of BMP4 in hepatocellular carcinoma (HCC) has no effect on cell growth (117), while in 2012, Chiu *et al.* showed that up-regulation of BMP4 strongly enhances proliferation and migration of HCC (104). The promotion of cell growth in

HCC by BMP4 results from induction of cyclin-dependent kinase inhibitor protein (CDK1) and CCNB1 expression after BMP4 the activation of ERK/MEK signaling pathway (104).

BMP4 has also been linked to cell migration and invasion, both of which are critical for the metastatic behavior of cancer cells. For example, BMP4 treatment promotes cell invasiveness in pancreatic (106, 118), ovarian (119) and colorectal cancer (106). Further supporting results were obtained where BMP4 inhibition resulted in reduction of cell migration and invasion (105, 117).

Although there are conflicting data regarding the contribution of BMP4 to tumor formation, it has been found that BMPR1A knock down resulted in reduced tumor growth of HCC (104).

The role of BMP4 in regulation of cancer cell apoptosis is still not fully established. However, few studies have reported that BMP4 treatment induces apoptosis in myeloma, retinoblastoma, glioma and in colorectal cancer stem cells (93, 109, 116, 120, 121).

In addition to the effect of BMP4 on cancer cell growth, BMP4 is an essential factor for the regulation of normal liver regeneration. A previous study reported that BMP4 is regularly expressed in hepatic stromal and endothelial cells; however, BMP4 expression in these cells was decreased after hepatectomy. This finding demonstrates the paracrine control of BMP4 exerts on liver regeneration, where BMP4 acts as an anti-proliferative agent. Moreover, *in vitro* treatment with high concentrations of BMP4 inhibited the proliferation of primary hepatocyte and HepG2 cells. In addition, maintaining BMP4 levels in a mouse model after partial hepatectomy led to inhibition of hepatocyte proliferation and consequently reduced the capability of restoring the liver mass. In a similar fashion, treatment with a BMP4 antagonist, Noggin, promoted liver regeneration. These findings suggest that BMP4 expression is essential for inhibiting liver regeneration (122).

BMP4 was also shown to affect the differentiation of hepatic progenitor cells (HPCs). HPCs are local stem cells in the liver that are able to differentiate into either hepatocytes or cholangiocytes. This process is critically regulated by HGF, ECM, and cell surface associated molecules (90, 123). A recent study demonstrated that treatment of rat HPCs (WB-F344) with BMP4 has induces the differentiation into the hepatocytes lineage (124, 125).

The crucial role of BMPs in regulating various cellular processes has led to the investigation of their role in other clinical disorders such as liver fibrosis. A previous study reported that BMP2 and BMP4 increased the expression of α-SMA in cultured HSC (63, 126). The expression of α-SMA is a marker of HSC trans-differentiation and transformation into their myofibroblast-like phenotype (44). In addition, it has been shown that BMPs have a potent effect in the regulation of trans-differentiation of HSC (63). Moreover, BMP4 itself is over expressed in other liver diseases, *e.g.* bile duct ligated liver (126) and in liver cancer tissue (104, 117).

Resolution of Fibrosis

Due to the significant involvement of HSC in the development of fibrotic liver, it is clear that the resolution of fibrosis is related to the reduction of HSC activation. There are two major pathways for the resolution of HSC activation: reversion of activated HSC to their quiescent status, or their clearance via stellate cell apoptosis (28). The reversion of activated HSC to quiescence has been verified in cultured cells (127); however, *in vivo* studies did not show the evidence that support this possibility. On the other hand, both *in vivo* and *in vitro* studies confirmed the activated HSC apoptosis during the resolution of fibrosis (128). Both CD95 (Fas), its ligand CD95L (Fas-ligand) and nerve growth factor receptor (NGFR) are expressed by activated HSC, which promote HSC apoptosis (129). Natural killer cells (NK) can also induce HSC apoptosis through the TRAIL-mediated pathway (130). Activated HSC also secrete soluble survival factors,

notably insulin-like growth factor 1 (IGF-1) and tumor necrosis factor alpha (TNF-α). The excessive secretion of IGF-I and TNF-α during liver injury promotes the survival of activated HSC (17, 129). In addition, TGF-β and PDGF also promote HSC survival and have little anti-apoptotic activity (128, 131). TIMP-1 reduces apoptosis generated by serum deprivation, NGF stimulation and cycloheximide exposure (132). The anti-apoptotic effect of TIMP-1 is based on its effect on inhibiting ECM degradation through inhibition of MMP (133). Inhibition of ECM degradation suppresses apoptotic cytokine release from HSC (132), whereas, pro-survival receptors such as IGF-1 are stimulated (134).

Antifibrotic therapeutic approaches

For many years, it has been believed that fibrosis is an irreversible process. Recent clinical studies, however, have indicated that fibrosis can be reversed (34, 135, 136). Many animal studies reported that the removal of the primary cause is the most effective strategy for fibrosis regression, especially in early stages (137, 138). For example, removal of excessive iron in haemochromatosis leads to reversion of fibrosis (139, 140). Using anthelmintic drugs for treating schistosomiasis is associated with fibrosis regression (141). In addition, inhibition of HBV (142, 143) or HCV (144) showed significant improvement in liver function and regression of fibrosis. Furthermore, fibrosis regression has also been observed after relief of bile duct obstruction (145). Other effective antifibrotic therapeutic approaches in preclinical or in clinical trials include: inhibition of HSC activation, reduction of inflammation, antioxidant administration, stimulation of activated HSC apoptosis, inhibition of collagen synthesis and promotion of ECM degradation (Table. 1) (45, 52, 146).

Table 1. Main antifibrotic therapies for treatment of liver disease

Agent	**Strategy**	**Antifibrotic effect in experimental fibrosis**	**Antifibrotic effect in human (Clinical trials)**
Angiotensin II Receptor Blocker *e.g.* losartan	Inhibition of HSC activation	Positive data (147, 148)	Positive data (149, 150)
Pentoxifylline		limited data (151, 152)	Limited negative data (153)
Colchicine		limited data (154)	inconsistent data (154, 155)
Interferon gamma		Positive data (85, 156, 157)	Positive data (158)
PPAR gamma ligands e.g. Rosiglitazone		Consistent positive data (159, 160)	Positive data in NASH (161-163)
Silymarin	Antioxidant	Positive data (164, 165)	Limited inconsistent data (166, 167)
Phosphatidylcholine		Consistent positive data (168)	Not proven in alcohol induced fibrosis (169)
α-tocopherol		Positive data (170, 171)	Isolated reports in NASH (172, 173)
Sho-saiko-to		Positive data (174, 175)	Isolated reports in hepatitis C (176)
S-adenosyl-methionine		Positive data (177)	effective in alcohol-induced fibrosis (178)
IL-10	Inhibits inflammatory	Positive data (179)	Isolated reports in chronic

	response		hepatitis C (180)
Colchicine	Inhibits collagen synthesis	Positive data (181, 182)	Inconsistent results (183-185)
Gliotoxin	Induction of HSC apoptosis	Positive data (186, 187)	Not tested

Gene Therapy

Gene therapy is a new therapeutic tool that may provide a solution to manage fibrosis. Antisense oligonucleotides or functional therapeutic genes located in plasmid DNA can be used to manage fibrosis through modulation of gene expression in diseased cells (188, 189). There are various methods used for gene transfer to a fibrotic liver. In this regard, viral vectors have shown the highest efficiency as a means for gene transfection into the target cells. Retroviruses and adenoviruses are the most common viral vectors for gene transfer both *in vitro* and *in vivo* (190, 191). Recombinant adeno-associated viruses (rAAV) have superior properties over adenoviruses, such as high cellular tropism, more stable transgenic expression and less stimulation of immune response (192).

TGF-β promotes HSC proliferation as well as increases the production of collagen type I and III proteins by activated HSC (63).Various studies reported that inhibition of TGF-β release causes reduction of liver fibrosis. For example, the administration of adenoviruses carrying a gene expressing a truncated type II TGF-beta receptor (AdTbeta-TR) to dimethylnitrosamine (DMN)-treated rats inhibited TGF-β binding to its receptor, reduced deposition of ECM and suppressed liver fibrogenesis (193). Adenoviral transfection of Smad 7 (known for its inhibitory effect on

TGF-β) (194) led to a reduction of HSC activation and prevented fibrogensis progression (195). The delivery of TGFβRII-specific short-hairpin RNA (shRNA) into rat activated HSC was accompanied by the knockdown of TGFβRII and reduced levels of α-SMA, collagen type I, III, IV and hyaluronic acid (HA) expression (196). Also, TGF-β1-siRNA has been used to knock down TGF-β1 expression in CCl4-treated mice. Another important cytokine is TNF-α, which is mainly produced by KCs. TNF-α is not only involved in activation of HSC and liver damage but also plays an important role in reduction of apoptosis in HSC (131). Targeting KCs with TNF-α antisense oligonucleotides utilizing liposomes as a carrier system resulted in reduction of liver fibrosis that was induced by ethanol (2, 197).

The Augmentation of liver regeneration (ALR) cloned gene plays a critical role in the regulation of liver regeneration and exerts potent anti-hepatitis effects. Therefore, the administration of ALR recombinant plasmid to a rat with hepatic fibrosis reduced the liver fibrosis, ALT, AST and TIMP-1 expression. The administration of ALR also inhibited the expression of collagen type I & III when compared with colchicine that has been used as an anti-fibrotic positive control (198).

Hepatocyte growth factor (HGF) is a major regulator of hepatocyte regeneration and it exhibits potent anti-apoptotic activity. Moreover, it displays anti-fibrotic effects through inhibition of TGF-β1 and collagen type III gene expression levels (199-201).

It has been reported that the delivery of MMPs can be a promising tool for resolving liver fibrosis and advanced cirrhosis through their role in digestion of the fibrillar collagen of ECM. MMP-1, MMP-8 and MMP-13 are considered the most potent MMPs (202, 203). In 2011, Kim *et al*. utilized a polyethylenimine polymer coupled to hyaluronic acid (HA) as a specific ligand

for the targeted delivery of plasmid DNA encoding MMP13 to the liver. The expression of MMP13 resulted in the reduction of aspartate transaminase enzyme levels, and also reduced the induction of liver fibrosis caused by CCL4 administration (204). The delivery of human pro-MMP-1 encoded on complementary DNA using an adenoviral vector to a rat model of liver fibrosis showed significant attenuation of liver fibrosis (205). Similarly, the adenoviral transfection of MMP-8 to a rat model of liver cirrhosis mediated by CCL4 administration was accompanied by significant resolution of liver damage (203).

In advanced stages of liver damage, TIMP-1 is overexpressed, leading to more fibrosis through disposition of ECM. This is because TIMP-1 binds to MMPs and inhibits their activity (206). In 2006, Roderfeld *et al*. reported that the adenoviral delivery of the proteolytically inactive MMP-9 to mice of CCl4-mediated hepatic fibrosis reduced liver damage accompanied by a decrease in collagen type-I expression (207).

RAAV has been utilized for the delivery of IFN-gamma to HSC (rAAV-IFN-gamma). The antifibrotic effect of rAAV-IFN-gamma has been investigated in both *in vitro* and *in vivo* rat models of CCL4-mediated hepatic fibrosis. The *in vitro* study revealed that rAAV-IFN-gamma inhibits HSC activation and decreases the expression of α-SMA, TIMP-1 and TGF-β. Concurrently, the *in vivo* study reported that treatment with rAAV-INF-gamma was associated with fibrosis regression. Furthermore, the hydroxyproline content, serum AST and ALT levels and TIMP-1 mRNA expression were significantly decreased; however, no significant changes were observed in TGF-β and MMP-13 expression (208).

RNA interference

RNA interference (RNAi) is a mechanism by which small double-stranded RNAs (dsRNAs) regulate specific gene expression. This process can be induced either endogenously through microRNAs (miRNAs) or exogenously through small interfering RNAs (siRNAs) (209, 210). RNAi was first observed in *Caenorhabditis elegans* by Fire and Mello when they discovered the ability of dsRNA to knock down the expression of specific genes (44, 211). In 2001, another study showed that siRNA could block gene expression in mammalian cells (212). The first successful trial of siRNA-mediated gene silencing was carried out in an HCV mouse infection model (213). In recent years, RNAi has increasingly become a novel therapeutic approach for the treatment of many human diseases (214, 215).

RNAi occurs when long pieces of dsRNA are cleaved into smaller fragments known as siRNA (21–23 nucleotides long) by the Dicer enzyme (216). However, siRNA can be chemically synthesized outside the body and directly introduced into the cell, therein avoiding Dicer-mediated cleavage and nonspecific off-target gene silencing. When siRNA forms intracellularly, it binds to a protein complex called the RNA-induced silencing complex (RISC) (112). RISC contains Argonaute-2, a protein that separates the siRNA into two single stranded RNA molecules, followed by the cleavage of the sense strand (217). The single antisense strand of the siRNA guides the activated RISC and selectively binds to mRNA that has a complementary sequence to the antisense strand resulting in the degradation of mRNA (218). The cleavage of mRNA is mediated by the endonuclease activity of Argonaute-2 at a position that is located between nucleotides 10 and 11 on the complementary antisense strand from the 5′-end (219). The activated RISC complex is then recycled and functions in multiple catalytic processes (220). This effect lasts up to one week in rapidly dividing cells, and for several weeks in non-dividing

cells (221, 222). The frequent administration of siRNA is required after its degradation within the cell to achieve a persistent inhibitory effect (223).

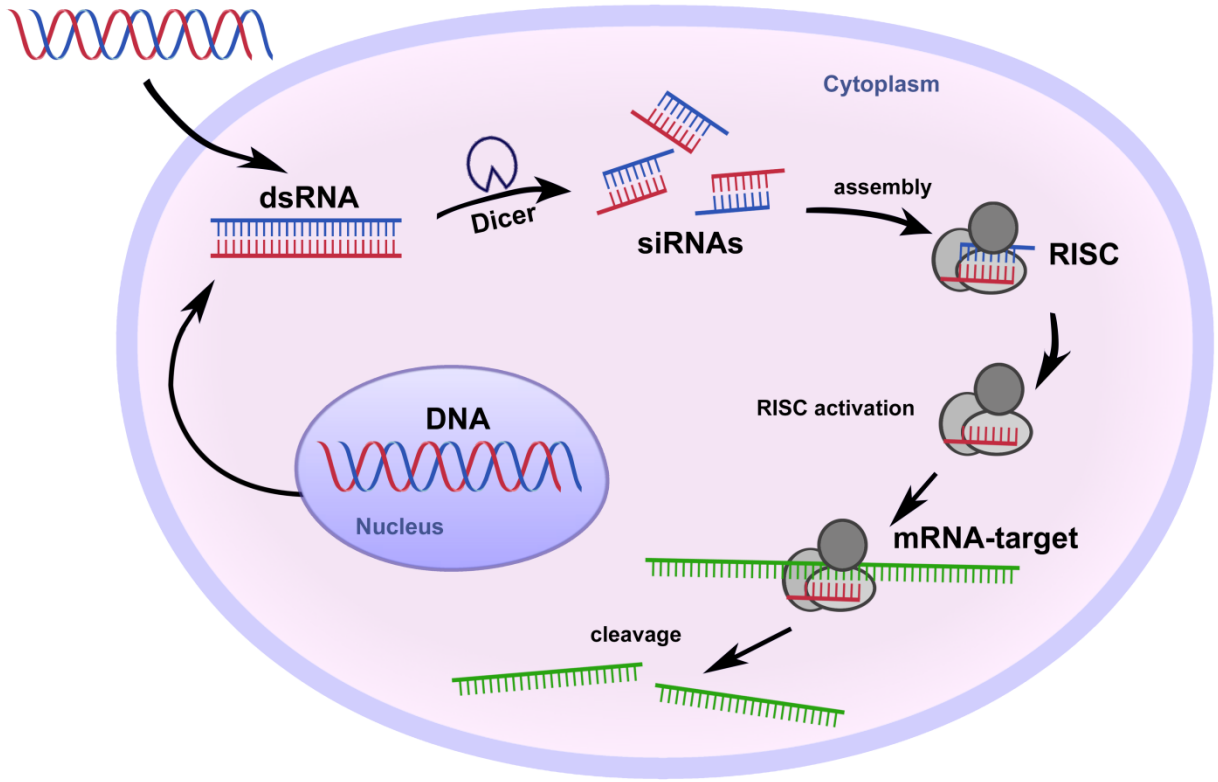

Figure 2: Mechanism of RNAi
Figure was created by Ms Jiaqi Yang

Barriers of siRNA delivery and therapy

Theoretically, RNAi can be used to silence almost any gene in the body. However, this faces many challenges in clinical practice, including safety, stability, and effective delivery of siRNA (224). The first obstacle is siRNA degradation by plasma RNAses as well as its rapid elimination by the renal and reticulo-endothelial system. This is especially the case for naked unmodified siRNA (225). Moreover, siRNAs are capable of stimulating the innate immune system, which recognizes them as foreign bodies. Therefore, this may lead to off-target immune-mediated side

effects (226). In order to achieve gene silencing, siRNA must enter the cytoplasm of the target cell. However this delivery is limited by the negative charge and the high molecular weight of siRNA, which makes it difficult to penetrate the cell membrane by passive diffusion or without the aid of a delivery system (227, 228). Another barrier is the intracellular endosomal trapping effect that will guide siRNA to degradation before it reaches the target mRNA (229). Furthermore, siRNA application can cause off-target effect, in which siRNA may interact and induce nonspecific silencing to genes whose expression should not be targeted, as these genes may share partial sequence similarity to the target gene (230, 231). The off-target gene silencing can be a significant problem and may lead to toxicity, mutation and unexpected changes in cell behaviour (232, 233). However, these challenges can be solved through rational design of siRNA, as well as the development of nanocarriers that ensure specific and safe delivery of siRNA into target cells without inducing any toxic or immunological side effects. In this sense, additional optimization of siRNA biostability and cellular delivery is of utmost importance (234). In 2005, Jackson *et al*. reported that off-target gene silencing can be minimized through substitution of the 2'-O-methyl group on the ribose ring of the guide strand (231). Rational siRNA design should consider several parameters, namely: GC content, the minimal repeated sequences that are responsible for the off-target effect, and an appropriate choice of siRNA length (19–22 bps). In practice, several companies provide an effective siRNA design online with the desired properties to reduce off-target effects (233, 235). To facilitate siRNA transport through biological membranes, one approach is to complex the siRNA to cationic polymers or with cationic lipids. The polymers form polyplexes and cationic lipid create lipoplexes that facilitate endosomal escape (236). Several nanocarriers (1-1,000 nm) can be utilized to deliver siRNA, however, it has been reported that the nanoparticles of 50-200 nm are easily taken up by

target cells via passive delivery and avoid rapid renal clearance as well as provide a large surface area that can improve drug release, extend bioavailability, bio-distribution and efficacy of drugs (236-238). In addition, these nanocarriers can be modified with targeting moieties to achieve active targeted delivery, which can be internalized via receptor-mediated endocytosis. These targeted nanoparticles can avoid or minimize off-target side effects, as well as achieve the desired therapeutic effect with the minimum required dose (239). Among the nanocarriers that have been successfully formulated to target liver fibrosis are cationic polymers, cationic liposomes, stable nucleic acid lipid particles (SNALP) and polylipid nanoparticles.

Liposomes in siRNA delivery

Over the last 25 years, liposomes have been extensively utilized for drug and gene delivery (240). This is due to their safety, biocompatibility, and comparative ease of preparation. In addition, they demonstrate a diverse range of morphologies, compositions, sizes, tissue targeting and controlled release characteristics. Furthermore, they are able to deliver and protect various types of therapeutic molecules of either hydrophilic or hydrophobic natures (241-243). To date, the FDA has approved seven liposomal drugs for targeting different health problems, such as cancer and infectious diseases (238, 244). Structurally, liposomes are spherical vesicles formed by self-assembly and characterized by an aqueous core surrounded by one or more phospholipid bilayers (unilamellar or multilamellar, respectively). In general, most liposomal preparations used for siRNA and gene delivery are made of neutral and cationic lipids.

Cationic liposomes such as DOTAP (1,2-dioleoyl-3-trimethylammonium-propane) and DOTMA (N-[1-(2,3-dioleoyloxy)propyl]-N,N,N-trimethyl-ammonium methyl sulfate) are mainly used for siRNA delivery to the liver (245). This is attributed to their ability to form lipoplexes with negatively-charged siRNA via electrostatic interaction, as well as facilitate interaction with

negatively charged cell membrane components resulting in the uptake of the particles (230, 246, 247). Moreover, cationic liposome provide protection for siRNA from enzymatic degradation and reduce renal clearance of siRNA (233). Further, cationic liposomes also provide high transfection efficiency of siRNA and exhibit relatively low cytotoxicity and immunogenicity (230).

Generally, lipoplexes are formed via electrostatic interactions between the cationic lipid head groups (quaternary amine head groups) with the anionic phosphate groups of siRNA. siRNA packaging into liposomes can be achieved either through encapsulation or adsorption. The former requires adding siRNA to the inner water of hydration during liposomes preparation or during liposomes recovery after lyophilization (internal addition). This method provides higher encapsulation efficiency and stability to siRNA. The latter strategy is adsorption of siRNA to the pre-formed liposomes nanoparticles. This requires mixing the cationic liposomes with the aqueous siRNA solution at a certain weight ratio and incubation for a period to allow complex formation (external addition). The positively charged head groups of liposomes are thought to associate and coat the surface of the siRNA, resulting in cationic lipid layers on siRNA or the siRNA associate on the surfaces of the liposomes. Although this strategy has a lower siRNA loading efficiency, we employed it in the present study because it offers a simple and rapid way of siRNA loading compared with encapsulation of siRNA into liposomes (248).

Although cationic liposomes offer high siRNA encapsulation efficiency, the *in vivo* preclinical application encountered some challenges. Namely, these included systemic administration-associated toxicity, poor stability in plasma and immune response activation (244, 249, 250). The major concern in this context is systemic administration-associated toxicity, a phenomenon largely thought to arise from the excessive charge on the lipid surface (249, 251). Dokka et al.

reported that this toxic effect is related to activating the release of reactive oxygen species (ROS) and increased intracellular calcium levels induced by cationic liposomes (252). Another challenge is that cationic liposomes possess poor stability in plasma, wherein they tend to aggregate. This aggregation is attributed to their interaction with negatively charged serum proteins (250). The interaction of cationic liposomes with serum components may result in undesirable off-target side effects that lead to their rapid clearance from the blood by macrophages of the reticulo-endothelial system (RES), and failure of siRNA release to the targeted cells. Reports have also shown that multivalent cationic liposomes like Lipofectamine® are highly toxic to macrophages and other immune cells in contrast to monovalent cationic lipids like DOTAP (244, 253, 254). In order to overcome these challenges and to achieve successful delivery of siRNA by liposomal delivery systems, important measures should be taken, such as optimization of lipid content ratio, lipid-to-siRNA ratio, size of particles and zeta potential. Additional parameters worthy of optimization may include siRNA encapsulation or binding efficiency, as well as incorporation of specific ligands to liposomal surfaces in order to enhance their selective interaction with the target cells (244).

The development of a targeted delivery system for anti-fibrotic therapeutics is a preferred approach, as most of these drugs lack *in vivo* cellular specificity to HSC, leading to off-target side effects. However, the selective targeted delivery system increases the drugs' bioavailability at the target site and enhances their therapeutic efficiency with the minimum required therapeutic dose. Consequently, this eliminates the side effects that result from off-targeted delivery (1, 189, 255). In this regard, ligands such as galactosylated cholesterol, glycolipids or galactosylated polymers have been conjugated to liposomes, resulting in significantly improved targeting efficacy to the liver (256-258). Adrian et al. developed targeted liposomes for drug delivery to

HSC composed of dilinoleoylphosphatidylcholine (DLPC). Specifically, they used human serum albumin and mannose-6-phosphate (M6P-HAS) as a selective targeting group to HSC. M6P-HAS-coupled liposomes showed high specificity and enhanced uptake by HSC. In vitro investigation demonstrated that M6P-HAS liposomes exhibited anti-fibrotic activity on cultured HSC, where the expression levels of TGF-β, collagen- I and α-SMA in HSC were decreased (1).

In 2008, Sato et al. developed vitamin A-coupled liposomes for selective targeted delivery of collagen specific chaperone (gp 46) siRNA to HSC. These cationic liposomes are composed of cationic lipid (DC-6-14), cholesterol and DOPE. Vitamin A has been employed as a selective ligand based on the function of HSC in the storage of vitamin A, as they are the only liver cells with high retinol-storing capacity and high expression levels of RBP. The anti-fibrotic effect of vitamin A-coupled liposomes-gp46 siRNA has been investigated both in vitro and in three rat models of DMN, CCl4 and bile duct ligation (BDL)-mediated hepatic fibrosis. VA-lip-gp46 siRNA could silence gp46 gene expression both *in vitro* and *in vivo* as well as reverse the hepatic fibrosis in the three cirrhotic model treated rats with a systemic administration of relatively low doses of 0.75 mg/kg of VA-lip-gp46 siRNA. In addition to decreased production of collagen, hydroxyproline accumulation, bilirubin and hyaluronate levels have been normalized in all treated rat models by VA-lip-gp46 siRNA administration. It has also been revealed that treatment with VA-lip-gp46 siRNA, in contrast to treatment with Lipofectamine 2000®, did not stimulate the immune response, as TNF-α expression levels remained normal. All these findings strongly support a specific and selective action for VA-lip-gp46 siRNA complex on HSC without off-targeting effects (259). Similarly, Narmada et al. have cloned HGF gene to pDsRed2 plasmid DNA vector and transfected to HSC utilizing vitamin A coupled liposomes as a delivery system to rat model of DMN-induced liver fibrosis. Treatment with VA-lip-HGF leads to

increase HGF gene expression and resolution of the existing liver damage induced by DMN administration. In addition, TGF-β1, α-SMA and collagen-I mRNA levels decreased (255).

Moreover, polyethylene glycol (PEG) has routinely been used to modify liposomal surfaces through formation of a protective barrier. This protective coat prevents macrophage uptake and reduces interaction with serum components. Therefore, PEGylated liposomes, which are also referred as stealth liposomes, minimize RES clearance, immune response, cationic liposomes aggregation in serum, and consequently enhance the stability and transfection efficiencies of lipoplexes in presence of blood (244, 254, 260-262). Despite these advantages, PEGylated liposomes exhibit some shortcomings, notably: lack of target cell specificity, and decreased cellular uptake of lipoplexes. The latter stems from an inhibition of endocytosis in such a way that it is dependent on the amount of PEG found on liposomes (262, 263). Moreover, as PEGylation stabilizes DNA encapsulation into liposomes, this may decrease DNA-liposome complex dissociation and consequently result in a failure to release DNA into the cytoplasm (262). Although PEGylated liposomes lack specificity for targeting cells, PEGylation provides a good surface and facilitates the conjugation of target-specific ligands (244). In 2012, Gao J et al. developed PEGylated immunoliposomes composed of DOTAP and cholesterol conjugated with anti-EGFR antibody (TLPD) for the targeted delivery of siRNA to hepatocellular carcinoma (264).

Neutral lipids

As mentioned previously, cationic liposomes-related toxicity results from the excessive charge on the lipid surface; therefore, neutral lipids are commonly used in gene delivery in combination with cationic lipids to minimize the toxicity associated with the cationic liposomes. In addition, neutral lipids do not stimulate the immune response. Moreover, several *in vivo* studies have

reported that utilization of neutral lipids with cationic ones in siRNA delivery achieved higher transfection efficiency than did cationic liposomes alone (232, 244, 265, 266). The most commonly used neutral lipids are 1,2-dioleoyl-sn-glycero-3-phosphatidylcholine (DOPC) and 1,2-Dioleoyl-sn-Glycero-3-Phosphoethanolamine (DOPE). It is believed that DOPE leads to higher transfection efficiency than does DOPC (267, 268), as the former yields a hexagonal tubular structure that allows direct binding to DNA via electrostatic interactions and stabilizes DNA inside its tubules. Furthermore, reports showed that DOPE-containing cationic liposomes could destabilize the endosomal vesicle membrane, leading to endosomal escape of the lipoplex. In contrast, DOPC forms lamellar layers of DNA and lipids, and it has no effect on endosomes (262, 269, 270).

.

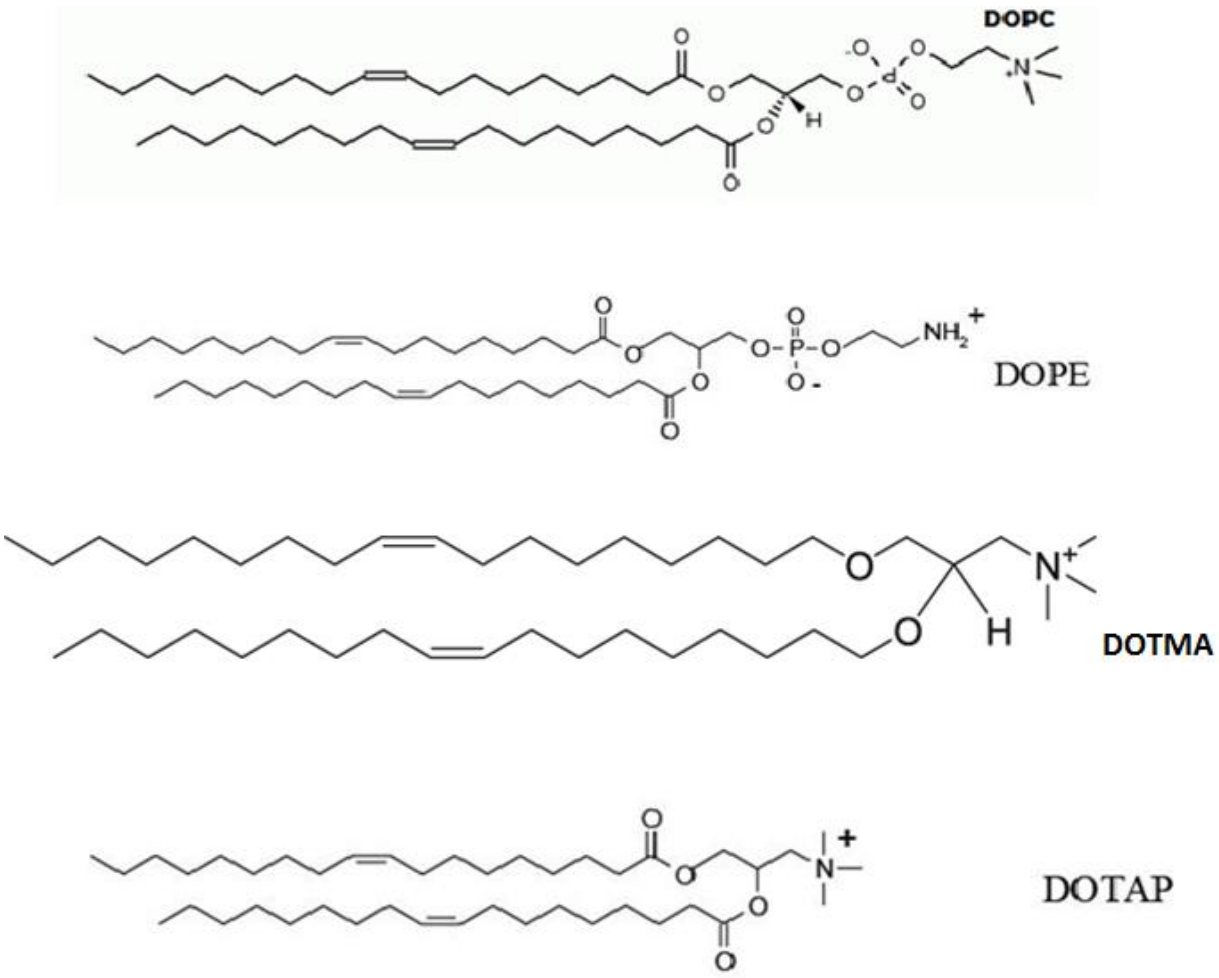

Figure 3: Chemical structures of commonly used synthetic lipids. Neutral lipids include 1,2-dioleoyl-sn-glycero-3-phosphatidylcholine (DOPC) and dioleoylphophatidylethanolamine (DOPE), while cationic lipids include N-[1-(2,3-dioleyloxy) propyl]-N,N,N-trimethylammonium methyl sulfate (DOTMA) and 1,2-bis(oleoyloxy)-3-(trimethylammonio) propane (DOTAP).

SiRNA-nanotherapeutics and liver fibrosis

Up to date, there have been significant developments in the clinical use of siRNA-based therapies. However, the most common application of siRNA-based therapeutics is based on the localized delivery form *e.g.* age-related macular degeneration (AMD) which causes vision loss (226). This study was carried out by Acuity Pharmaceuticals in 2004, which resulted in improved vision in some of the patients (238).

In addition, several clinical trials based on systemic delivery of siRNA are currently underway, including those for HBV infection and acute renal failure. In 2008, the first clinical trial started for siRNA-therapy against a human solid tumor (melanoma) (271). Currently there are eight clinical studies for the treatment of cancer using nanoparticle-based siRNA delivery (244). Calando Pharmaceuticals developed CALLA-01, which is the first siRNA-anticancer therapeutic entered phase I clinical trial. CALLA-01was designed based on cyclodextrin-based polymer to inhibit the expression of the M2 subunit of ribonucleotide reductase (R2) (272).

The application of siRNA-based therapies in the treatment and prevention of liver diseases has been reported to be effective (273, 274). The potential application of siRNA for the treatment of HCV infection has also been discussed by Chang Ho Lee (272). The intravenous administration of HCV-specific siRNA with liposomes and purified recombinant human apolipoprotein A-I (rhapo A-I) significantly reduced HCV protein expression (275).

Another study showed that VEGF-siRNA is able to silence VEGF expression. VEGF silencing is followed by reduction in growth of hepatocellular carcinoma both *in vivo* and *in vitro* (276).

Adenovirus was applied to deliver siRNA to inhibit the oncogene p28GANK in hepatocellular carcinoma (HCC) cell lines and nude mice. Results showed that siRNA for p28GANK could significantly inhibited tumor growth both *in vitro* and *in vivo* by inducing HCC apoptosis (277).

In terms of liver fibrosis, siRNA has been used to knock down TGF-β1 expression in CCl4-treated mice. TGF-β1 gene inhibition resulted in reduced expression levels of type I collagen and α-SMA. In addition, ALT and AST levels also decreased and consequently reduced the progression of liver fibrosis (278). Similarly, plasmid vectors harboring TGF-β1-siRNA have been utilized to target TGF-β 1 in both CCL4- and high-fat diet-mediated fibrosis. TGF- β1 siRNA successfully silenced the expression of TGF-β1, leading to inhibition of HSC activation, as well as reduced the production of type I and type III collagen (279).

In 2006, Li *et al*. evaluated the anti-fibrotic activity of connective tissue growth factor (CTGF)-siRNA in a rat model of CCl4-mediated hepatic fibrosis. They observed reduction in type I and III collagen and TGF-β1 levels, as well as inhibition of HSC activation (280). Two different working groups have also used CTGF-siRNA to treat the progression of hepatic fibrosis; one study was conducted in hepatic fibrosis induced by N-nitrosodimethylamine (NDMA) (281) and the other recent study was against liver fibrosis in CCL4-treated rats (282). Both studies demonstrated that CTGF knockdown led to reduced HSC activation and resolution of liver fibrosis. In addition, down-regulation of TGF-β1 levels and reduced accumulation of connective tissue proteins in the liver have been reported in the first study (281), whereas the latter showed decreased α-SMA levels (282). In 2008, Chen *et al*. investigated the influence of PDGFR β-siRNA on cultured activated HSC and in rat models of liver fibrosis induced by DMN and bile duct ligation. PDGFR β-siRNA delivery was carried out using a hydrodynamics-based transfection method. They found that down-regulation of PDGFR-β could inhibit HSC activation

and proliferation, and block the MAPK pathway *in vitro*. Fibrotic rats treated with PDGFR-β siRNA showed significant improvement in their liver function as well as suppressed fibrosis progression (283).

In 2009, Cheng *et al*. constructed and evaluated different sequences of TGF-β1 siRNA and TGF-β1 shRNA on cultured HSC-T6. Lipofectamine 2000® was used to deliver TGF-β1 siRNAs while pyridinium liposomes were used to transfect TGF-β1 shRNA into the activated HSC-T6. There were significant decreases in TGF-β1 and TIMP-1 expression levels upon transfection of HSC-T6 with both TGF-β1 siRNA and TGF-β1 shRNA, which advocated a synergistic effect. Furthermore, TGF-β1 gene silencing was accompanied by reduced expression of both TNF-α and IL-1β (284).

The development of liver-targeted specific delivery system of siRNA therapeutics is an important approach to minimize the toxicity and to improve the transfection efficiency (285, 286). In 2010, Kang *et al*. used polyethyleneimine (PEI), cationic polymer utilizing pullulan polysaccharide as targeted conjugate, to achieve specific delivery of PEI-siRNA complexes to liver. The use of PEI-pullulan/siRNA complexes not only improved the liver targeting efficiency, but also minimized *in vivo* toxicity and mortality rates in rats when compared with the use of PEI-siRNA complexes (286). Another study carried out by Park *et al*. developed siRNA delivery system targeting HSC in the liver. They used reducible PEI conjugated to hyaluronic acid as a targeting ligand to deliver TGF-β1 for treatment of liver fibrosis. The anti-fibrotic effect of (PEI-SS)-g-HA/siRNA has been evaluated on cultured HSC-T6 and *in vivo* in cirrhotic mice treated with CCl4. PEI-SS-g-HA/siRNA complex demonstrated low toxicity and high transfection efficiency both *in vitro* and *in vivo*. Moreover TGF-β1 siRNA/(PEI-SS)-g-HA delivery showed a significant protective effect against liver cirrhosis, exemplified by a strong reduction in nodule

formation, collagen production, α-SMA expression and HSC activation (285). Recently, another group used a PEI polymer conjugated to N-acetylglucosamine (GlcNAc) and indocyanine green (ICG) to successfully deliver TGF-β1 siRNA to activated cultured HSC and to CCl4-treated mice. The transfection of TGFβ1-siRNA using PEI-D-GlcNAc-ICG showed higher accumulation of PEI-D-GlcNAc-ICG/TGFβ1siRNA complex on the fibrotic mice's livers than the accumulation in normal liver. In addition, TGF-β1 and α-SMA levels have been significantly reduced. This finding suggests that the specific targeting of the complex to HSC was responsible for the fibrosis (287).

Currently there are about 25 siRNA-based drugs in clinical trials for the treatment of various of diseases including viral infections, cancer and liver diseases (288). As a result, siRNA-based therapy has become a promising potential for the treatment of a wide range of diseases.

Hypothesis

The targeted specific delivery of BMP4-siRNA to HSC inhibits BMP4 gene expression and decreases transformation of quiescent HSC into myofibroblast–like phenotype, consequently decreasing development to fibrosis.

Aim of Study

The objective of this study was to utilize RNAi to silence BMP4 expression in LX-2 cells in an attempt to decrease the transformation of quiescent HSC into myofibroblast–like phenotype, and to provide a potential therapeutic approach for liver fibrosis

The specific aims for this study are:

1- To develop and characterize VA-coupled liposomes for the targeted delivery of siRNA to HSC.
2- To evaluate the delivery efficiency of siRNA to LX-2 cells by VA-coupled liposomes and VA-free liposomes using FACS analysis.
3- To investigate *in vitro* BMP4 gene silencing
4- To examine the effect of BMP4 suppression on α-SMA expression as an indicator of BMP4 activity on HSC trans-differentiation

Chapter 2: Materials and Methods

Materials

1, 2-Dioleoyl-sn-Glycero-3-Phosphoethanolamine (DOPE) (CAT#ME-8181) and

1, 2-Dioleoyl-3-Trimethylammonium-Propane (DOTAP) (CAT#CL-8181TA) were purchased from NOF, America Corporation (NY, USA), D-(+)-Trehalose dehydrate (CAT# 90210-50G), vitamin A (CAT#95144) and Dimethyl sulfoxide (DMSO) (CAT#D4540) were purchased from Sigma Aldrich (ON, Canada). Chloroform was obtained from Fisher Scientific Company (ON, Canada). Amicon® Ultra-4 centrifugal filters devices (30,000 NMWL) (CAT#UFC803024) were from EMD Millipore (Massachusetts, USA). Premixed WST-1 Cell proliferation reagent (CAT#630118) was purchased from Clontec (ON, Canada). Polymerase chain reaction (PCR) primers were designed by the Oligo 7 computer software and synthesized by Life Technology™ (ON, Canada). BMP4 qPCR Template Standard (CAT# HK201114), α-SMA qPCR Template Standard (CAT#HK200549) were obtained from OriGene Technologies (Maryland, USA). PureLink® RNA Mini Kit (CAT# 12183018A) was from Life Technology™ (ON, Canada). Halt™ Protease and Phosphatase Inhibitor Cocktail (100X) (CAT#78442) was supplied by Life Technology™ (ON, Canada). BCA Protein Assay Kit (CAT#23227) was purchased from Thermo Scientific (ON, Canada), The iScript^{TM} cDNA Synthesis Kit (CAT#170-8891) and Microseal® 'B' Adhesive Seals (CAT#MSB-1001) were purchased from the Bio-Rad Laboratories Ltd. (ON, Canada) and Power SYBR® Green PCR MASTER MIX (CAT# 4368706) and MicroAmp® Fast Optical 96-Well Reaction Plate (CAT# 4346906) were obtained from Life Technology™ (ON, Canada). Human BMP4 ELISA kit (CAT# ab99983) was purchased from abcam (ON, Canada) Lipofectamin 3000 (CAT# L3000008) was supplied by

Life Technology™ (ON, Canada). Human Alpha-Smooth muscle actin, Alpha-SMA ELISA Kit (CAT# NB-E11172) was obtained from Novatein Biosciences (Massachusetts, USA).

Cell culture

Human hepatic stellate LX-2 cells (CAT# SCC064), Dulbecco's Modified Eagle Medium (DMEM)(CAT#SLM-021-B), FBS (CAT#ES009-B), penicillin/streptomycin (CAT#TMS-AB2-C) and 1 X Glutamine (CAT#TMS-002-C) were purchased from EMD Millipore (Massachusetts, USA), Opti-MEM® Reduced Serum Medium (CAT#31985-070) and trypsin–EDTA (CAT#15050057) were supplied by Life Technology™ (ON, Canada).

LX-2 cells were recovered from liquid nitrogen by incubating the cryotube briefly at 37 ºC in a water bath. When cells were completely thawed, the outside of the cryotube was disinfected with 70% ethanol. In a laminar flow hood, the contents of the cryotube were transferred into a sterile 15 mL conical tube. 10 mL of pre-warmed DMEM media with high glucose supplemented with 10% fetal bovine serum (FBS), 1 X penicillin/ streptomycin and 1 X glutamine were slowly added to the conical tube. The cell suspension was gently mixed by pipetting up and down avoiding formation of air bubbles, and then centrifuged at 600 x g for 5 min to remove residual cryopreservative (DMSO). The supernatant was discarded and the pellet was resuspended in 5 mL of the culture media mentioned above, and the cell suspension was transferred into a sterile T25 tissue culture flask and placed in a humidified 37°C incubator of 5% CO2 and 95% air.

When cells were 80% confluent after 3-4 days of culturing, they were passed by trypsinization. The culture medium was aspirated from the T25 flasks. Then, cells were washed twice with 1x Phosphate buffer saline (PBS) solution. PBS solution was then removed by aspiration. Cells were de-attached by adding 1 mL trypsin 0.25 % w/v, and incubated for 3 min at 37°C incubator.

After that, 10 mL of 10% FBS DMEM medium was added to the flask to stop trypsinization. The cell suspension was then transferred into a T75 tissue culture flask and maintained in a humidified 37°C incubator of 5% CO2 and 95% air for next passage.

siRNAs

Two pre-designed siRNA silencer select targeting human BMP4 were purchased from Life technologies™ (ON, Canada). The two siRNAs were 21 bps long (MW~ 13 kDa), and their sequences are shown in Table 2.

Silencer® Negative Control siRNA (CAT# AM4635) and Silencer® FAM-labeled Negative Control siRNA (CAT# AM4620) were also purchased from Life technologies™ (ON, Canada).

Table 2: Sequences of specific BMP4-siRNAs.

Name	Sequences	siRNA Location	RefSeq
BMP4-siRNA (CAT#s2026)	Sense: AGAGUGCCGUCAUUCCGGATT Antisense: UCCGGAAUGACGGCACUCUTG	651	NM_001202.3
BMP4-siRNA (CAT#s2027)	Sense: GCAUGUCAGGAUUAGCCGATT Antisense: UCGGCUAAUCCUGACAUGCTG	968	NM_130850.2

Methods

Preparation of liposomes

Liposomes were prepared using the thin-film hydration method as described previously with some modifications (289). Briefly, cationic liposomes were prepared from DOTAP and DOPE at a 1:1 molar ratio. Lipids (containing 50 mg DOTAP and 47 mg DOPE) were dissolved in HPLC-grade chloroform in a round bottom flask. After mixing the lipids, the solvent was dried at 55˚C using a rotary evaporator yielding a lipid film. The thin lipid film was thoroughly dried to remove any residual chloroform by placing the flask on a vacuum pump for 1 hr. The resulting dried film was hydrated in ddH_2O to make a stock solution of 10 mg/mL. The lipid dispersions were warmed and mixed using a rotatory evaporator in which the round bottom flask was spinning in a warm water bath without vacuum for 10 min at 50˚C above the lipid transition temperature (gel liquid crystal transition temperature). The resulting lipid dispersions were large multilamellar vesicles (LMVs). The liposomes size was reduced to small unilamellar vesicles (SUVs) by sonication for 80 sec at 7 kHz (using Branson Sonifier 150 Danbury, USA).

Conjugation of Vitamin A to liposomes and Lyophilization

To prepare Vitamin A (VA)-coupled liposomes, VA was first dissolved in a minimal volume of DMSO (2.6 W/V % VA). VA was then mixed with liposomal suspensions at a molar ratio of VA/lipids (2:1) (259). The mixture was incubated overnight at -20 ˚C to allow complete adsorption of VA on liposomal surfaces. After that, DMSO and the free fraction of VA were removed by ultra-filtration three times using Amicon® Ultra-4 centrifugal filters devices (30,000 NMWL) at 4,000 rpm for 20 min (259). The resultant liposomes were reconstituted in double distilled water (ddH_2O) and stored in amber colored vials at 4 ˚C overnight. To increase the

stability of the liposomes for long-term storage and protect liposomes against hydrolysis and oxidation of phospholipids, they were lyophilized (290, 291). However, lyophilization is associated with changes in physicochemical properties of liposomes due to damage and rupture of the lipid bilayers by ice crystals during freezing, particle aggregation after dehydration and phase transition during rehydration (292-294). To stabilize liposomes during lyophilization, lyoprotectants *e.g* carbohydrates were used to maintain transfection efficiency (293-295). Liposomes employed for the present study were lyophilized utilizing trehalose as lyo-protectant as described previously (290). Firstly, trehalose was added to liposomes at a mass ratio of 1:10 liposomes/trehalose in ddH_2O and mixed using a vortex mixer for 15 sec at 25 °C in amber colored vials. The liposomes were then frozen at −80 ˚C for 8 hr followed by lyophilization at −50 ˚C under reduced pressure 0.310 mBar for 24 hr (Labconco freeze dryer; Labconco Corp., MO, USA). The lyophilized samples were stored at −20˚C in amber colored vials for further characterization and for siRNA loading.

Preparation of Lipoplexes (siRNA-liposomes complex)

Lyophilized samples were reconstituted in pre-warmed ddH2O to their original volume. The reconstituted liposomes were warmed in a water bath at 50˚C and mixed using a vortex mixer until the samples were totally dispersed (without any visually inspected particulate matter). To prepare lipoplexes, VA-liposomes were first prepared as mentioned above, and siRNA was diluted to a concentration of 1.0 µg/µL in nuclease-free water prior to lipoplex preparation. Lipoplexes were prepared by the addition of VA-liposomes to siRNA solution at various VA-liposomes /siRNA molar ratios of (10:1, 10:2 and 10:3 mol: mol). The mixture was gently mixed by pipetting up and down forty times and then incubated at RT for 30 min to allow complex formation (296).

Characterization of liposomes

Measurement of particle size and Zeta potential

The particle size was recorded to evaluate the effectiveness of size reduction and liposomes stability following lyophilization. It is also an important parameter for entry across cellular membranes by endocytosis.

The zeta potential of a particle is the overall charge that a particle acquires in a particular medium. Zeta potential depends on several factors, including: pH, ionic charge, ion size, and concentration of ions in solution (297). Zeta potential is another important parameter that indicates stability because it measures the degree of aggregation or repulsion between particles. It is also an important factor that helps to predict the permeability across biological membranes. The change in particle size and zeta potential of particle could cause change of the transfection efficiency (298)**.**

Liposomes and lipoplexes were suspended in deionized water at 100-200 µg/mL of NP suspension, pH 7.4. The average size, polydispersity (particle size distribution) and zeta potential of VA–coupled liposome, VA-lipoplexes, VA-free liposomes and VA-free lipoplexes were determined at 25ºC by dynamic light scattering (DLS) using ZetaPALS (Brookhaven Instruments, Holtsville, NY, USA). Each sample was run for two min three times and all samples were tested in triplicates.

SiRNA binding efficiency (BE)

To measure siRNA-binding efficiency (BE), lipoplexes were prepared with FAM-labeled siRNA. The siRNA BE was determined by comparing the amount of initially added siRNA with

the unencapsulated siRNA in the sample using ultra-centrifugation and a fluorescence assay (264). Briefly, the lipoplexes were prepared by adding different concentrations (1, 3, 5, 9 µg) of fluorescein amidite (FAM™)-labeled siRNA to a fixed volume (3µL) of VA-liposomes (10 mg/mL). The final concentrations of the liposomes and siRNA were 30 µg/mL (259, 299). Lipoplexes were filtered using Amicon ®Ultra-4 centrifugal filter devices (30,000 M.W. cut-off) at 4,000 rpm for 15 min. Afterwards, the filtrate containing the free fraction of FAM-siRNA was collected and quantified using a calibration line obtained by serial dilution of standard FAM-siRNA solutions. The fluorescence intensity of FAM-siRNA was determined using a microplate reader (Synergy™ 4, Biotek, Wi, USA) at excitation and emission wavelengths of 495 and 525 nm, respectively. The siRNA BE was calculated using the following formula:

$$\boldsymbol{BE = \frac{\text{Initially added siRNA} - \text{mass of unencapsulated siRNA}}{\text{Initially added siRNA}} X100}$$

Vitamin A Assay

Vitamin A concentration was determined by Reverse Phase High-Performance Liquid Chromatography (RP-HPLC) as described below (300).

HPLC conditions

Vitamin A analysis was carried out using HPLC with UV detection (Waters Corp, USA). The HPLC system consisted of a Model 600 E System Controller pump, a Model 700 Satelite Wisp injector and Waters™ 996 Photodiode Array Detector (PDA), interfaced with an NEC power mate 386/33i personal computer and millenium™ 2010 chromatogram measuring software. The separation of Vitamin A was carried out using a Nova-Pak C18 column, 3.9 X 150 mm, 60

nominal pore size, 4 µm spherical particles with an isocratic mobile phase composed of acetonitrile, tetrahydrofuran and water (55%: 37%: 8%) respectively. The flow rate was adjusted to 1.2 mL/min. Detection was performed at a wavelength of 325 nm and the injection volume was 20 µL. The samples and standards were prepared in the dark and kept in amber colored vials due to the light-sensitive nature of retinol.

Preparation of mobile phase

The mobile phase used in the study was composed of acetonitrile, tetrahydrofuran and water (55 %: 37 %: 8 %) respectively. The mobile phase solution was filtered through 0.45 mm nylon membrane filters using vacuum and subsequently degassed for 20 min with an ultra-sonic bath.

The analytical column was washed with the mobile phase and then adjusted to a flow rate of 1.2 mL/min.

Standards preparation

4 mg of retinol were accurately weighed on an analytical balance and dissolved in 4 mL of HPLC grade methanol in an amber-colored vial to make a stock standard solution with a concentration of 1 mg/mL. The solution was mixed by vortexing for 30 sec and stored in the dark at - 20ºC between uses. Working solutions of the standard were prepared by serial dilution using HPLC grade methanol yielding the following concentrations: 62.5, 125, 250, 500 and 1000 µg/mL.

Sample Preparation

The free fraction of vitamin A was removed by ultra-centrifugation of VA-liposomes three times using Amicon® Ultra-4 centrifugal filters devices (30,000 M.W. cut-off) at 4,000 rpm for 20 min each (259). Then, 500 µL of liposomes with a final lipid concentration of 10 mg/ml were dissolved in an equal volume of HPLC grade methanol and protected from light in amber vials. The sample was mixed by vortexing for 30 sec at RT. For vitamin A analysis, aliquots of the sample and the diluted standard solutions were transferred into small HPLC amber vials. A volume of 20 µL of all the samples and the standards was injected into the column.

Methanol was used for sample extraction and standards preparation. Retinol was used as an internal standard. Samples and standards were prepared in the dark and kept in amber colored vials. Aliquots of the sample and the diluted standard solutions were transferred into small HPLC amber vials. A volume of 20 µL of all samples and standards was injected into the column. Vitamin A analysis was carried out using HPLC with UV detection (Waters Corp, USA). The separation of Vitamin A was carried out using Nova-Pak® C18 4 µm particle size 3.9 X 150 mm column with a mobile phase composed of acetonitrile, tetrahydrofuran and water (55 %: 37 %: 8 %) respectively, at a flow rate of 1.2 mL/min. Detection was performed at 325 nm. To avoid interfering peaks from the liposomes, Vit A-free liposomes were used as negative controls. The standard curve was established by plotting the amount of each standard dilution against the corresponding peak area. The concentration of vitamin A was determined by relating the area under the peak acquired by reverse-phase HPLC to the equation of the standard curve.

WST-1 Assay

WST-1 assay is a quantitative measurement of the metabolic activity of viable cells *in vitro*. The assay can be used for determination of cell viability, factor-mediated toxicity and for cell proliferation. The assay is based on the enzymatic cleavage of the slightly red tetrazolium salt WST-1 to the dark formazan by cellular mitochondrial dehydrogenases in viable cells. Expansion in the number of viable cells or mitochondrial enzyme activity results in an increase in the intensity of formazan dye formed, which could be quantified by measuring the absorbance at 540 nm using a microplate reader (Synergy™ 4, Biotek, Wi, USA).

Cytotoxicity of Vit A-coated liposomes

The cytotoxicity of Vit A-liposomes was evaluated by premixed WST-1 cell proliferation reagent according to the manufacturer's protocol. Briefly, LX-2 cells were seeded on 96-well plates at a density of 1 X 10^4 cells per well in 100 µL of DMEM media, and incubated for 24 hr. The following day, cell culture media was replaced with Opti-MEM® reduced serum medium. A volume of 10 µl of Vit-A free liposomes and Vit-A coupled liposome was added to each well, at a concentration of 25 to 250 µg/mL, and incubated for an additional 24 h. Blank cell media was used as a negative control while untreated cells were used as positive controls. Cell proliferation was evaluated by adding 10 µL of WST-1 solution to each well and incubated at 37 ˚C for 2 hr. All concentrations were measured in triplicate. The absorbance was measured using a microplate reader (Synergy™ 4, Biotek, Wi, USA) at 540 nm. Cell viability was calculated according to the following formula:

$$\text{Cell viability } \% = \frac{\text{Absorbance of treated cells } - \text{ Absorbance of Blank}}{\text{Absorbance of control } - \text{ Absorbance of Blank}} \text{X100}$$

***In vitro* cellular uptake**

The intracellular delivery of VA-liposomes-siRNA complex was assessed by Flow Cytometry analysis. LX-2 cells were seeded on 6-well plates at a density of 2 X 10^5 cells per well. After 24 h, the culture medium was exchanged with Opti-MEM® reduced serum medium. Cells were treated with 15 µg liposomes containing 3 µg FAM-labeled siRNA per well in 2 mL of the culture media and incubated for 4 h. After that, cell medium was removed by aspiration and cells were washed twice with PBS. Cells were detached by trypsinization. The cell suspensions were centrifuged at 600 rpm for 5 min and washed three times with 1X PBS to remove any free FAM-labeled nanoparticles. Pellets were resuspended in 500 µL PBS and the fluorescence intensity was measured by Flow Cytometer (BD Biosciences, San Hose, CA, USA) (**296**). Approximately 1 X 10^4 cells were counted by the flow cytometer to determine the trend of the VA-liposomes-siRNA taken by the LX-2 cells. The instrument was calibrated using non-treated cells (**301**, **302**). The Flow Cytometry data were analyzed using CELLQUEST v.1.0 software.

Intracellular delivery of siRNA to LX-2 cells was also evaluated using a microplate reader. Briefly, LX-2 cells were seeded in 24-well plates at density of 5 X 10^4 cells per well 20 h before experiments. Cells were treated with different liposomes formulations containing 2 µg/well FAM-siRNA in the culture medium at 37 °C for 4 h. Cells were washed three times with PBS followed by incubation with 300 µL lysis buffer (0.3% Triton X-100 in PBS) at RT for 30 min.

The fluorescence intensity of 100 µL cell lysate was determined using a microplate reader (Synergy™ 4, Biotek, Wi, USA) at excitation and emission wavelengths of 495 and 525 nm, respectively.

SiRNA Transfection

LX-2 cells were pre-seeded in 12-well plates at density of 1 X 10^5 cells per well and incubated at 37˚C for 12 h before experiments. Cells were treated with different formulations carrying 3 µg of BMP4-siRNA per well in 1 mL of Opti-MEM® reduced serum medium. The cells were divided into three groups. BMP4-siRNA was transfected into LX-2 cells using Vit A–coupled liposomes, Vit A–free liposomes and the commercial transfection agent Lipofectamine 3000. The second group was the control group including cells treated with negative control siRNA and normal control (non-transfected cells). LX-2 cells were incubated with BMP4-siRNA at 37˚C for different time points (24 h, 48 h and 72 h).

Gene Expression Analysis- RT-PCR

RNA Extractions

Total RNA was extracted from cultured LX-2 cells using PureLink® RNA Mini Kit according to the manufacturer's protocol. In brief, culture media were aspirated and cells were homogenized with 300 µL lysis buffer (containing 1% 2-mercaptoethanol) per well. Cells were lysed directly in culture plates by pipetting the cell suspension up and down several times. Cells were completely harvested in microcentrifuge tubes by vortexing for 1 min using a vortex mixer. Cell lysates were transferred to clean tubes and filtered through homogenization columns by centrifugation at 12,000 *g* for 2 min at room temperature (RT). Filtrates were collected and washed by addition of an equal volume of 70 % ethanol. A volume of 700 µL of each sample was transferred into spin cartridge (with the collection tube) and samples were centrifuged at 12,000 *g* for 15 sec at RT. The flow-through was discarded and RNA pellet was washed by adding 700 µL Wash Buffer I to the spin cartridge followed by centrifugation at 12,000 x g for

15 sec at RT. The flow-through and the collection tubes were discarded, and the spin cartridge was placed into new collection tube. The spin cartridge was washed twice by adding 500 µL Wash Buffer II followed by centrifugation at 12,000 x g for 15 sec (wash I) and 2 min (wash II) at RT. The flow-through was discarded, and the spin cartridge membrane was dried by centrifugation the spin cartridge at 12,000 x g for 1-2 min at RT. The collection tube was discarded, and the spin cartridge was placed into a recovery microcentrifuge tube. A volume of 30-60 µL RNase-free water was added to the center of the spin cartridge and incubated for 1 min at RT. RNA was eluted from the membrane into the recovery tube by centrifugation the spin cartridge at 12,000 x g for 2 min at RT. RNA concentration was determined by measuring the spectrophotometric absorbance at 260 nm, and RNA purity was determined by evaluating A_{260}/A_{280} wavelength ratio using Thermo Scientific™ NanoDrop™ 2000/2000c Spectrophotometers. RNA samples were stored at -80°C for further cDNA synthesis.

cDNA Synthesis

Total RNA was converted to cDNA using iScript™ cDNA Synthesis Kit. The total reaction volume was 20 µL containing 500 ng total RNA and 4 µL of 5 x iScript RT supermix (reverse transcriptase (RT), RNase inhibitor, dNTPs, oligo (dT), random primers, buffer, $MgCl_2$ and stabilizer). The volume was adjusted to 20 µL using Nuclease-free water. cDNA synthesis was carried out using S1000™ Thermal Cycler (Bio-Rad Laboratories, ON, Canada) using the following condition: 5 min at 25°C for priming, 30 min at 42°C for reverse transcription and 5 min at 95°C for reaction inactivation. cDNA samples were stored at -20°C until analysed by real time PCR.

Real time PCR

Gene expression levels were determined by absolute quantification using standards of known quantity. Briefly, BMP4 and α-SMA qPCR template standards from OriGene Technologies were prepared according to the manufacturer's protocol. Stock solution of qPCR template standard (10^7 copies/ µL) was prepared by dissolving the qPCR template pellet in 50 µL RNase-free water and mixing by gentle vortexing. A ten-fold dilution series was used to prepare working solutions of the standard over the range 10^6 to 10 copies/ µL. 10 µL of stock solution was added to microtubes containing 90 µL 1x dilution buffer and was mixed by vortexing, resulting in a working solution of 10^6 copies/ µL. To prepare the second working solution, 10 µL of 10^6 copies/ µL was transferred into a microtube containing 90 µL 1x dilution buffer and mixed gently. The remaining dilutions were prepared by repeating this step. 5 µL of each template solution from each tube was added to a 96-well PCR plate.

The obtained cDNA was diluted to a concentration of 5 ng/ µL. Real time PCR was carried out for BMP4 and α-SMA using the oligonucleotides synthesized by Invitrogen. The specific primers for each gene were designed by the Oligo 7 program based on the respective sequences obtained from GenBank (BMP4# NM_001202.3 and α-SMA# NM_001141945.1). A list of primer sequences is shown in Table 3. The total reaction volume was 20 µL with 5 µL of cDNA, 10 µL of 2X of Power SYBR® Green, 0.5 µL of 10 µM forward and reverse primers and 4 µL Nuclease-free water. Reaction components were added to the MicroAmp® Fast Optical 96-Well PCR Plate. The standard was run on the same PCR plate. PCR plates were sealed with adhesive cover sheet and centrifuged at 1,000 x g for 1 min. qPCR amplification was carried out using a PCR Detection System (Bio-Rad Laboratories, ON, Canada) by running 10 min at 95 ºC for pre-denaturation and 50 cycles under the following cycle conditions: 30 sec at 95 ºC for

denaturation; different annealing temperatures for 1 min; elongation at 72 ºC for 2 min; followed by a final elongation at 72 ºC for 10 min. The data were analyzed by Bio-Rad CFX Manager software version 3.1. The standard curve was established by plotting the log of the starting quantity of each template dilution against the respective fluorescence intensity acquired during the amplification known as Ct (cycle threshold) of each dilution. The slope, intercept and coefficient of determination R^2 were determined after plotting the Δ Ct value versus log concentration to evaluate whether the qPCR assay was optimized. The amplification efficiency (E) and the concentrations of unknown samples were calculated based on standard curve equation as follow:

$$Sample\ (number\ of\ copies) = \frac{\text{Ct sample} - \text{Intercept}}{\text{slope}}$$

$$E = 10^{-1/slope}$$

$$\%\ Efficiency = (\text{E} - 1)\text{X}\ 100$$

The comparative Δ Ct method was applied to determine the change in gene expression between treated samples relative to control group. To examine regulation of BMP-4 or α-SMA, the Ct from each treated sample was subtracted from the control-treated sample cycle values (Δ Ct= Ct control-Ct treated). The fold change of the test gene was determined as follow: $2^{-\Delta Ct}$

Table 3: List of primer sequences used for gene isolation and PCR

Gene	Primer sequence	Annealing Tem ºC	Amplicon size (bp)
BMP-4	F-5′-ATGTGGGCTGGAATGACTGG -3′ R-5′-GCACAATGGCATGGTTGGTT -3′	60ºC/30 s	Amplicon Length: 117 bp
SMAa	F-5′- GAGACCCTGTTCCAGCCATC-3′ R-5′-TACATAGTGGTGCCCCCTGA -3′	60ºC/30 s	Amplicon Length: 143 bp
SMAb	F-5′- GTCACCCACAATGTCCCCAT-3′ R-5′- GGAATAGCCACGCTCAGTCA-3′	58ºC/30 s	Amplicon Length: 123 bp

Protein Isolation

Control and treated cells were grown in 6-wells plate as mentioned above. Cells were washed with ice-cold PBS, and the cells were trypsinized and centrifuged at 600 rpm for 5 min. The supernatant was discarded and the cell pellet was lysed in 100 µL ice-cold protein extraction solution (1× 50 mM Tris, pH 8.0, 0.5 mM EDTA, 150 mM NaCl, 0.5%NP-40) containing 1× protease inhibitor cocktail (10µL/mL lysis buffer: protease inhibitor). Cell lysates were maintained at constant agitation for 30 minutes at 4°C. Samples were centrifuged at 13,000 *g* for 15 min at 4^0C. The supernatant of each sample was carefully collected and transferred into a new tube. The protein concentration was determined by the BCA protein assay.

Determination of protein concentration (BCA protein assay)

The BCA protein assay is a colorimetric assay used for quantitation of protein concentration, and is based on reduction of Cu^{+2} to Cu^{+1} by protein in an alkaline medium. When cuprous ion (Cu^{+1}) is formed, it can be detected using a unique reagent containing bicinchoninic acid resulting in a purple colour. The purple-colored reaction product results from chelation of two molecules of BCA with one cuprous ion, hence forming a purple-coloured, water-soluble complex.

The BCA protein assay kit includes: Reagent A (containing sodium carbonate, sodium bicarbonate, bicinchoninic acid and sodium tartrate in 0.1 M sodium hydroxide), Reagent B (containing 4% cupric sulfate), standard solution of bovine serum albumin (BSA) ampoules with a concentration of 2 mg/mL. BCA Working Reagent (186) was prepared by mixing stock solution A and B at a ratio of 50:1, respectively. A series of dilutions over the range of 20-2000 µg/mL of BSA standard solution was prepared, and assayed alongside the unknown samples. A volume of 10 µL of each standard dilution and unknown sample replicate was transferred into 96-well plates. 200 µL of the BCA WR was added to each well, and the plate was mixed on a plate shaker for 30 seconds. The plate was then incubated at 37°C for 30 min. The absorbance intensity is related to protein concentration, and was determined using a microplate reader (Synergy™ 4, Biotek, Wi, USA) at 562 nm. The total protein concentration of tested samples was determined based on the equation acquired by the standard curve. The standard curve was established by plotting concentration of each standard dilution against the respective absorbance intensity.

ELISA (Enzyme-Linked Immunosorbent Assay) for detection of BMP4

Following total protein isolation and quantification, an ELISA was established to determine the concentration of BMP-4 in cell lysates according to the manufacturer's instruction. Briefly, 100 µL of each standard and appropriately diluted sample (1/149) was pipetted into each well of the 96–well ELISA plate pre-coated with BMP-4 monoclonal antibody. All samples and standards were run in duplicate. Plates were sealed and incubated overnight at 4°C. The solution was then aspirated, and washed 4 times with 300 µL 1x wash buffer. A volume of 100 µL of 1X BMP-4 biotin-conjugated detection antibody was added to each well and incubated for 1 h at RT with gentle shaking. The solution was removed, and plates were washed again with the wash buffer. After four washes, 100 µL of 1X HRP-Conjugated Streptavidin solution (consisting of streptavidin protein that is covalently conjugated to horseradish peroxidase (HRP) enzyme) was added to each well, and incubated at RT for 45 min with gentle shaking. The solution was then discarded and washing was repeated. A volume of 100µL tetramethylbenzidine (TMB) substrate solution was added to each well and incubated in the dark for 30 min at RT with gentle shaking. 50 µL of stop solution was added to each well. The absorbance was measured immediately at 450 nm using a microplate reader (Synergy™ 4, Biotek, Wi, USA). The specific protein concentration of tested samples was determined based on the equation acquired by the respective standard curve. The standard curve was established by plotting the concentration of each standard dilution against the respective absorbance intensity.

ELISA for detection of α-SMA

An ELISA was also established to determine the concentration of α-SMA in cell lysates according to the manufacturer's instruction with some modification. Briefly, samples were first appropriately diluted (1 : 4) using sample diluent. A volume of 50 µL of each standard dilution

and sample was pipetted into each well of the 96–well ELISA plate pre-coated with the α-SMA monoclonal antibody. All samples and standards were run in duplicate. Plates were sealed and incubated for 1.5 h at 37°C. The solution was then removed, and the plate washed five times with 300 µL 1x wash buffer. A volume of 100 µL of HRP-Conjugate reagent was added to each well and incubated for 1.5 h at 37°C. The solution was removed, and plates were washed. A volume of 50 µL each of chromogen A and chromogen B solution was added subsequently to each well and incubated in the dark for 15 min at 37°C. A volume of 50 µL of stop solution was added to each well. The absorbance was measured immediately at 450 nm using a microplate reader (Synergy™ 4, Biotek, Wi, USA).

Statistical analysis

Data were analyzed using Prism 6.0 (Graph-Pad Software Inc.). Results were expressed as mean ± standard deviation (SD) of $n \geq 3$ unless otherwise specified. One and two way analysis of variance (ANOVA) tests were used to test significant differences between treatments with *p*-values < 0.05 considered significant, < 0.01 very significant, < 0.001 highly significant and < 0.0001 very highly significant.

.

Chapter 3: Results

Characterization of Liposomes and Lipoplexes

Particle size and zeta Potential

The average particle size of VA-free liposomes and VA-coupled liposomes ranged between 100 and 120 nm with a polydispersity index (PDI) around 0.20 (Table 4). The small PDI of liposomes indicates a narrow size distribution. The average zeta potential measurement for VA-free liposomes and VA-coupled liposomes in ddH2O (pH 7.4) remained nearly constant at ~ 45 mV. When liposomes were conjugated with siRNA, the average size was considerably increased forming lipoplexes. The size of lipoplexes was below 200 nm with PDI less than 0.2. However, the measured zeta potential of the resulted lipoplexes was greatly decreased from ~ 45 to ~ 25 mV.

Table 4: The average particle size, zeta potential and polydispersity index (PDI) of liposomes and lipoplexes measured by dynamic light scattering using ZetaPALS**.**

LIPOSOMES FORMULATION	**PARTICLE SIZE (nm)**	**ZETA POTENTIAL (mV)**	**POLYDISPERITY Index (PDI)**
VA-free liposomes	112.5±6.6	46.25±7.7	0.21475±0.034
Vit A-liposomes	113.5±5	43.75±6.99	0.20775±0.022
VA-free–siRNA lipoplexes	153.5±8	27±3.65	0.15±0.0139
VitA-siRNA lipoplexes	158.5±9.8	23.75±3.40	0.1395±0.013

Data represent means ± SD; n = 4.

siRNA Binding Efficiency

Another important factor to evaluate the quality of the liposomes is the siRNA loading efficiency. siRNA BE determined by ultra-filtrating method and fluorescence assay were shown in Figure 4. The amount of unbound-siRNA was measured in the clear filtrate. To consider any loss of siRNA onto the ultrafiltration membrane, the amount of liposomes-bound siRNA retained over the membrane were resuspended and measured. A small amount of siRNA content (0.8 %) was adsorbed onto the filtration membrane. Any loss of siRNA by adsorption to the filtration membrane was included in the calculation of BE results.

The BE of VA-coupled liposomes prepared with FAM-labeled siRNA of varying concentrations 1, 3, 5 and 9 µg/mL resulted in BE % of 95.3 ± 1.23, 93.76 ± 3.064, 93.75 ± 3.58, 92.68 ± 8.75 respectively. Similarly, The BE of VA-free liposomes was found to be 94.62 ± 1.72, 93.501 ± 6.250, 91.62 ± 7.159, 88.195 ± 5.89 at siRNA concentration of 1, 3, 5, and 9 µg/mL.

HPLC Analysis

Separation of vitamin A in liposomes was achieved successfully using a mobile phase of acetonitrile-tetrahydrofuran-water (55: 37: 8) with a flow rate of 1.2 mL/min. There were no interfering peaks. The retention time was 1.3 min (Figure 6). The data from the mean calibration curves of vitamin A using Retinol (Sigma) as an internal standard are shown in Table 5 and Figure 5. The standard curve was constructed by plotting the mean AUC versus concentrations of Retinol. Reproducibility was expressed as the percent coefficient of variation (% C.V). The calibration curves were linear over the range 100-1000 µg/mL with R2 = 0.9991. The linear equation y = 74.982x + 3206.5 derived from average data was used to calculate vitamin A concentrations in liposomes samples. The concentration of vitamin A in liposomes was determined according to AUC acquired by reverse-phase HPLC using the equation of the standard curve. HPLC analysis showed that our liposomes contain 3.25 mg/mL of vitamin A, which makes up around 80 % of the initially added amount of vitamin A.

Liposomes toxicity study

The major concern about utilization of the cationic liposomes is systemic administration-associated toxicity. Therefore, the liposomes should possess good biocompatibility and low cytotoxicity. The cytotoxicity at various concentrations of VA-coupled liposomes and VA-free liposomes was evaluated in the presence of LX-2 cells *in vitro* using the WST-1 assay Figure 7.

The data showed that VA-coupled liposomes and VA-free liposomes have very similar toxicities. Both VA-coupled liposomes and VA-free liposomes at concentrations up to 100 µg/mL were not toxic to LX-2 cells (~100%) as indicated in Figure 7. However, a significant reduction in cell viability ~80% ($p < 0.05$) was observed for both liposomes at 150 µg/mL. The highest toxic concentrations of VA-coupled liposomes were at 200 and 250 µg/mL reaching up to 57.16 % ($p < 0.0001$) and 45.34 % ($p < 0.0001$), respectively. The similar toxic effect was also observed for VA-free liposomes at 200 and 250 µg/mL ~ 60 % ($p < 0.0001$). Despite the concern about vitamin A toxicity, the chosen amount of vitamin A conjugated to liposomes did not alter the cytotoxicity of liposomes.

Cellular uptake study

To evaluate the delivery efficiency of VA-liposomes, LX-2 cells were treated with VA-liposomes containing FAM-siRNA. The delivery efficiency was measured by flow cytometry, which determines the number of fluorescence-positive cells. Flow Cytometry analysis showed that VA- liposomes possess significant higher transfection efficiency compared with VA free liposomes. Lx-2 cells transfected with VA liposomes were 55 ± 7 % ($p <0.01$) FAM-positive, whereas those transfected with VA-free liposomes were 30 ± 9% ($p <0.05$) FAM positive. However, treatment with naked siRNA did not increase the fluorescence intensity (Figure. 8).

The transfection efficiency of liposomes was further determined by a microplate reader. The fluorescence intensity of the cell lysate, which represents the intracellular delivery efficiency for siRNA by a given formulation, is shown in Figure 9. The cells treated with VA-liposomes ($p < 0.001$) showed significantly higher fluorescence intensities than did VA-free liposomes ($p < 0.05$). The mean fluorescence intensity was 1592.3 ± 238.7 for VA-free liposomes treated cells

and 2876.3 ± 320.75 for VA-coated liposomes treated cells. These results show that better cellular uptake was achieved when siRNA was complexed to VA-coupled liposomes.

In vitro BMP4 gene silencing

RT-PCR analysis showed that there is significant BMP4 gene silencing >50% after treatment with BMP4-siRNA. RT-PCR was conducted to examine the effect of BMP4-siRNA on BMP4 gene expression. BMP4-siRNA was transfected into activated human hepatic stellate LX-2 cells using Lipofectamine 3000, VA-free liposomes and VA-coupled liposomes. The optimized standard curve is shown in Figure 10. At 24, 48 and 72 h post-transfection, the amount of BMP-4 mRNA acquired by template standard curve using absolute RT-PCR was compared with normal untreated control. Results are shown as a ratio of BMP4 mRNA of the experimental group to the BMP4 mRNA of the untransfected control. The data showed no significant change in BMP-4 expression for the same treatment between 24 h, 48 h and 72 h time points (Figure 11). The highest silencing effect at all pre-determined experimental time points was achieved using BMP4-siRNA complexed into VA-liposomes. The gene silencing efficiency of BMP4-siRNA/VA-liposomes at 24 h, 48 h and 72 h post transfection was 72 ± 11.5625 % ($p < 0.0001$), 74.47 ± 3.17 % ($p < 0.0001$), and 81.12 ± 5.42 % ($p < 0.0001$), respectively. In addition, BMP4 expression was also significantly inhibited by BMP4-siRNA/VA free liposomes lipoplexes: 60.65 ± 6.45 % ($p < 0.0001$), 54.64 ± 7.36 % ($p < 0.0001$), and 55.68 ± 6.74 % ($p < 0.0001$), at 24, 48 and 72 h respectively. Similarly, after treatment with BMP4-siRNA/lipofectamine complex at all-time points, the BMP4 level was reduced to 45.96 ± 5.56 % ($p < 0.0001$), 51.10 ± 5.23 % ($p < 0.0001$), and 40.64 ± 9.69 % ($p < 0.0001$) compared to untreated control.

Effect of BMP4 Gene Silencing on α-SMA mRNA Expression

BMP is involved in regulating many cellular processes including HSC trans-differention. A previous study indicated that BMP4 is the key cytokine that can increase the expression of α-SMA in cultured HSC (63, 126). The expression of α-SMA indicates HSC trans-differentiation and transformation into their myofibroblast-like phenotype (44). Therefore, we measured α-SMA mRNA expression of HSC cells after transfection with BMP4-siRNA (Figure 12).

Interestingly, we observed that treatment with BMP4-siRNAcaused significant reduction of α-SMA expression in a similar fashion as observed in the case of BMP4. All groups treated with VA-liposomes, VA-free liposomes and Lipofectamine-3000 carrying BMP4-siRNA caused significant α-SMA knockdown at all-time points. The α-SMA expression was lowest in the group treated with siRNA bound to VA-liposomes [22.84 ± 3.31 % ($p < 0.0001$), 36.04 ± 5.67 % ($p < 0.0001$), and 34.45 ± 8.27 % ($p < 0.0001$) at 24 h, 48h and 72 h respectively]. BMP4-siRNA delivered with VA-free liposomes and lipofectamine 3000 showed similar expression of α-SMA compared with that of untreated control at all-time points assessed [VA-free liposomes = 32.73 ± 8.76 %, 39.23 ± 13.05 % and 36.33 ± 12.58 % ($p < 0.0001$) while, lipofectamine 3000 = 29.99 ± 2.82 %, 43.53 ± 11.08 % and 41.39 ± 16.14 % at 24 h, 48 h and 72 h respectively ($p < 0.0001$)]. However, we did not observe any significant change in α-SMA expression following treatment with the negative control siRNA at all-time points tested.

BMP4 protein expression analysis by ELISA

We examined the efficiency of siRNA in silencing BMP4 protein expression using ELISA. The method measures the concentration of BMP4 protein inside the cells. Results are given as percentage of BMP4 expressed in the experimental group compared with BMP4 expressed in the untreated group Figure 13.

Our data showed that at 48 h and 72 h, VA-liposomes, VA-free liposomes and lipofectamine 3000 caused significant reduction in BMP4 protein level.

At 48 h post siRNA transfection BMP4 expression level significantly went down to 52.76 ± 4.57 % ($p < 0.0001$), 63.69 ± 4.28 % ($p < 0.0001$) and 50.60 ± 3.97 % ($p < 0.0001$) following treatment with VA-liposomes, VA-free liposomes and Lipofectamine 3000, respectively, compared with untransfected control. Similarly, at 72 h post transfection VA-liposomes, VA-free liposomes and Lipofectamine 3000 showed significant suppression of BMP4 by 47.01 ± 3.31 % ($p < 0.0001$), 44.01 ± 5.13% ($p < 0.0001$) and 50.08 ± 5.18 % ($p < 0.0001$) respectively.

However, 24 h post transfection, only siRNA complexed to Lipofectamine 3000 could significantly knock down BMP4 expression by nearly 36.86 ± 3.83 % ($p < 0.0001$).

α-SMA protein expression analysis by ELISA

α-SMA protein expression in LX-2 cells at different time points following BMP4-siRNA treatment is shown in Figure 14. Results are given as percentage of α-SMA expressed in each sample compared with α-SMA expressed in the untreated group. In ELISA performed on α-SMA, the pattern was very similar to that obtained in BMP4 ELISA analysis

At 24 h post transfection, there was no significant change in α-SMA protein levels for group treated with VA-coupled liposomes and VA-free liposomes. In contrast, Lipofectamine 3000 could knock down α-SMA protein expression to 71.97 ± 8.68 % ($p < 0.05$).

However, 48 h post siRNA transfection α-SMA levels significantly went down to 63.59 ± 2.89 % ($p < 0.01$), 50.42 ± 3.63 % ($p < 0.0001$) and 63.40 ± 10.59 % ($p < 0.01$) following treatment with VA-coupled liposomes, VA-free liposomes, and Lipofectamine 3000, respectively, compared with un-transfected control.

Similarly, at 72 h post transfection VA-liposomes, VA-free liposomes and Lipofectamine 3000 showed significant suppression of α-SMA by 30.89 ± 7.24 % ($p < 0.01$), 45.04 ± 13.76 % ($p < 0.001$) and 32.34 ± 4.84 % ($p < 0.01$), respectively, compared with un-transfected control. In contrast, there was no significant change in α-SMA expression in the group treated with control siRNA.

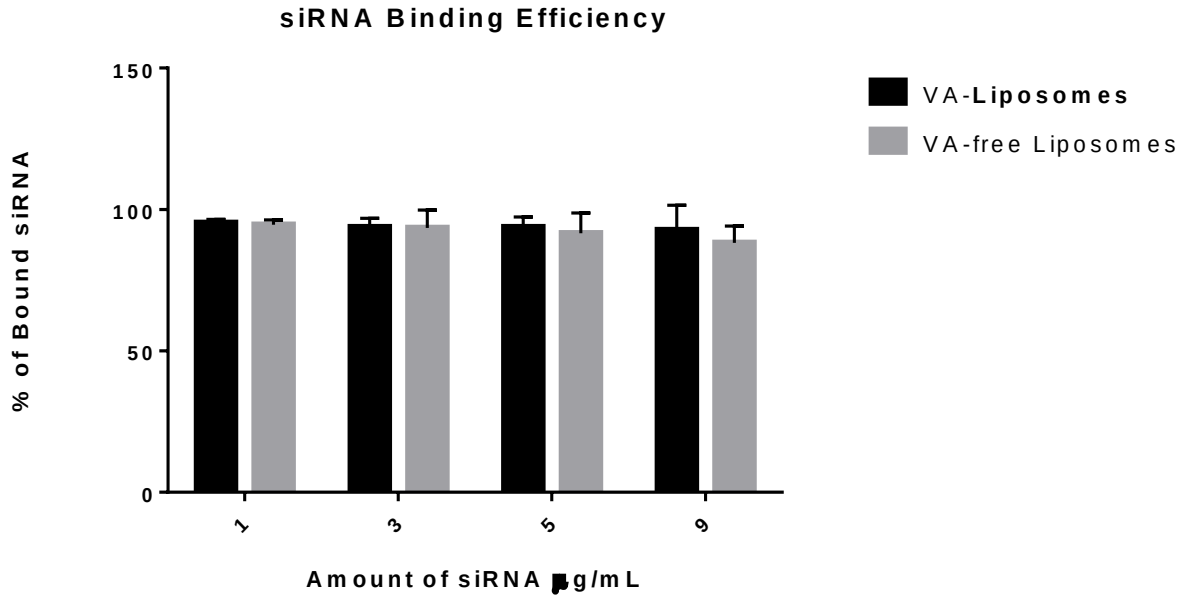

Figure 4: siRNA binding efficiency using fixed concentration of liposomes (30 µg/mL) at different siRNA concentrations (1, 3, 5, 9 µg/mL) determined by the ultra-filtration method. The free fractions of siRNA in different samples were collected after ultra-filtration and then measured by a fluorescence assay. The siRNA BE was calculated using the formula: (Initially added siRNA-mass of unencapsulated siRNA/Initially added siRNA) X 100. The results represent mean ± SD (*n* = 3).

Table 5: HPLC calibration of Retinol, *n*=4, % C.V. = % coefficient of variation

Concentration of Retinol µg/mL	Average AUC	%C.V.
62.5	6810.5	2.849741
125	12589.75	2.788132
250	22704.75	6.95524
500	41579.25	8.224421
1000	77625.75	10.20611

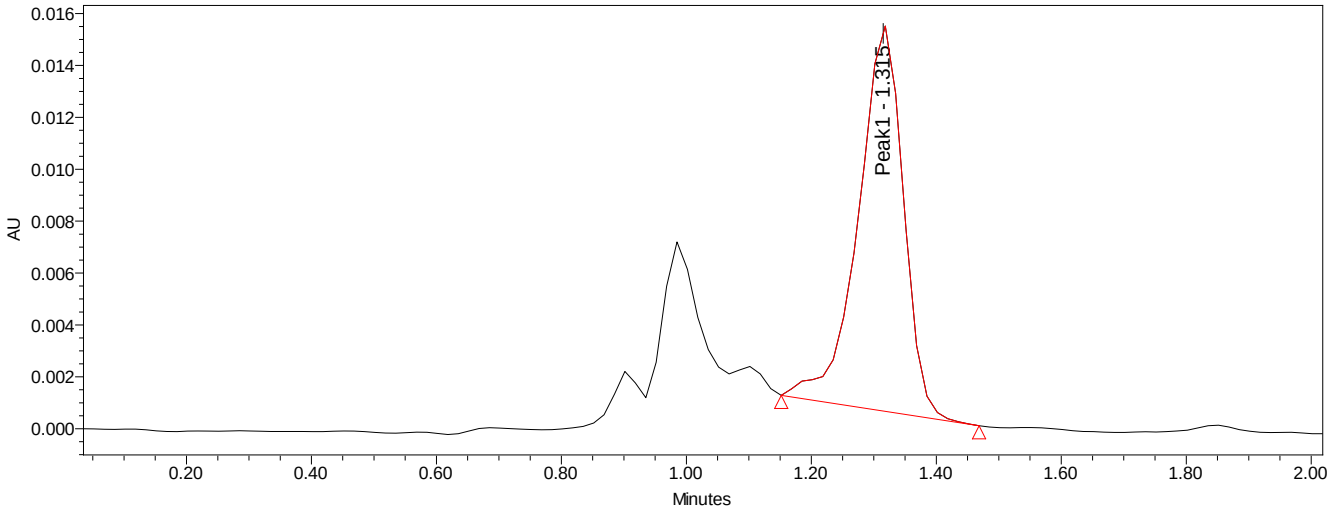

Figure 5: A reversed-phase HPLC chromatogram of retinol (Vit A) was detected by UV absorbance at 325 nm using reversed-phase (Nova-Pack C18, 4 ~m) column with a mobile phase of acetonitrile-tetrahydrofuran-water (55: 37: 8) and a flow rate of 1.2 mL/min

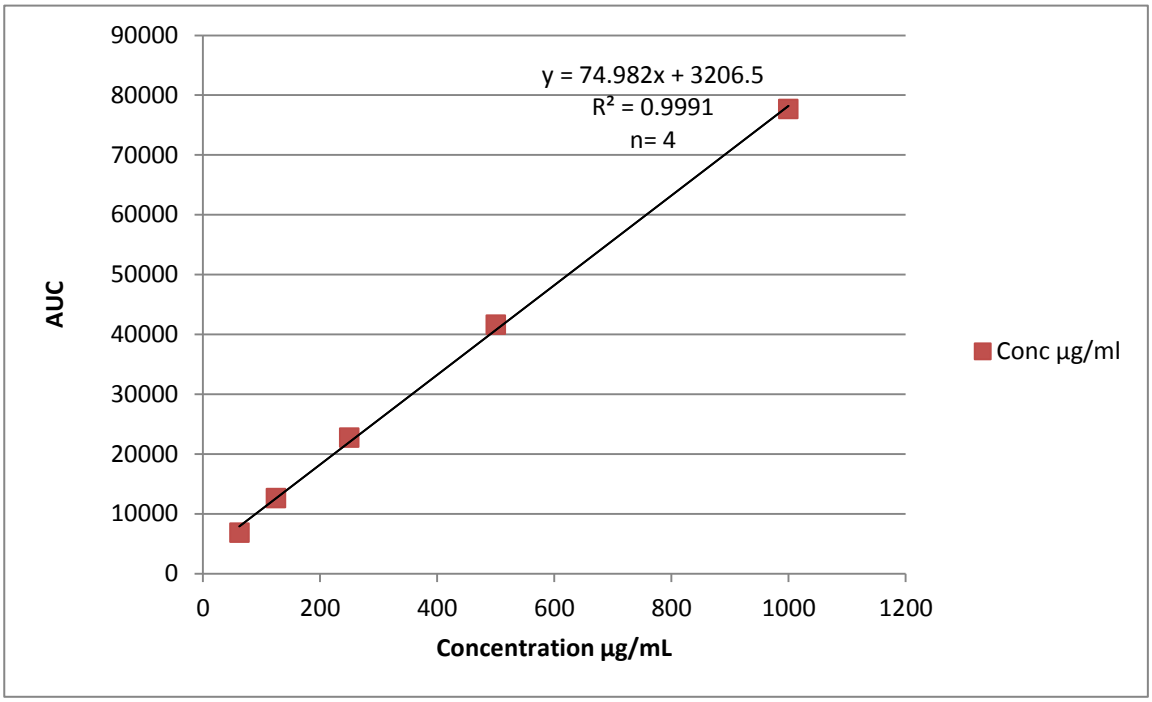

Figure 6: Standard curve of Retinol showing correlation coefficient and trend line. (*n* = 4), correlation coefficient = R^2

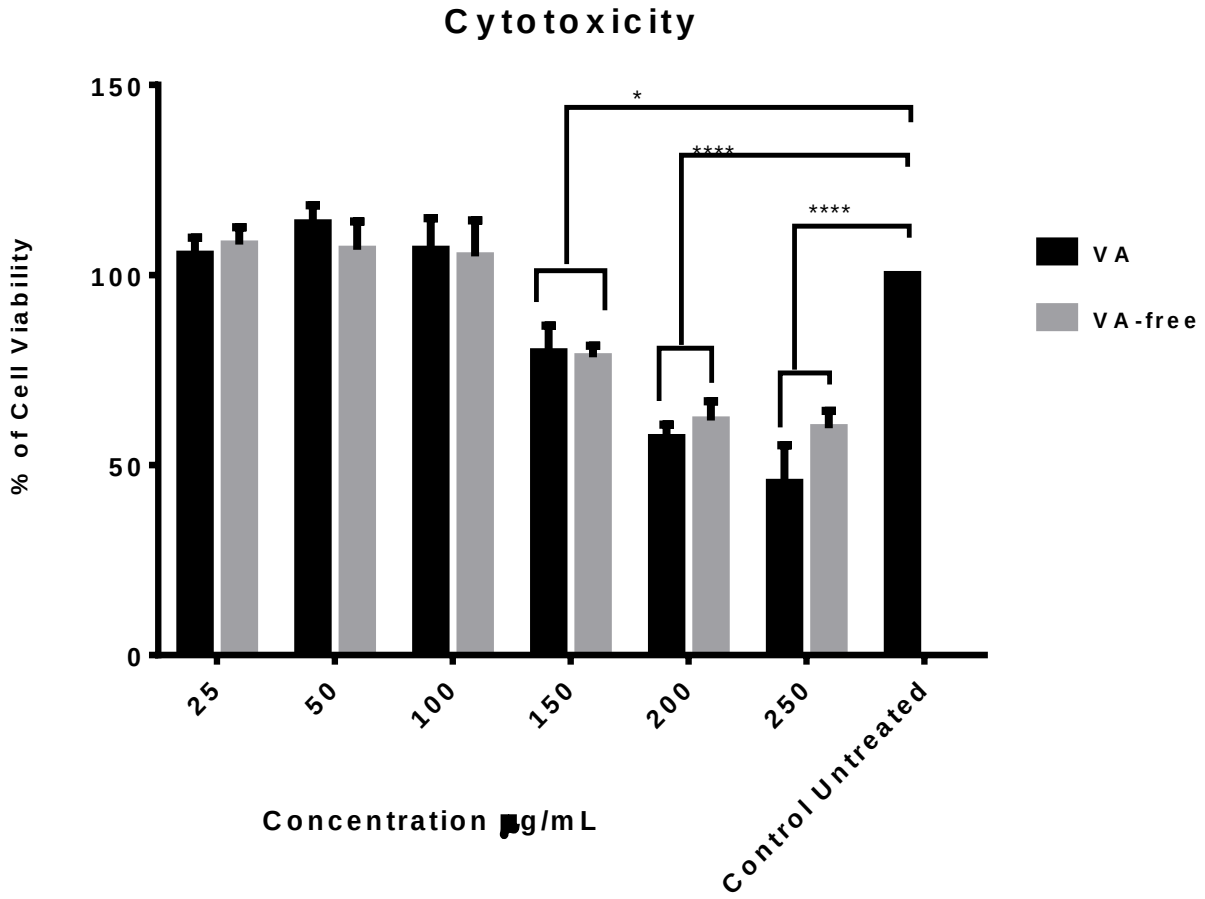

Figure 7: Cytotoxicity analysis determined by WST-1 assay on LX-2 cells. The data show the percentage of viable LX-2 cells after treatment with different concentration of VA-coupled and VA-free liposomes in comparison with untreated cells at 24 h post-transfection using the WST-1 assay. The data show three different experiments (each performed in triplicate) and are expressed as mean ± SD (n = 3). Both VA-coupled liposomes and VA-free liposomes at concentrations up to 100 µg/mL were not toxic to LX-2 cells. However, a significant reduction in cell viability by ~20% ($p < 0.05$) was observed for both liposomes at 150 µg/mL. The highest toxic concentrations for both liposomes were at 200 and 250 µg/mL ($p < 0.0001$).

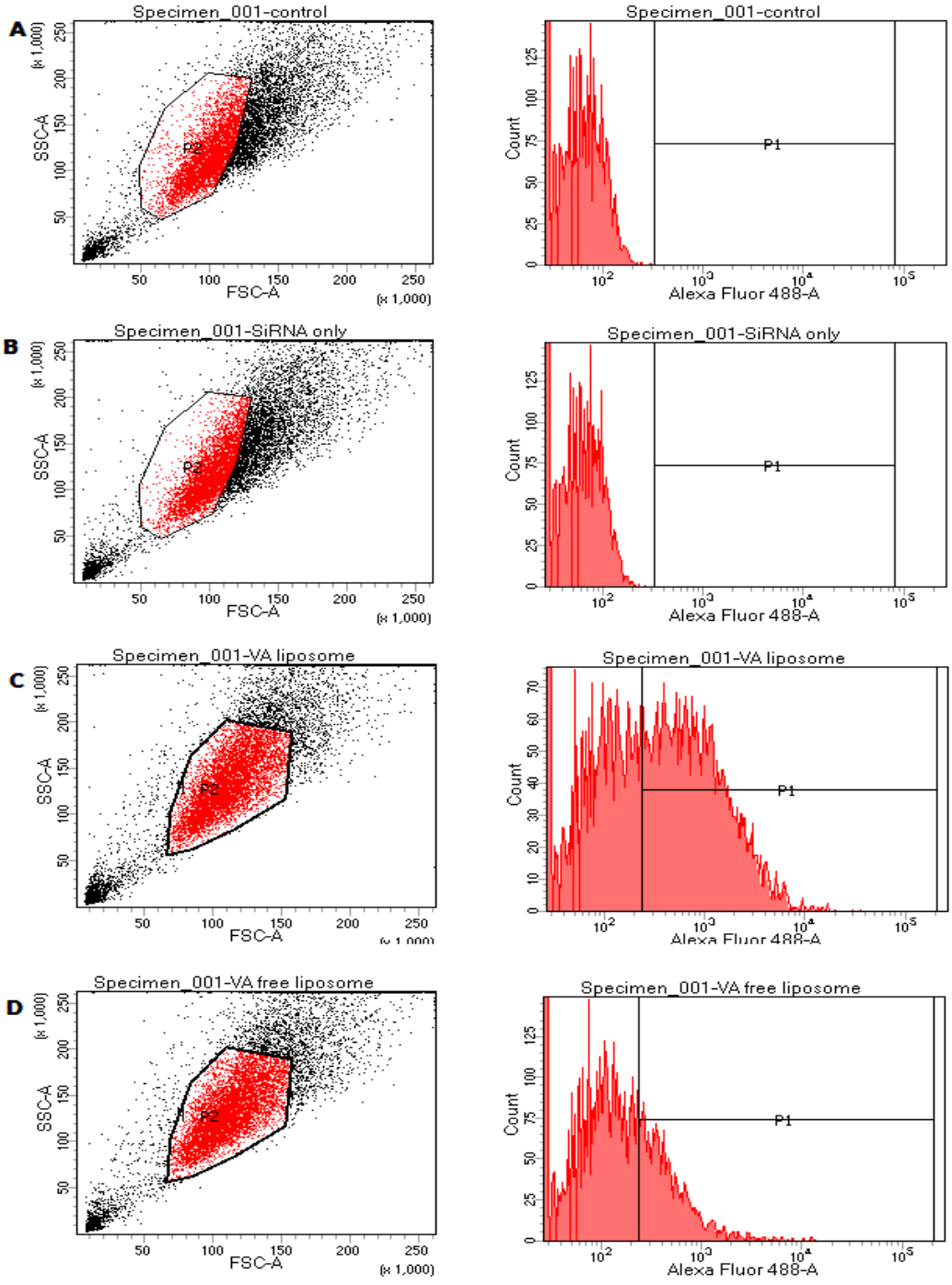

Figure 8: Flow cytometer analysis of 300 nM FAM-labeled siRNA complexed to the liposomal formulation transfected into LX-2 cells at 4 h incubation. (A) Untreated cells (B) free siRNA as negative control (C) VA-liposome/siRNA (D) VA-free liposomes/siRNA.

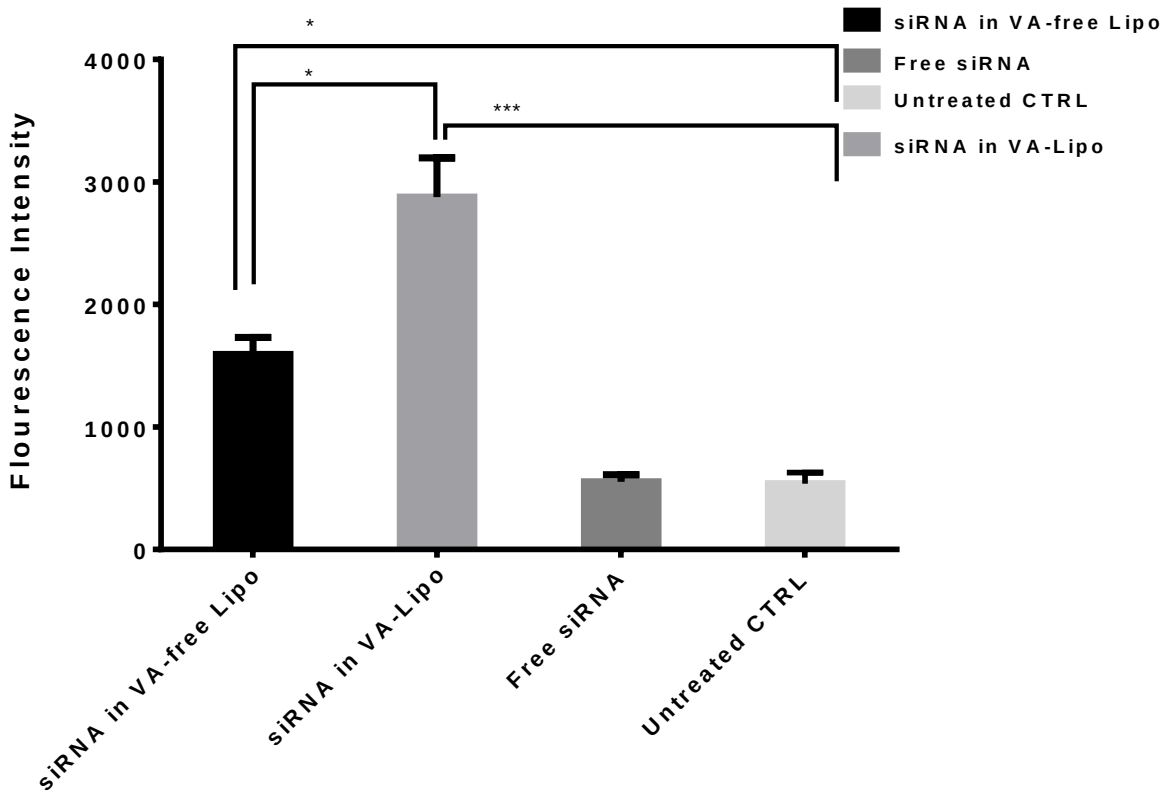

Figure 9: *In vitro* cellular uptake analysis determined by microplate reader. The fluorescence intensities of cell lysates from LX-2 cells treated with FAM-siRNA represent the intracellular delivery efficiency for siRNA by a given formulation. LX-2 cells were incubated with VA-coated liposomes, VA-free liposomes and free siRNA at 37 °C for 4 h. Cells were washed and lysed. Each value represents the mean ± S.D. (n = 3).* = p-values < 0.05 considered significant and*** = p< 0.001 highly significant. Statistics were performed using one way ANOVA with post-hoc Tukey. There are significant uptake differences for both vitamin A–coupled liposomes ($p < 0.001$) and vitamin A–free liposomes ($p < 0.05$) in comparison with free-siRNA, which showed no fluorescence intensity. However, vitamin A–coupled liposomes showed higher fluorescence intensity ($p < 0.05$) vs vitamin A–free liposomes.

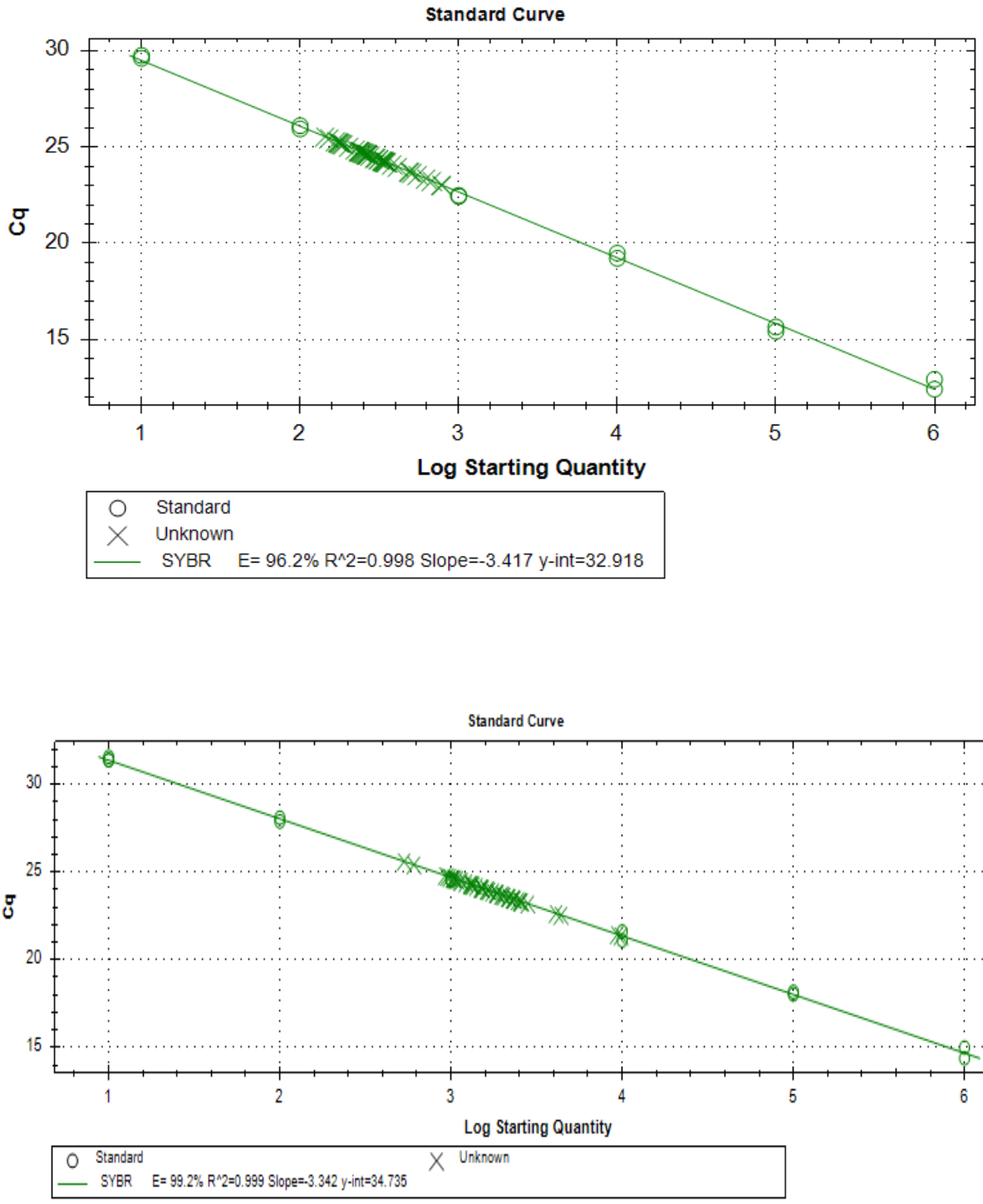

Figure 10: Real time PCR plots for BMP4 (A) and α-SMA (B). Real time PCR data were obtained by using serial dilutions of a PCR standard template. The standard curve shows log of starting quantity of each template dilution (x-axis) against the respective fluorescence intensity acquired during the amplification known as Ct (cycle threshold) of each dilution (Ct on y axis). R^2 value is close to 1. The slope, intercept and coefficient of determination R^2 were determined to evaluate whether the RT-PCR assay was optimized. E is the amplification efficiency.

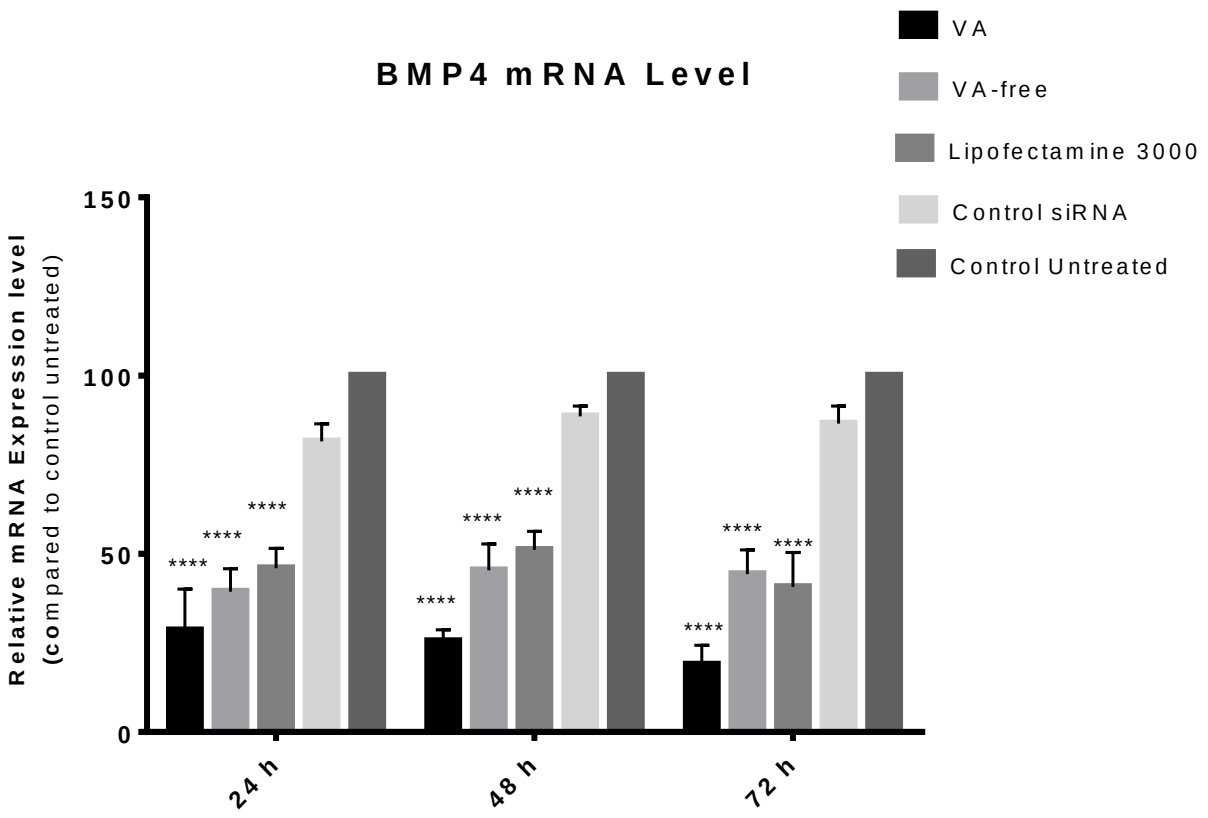

Figure 11: Inhibition of BMP4 in LX-2 cells determined by absolute RT-PCR assay at 24, 48 72 and h post-transfection after treatment with 3 µg/well of BMP4-siRNA using vitamin A–coupled liposomes, vitamin A–free liposomes, Lipofectamin 3000 and Control siRNA. Results were normalized and compared to normal control (non-transfected cells) within same time point, **** = $p < 0.0001$ considered highly significant. Statistics were performed using 2-way ANOVA with post-hoc Tukey. All groups treated with vitamin A–coupled liposomes, vitamin A–free liposomes, Lipofectamin 3000 showed significant reduction in BMP4 mRNA ($p < 0.0001$) in all time points assessed compared to control untreated.

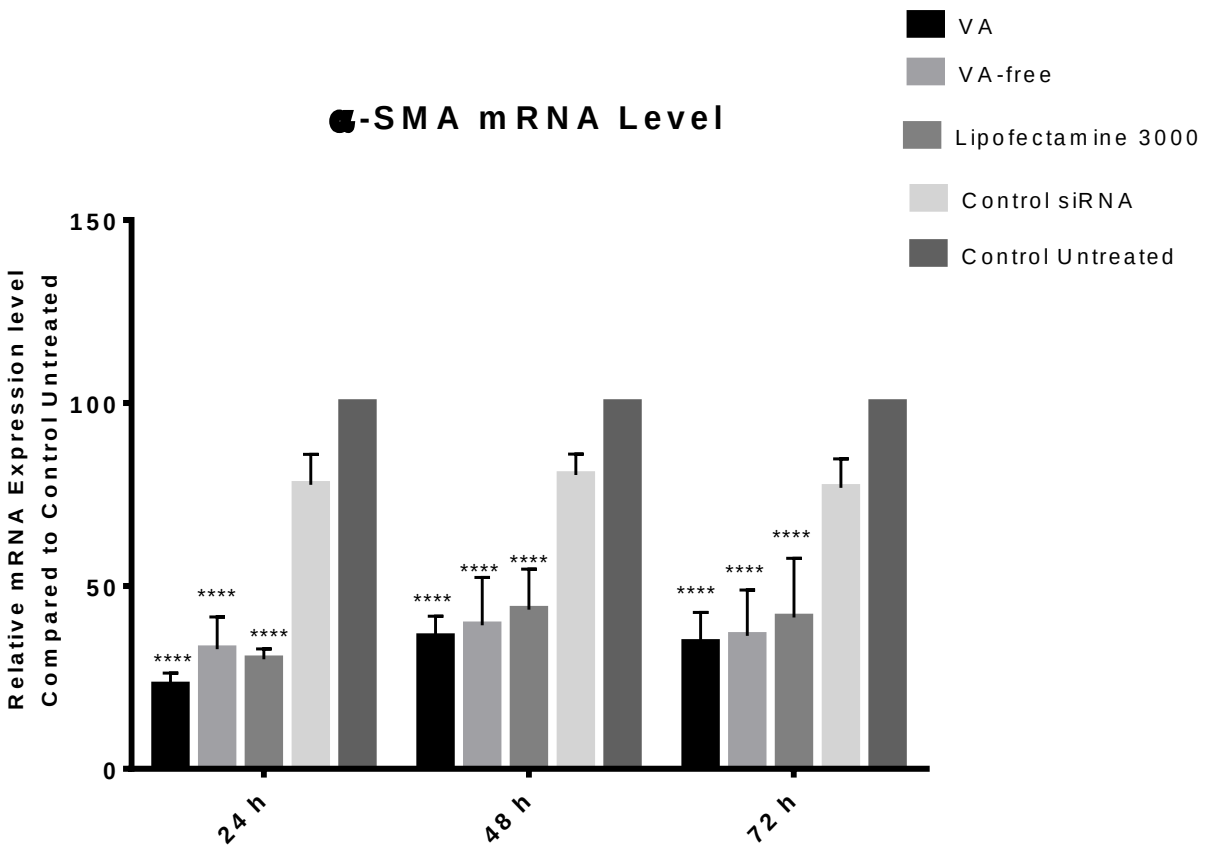

Figure 12: Inhibition of α-SMA in LX-2 cells determined by absolute RT-PCR assay at 24, 48 and 72 h post-transfection after treatment with 3 µg/well of BMP4-siRNA using vitamin A–coupled liposomes, vitamin A–free liposomes, Lipofectamin 3000 and Control siRNA. Results were normalized to normal control (non-transfected cells) within same time point. Statistics were performed using 2-way ANOVA with post-hoc Tukey. Treatment with BMP4-siRNA caused significant inhibition in α-SMA mRNA in all groups treated with vitamin A–coupled liposomes, vitamin A–free liposomes, Lipofectamin 3000 ($p < 0.0001$) in all time points assessed compared to control untreated.

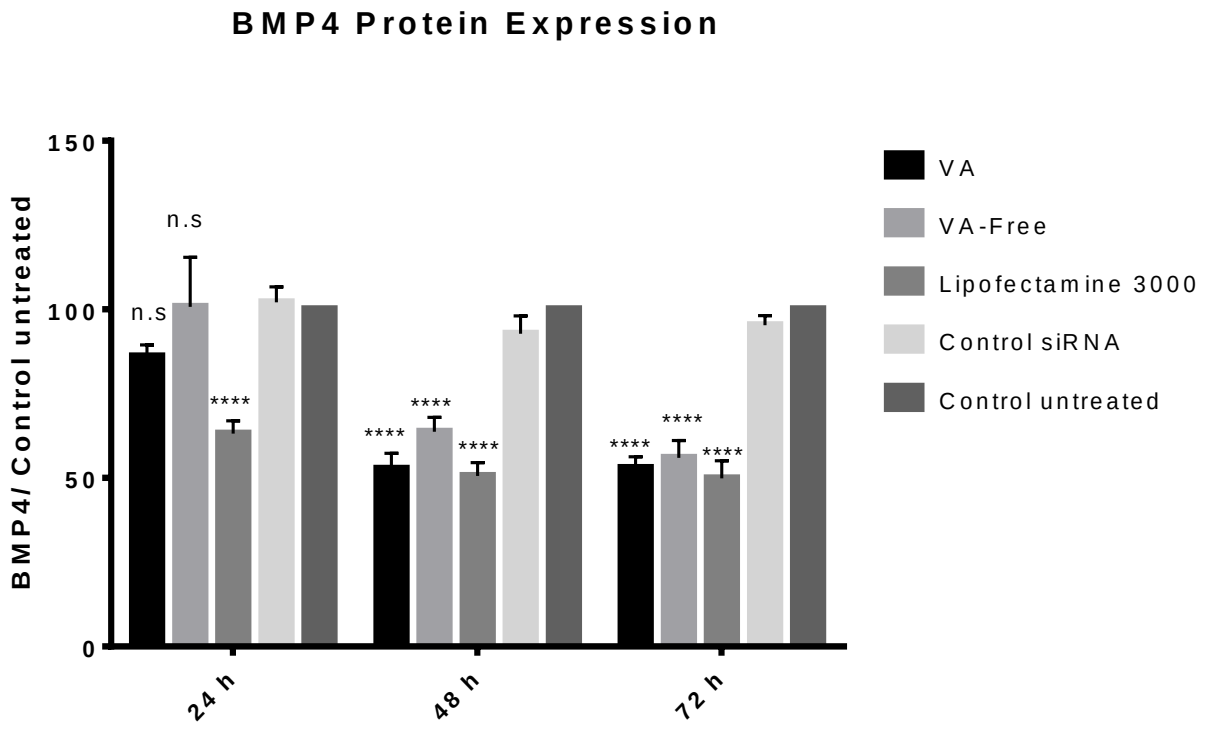

Figure 13: Effect of BMP-4 gene silencing on BMP4 protein expression determined by ELISA at 24, 48 and 72 h post-transfection after treatment with 3 μg/well of BMP4-siRNA using vitamin A–coupled liposomes, vitamin A–free liposomes and Lipofectamine 3000. Negative control siRNA was used as internal standard. Results were normalized and compared with normal control (non-transfected cells) within same time point. Statistics were performed using two-way ANOVA with post-hoc Tukey. At 48 h and 72 h post transfection, all groups treated with vitamin A–coupled liposomes, vitamin A–free liposomes, Lipofectamin 3000 showed significant decrease in BMP4 protein ($p < 0.0001$). However, at 24 h, only the group treated with Lipofectamine 3000 caused significant reduction in BMP4 protein ($p < 0.0001$).

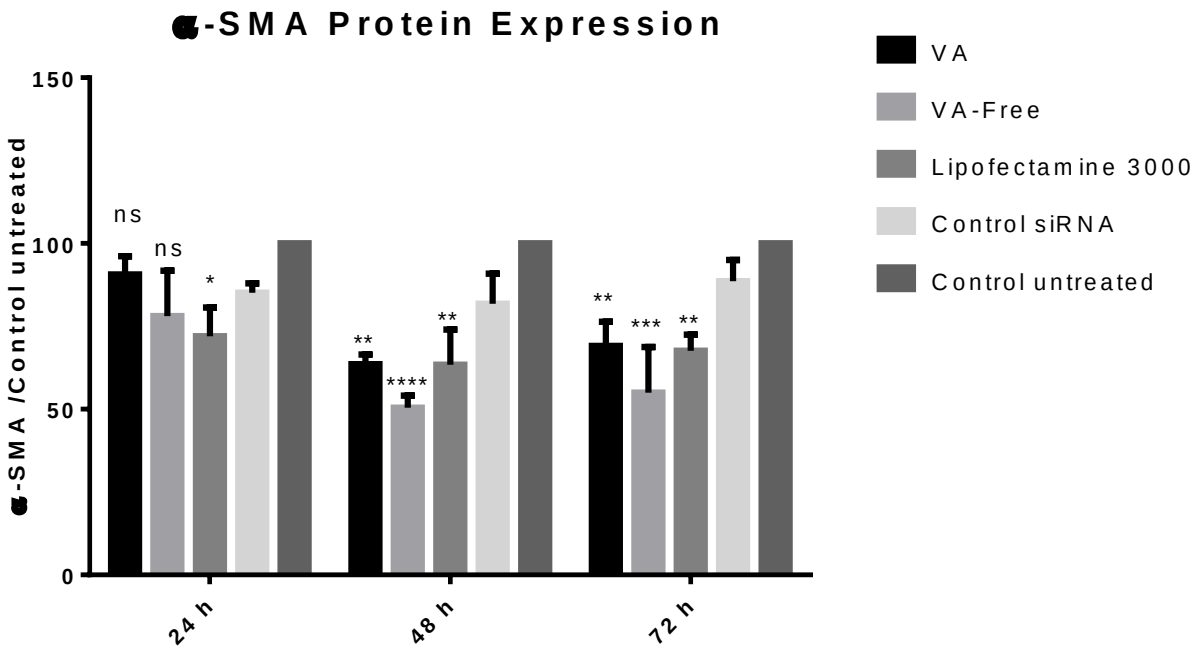

Figure 14: Effect of BMP-4 gene silencing on α-SMA protein expression determined by ELISA at 24, 48 and 72 h post-transfection after treatment with 3 μg/well of BMP4-siRNA using vitamin A–coupled liposomes, vitamin A–free liposomes, Lipofectamine 3000 and control siRNA. Results were normalized and compared with normal control (non-transfected cells). * = p-values < 0.05 considered significant,** = p< 0.01 very significant,*** = p< 0.001 highly significant and ****= p< 0.0001 considered very highly significant. Statistics were performed using two-way ANOVA with post-hoc Tukey. At 48 h and 72 h post transfection, all groups treated with vitamin A–coupled liposomes ($p < 0.01$), vitamin A–free liposomes { at 48 ($p < 0.0001$), at 72 ($p < 0.001$) }Lipofectamin 3000 ($p < 0.01$) showed significant decrease in α-SMA protein. However, at 24 h, only the group treated with Lipofectamine 3000 caused significant reduction in α-SMA protein ($p < 0.05$).

Chapter 4: Discussion

Hepatic fibrosis affects millions of people worldwide and it has a poor prognosis. This is because fibrosis can lead to cirrhosis, hepatocellular carcinoma, liver failure, and eventual death (303). According to a report released by the Canadian Liver Foundation in 2013 over an eight-year period, there was an increase in the death rate by nearly 30 % due to liver diseases.

Hepatic fibrosis is a reversible response that develops following liver injury (44) in an attempt to minimize the liver damage. Despite this attempt to minimize damage, liver function is significantly impaired (44). Recent clinical studies have reported that fibrosis can be reversed (34, 135, 136).

HSC are the principal players responsible for the pathogenesis of liver fibrosis. (6, 50). This is because when the liver is injured, HSC are activated, allowing them to proliferate, contract, and transform into fibrogenic myofibroblasts phenotype. This then enables their migration to regions of fibrosis (9). Activated HSC also express α-SMA protein and produce larger amounts of extracellular matrix (ECM) proteins, which accumulate as insoluble substances, causing fibrosis (48). Therefore, targeting HSC is an effective strategy for treatment of liver fibrosis (255).

The specific association of BMP4 with various liver diseases including liver fibrosis renders it an excellent candidate for targeting HSC cells using siRNA (63, 104, 117, 126). RNAi is a promising therapeutic approach by which dsRNAs can regulate specific gene expression (209, 210). However, siRNA therapy is encountering some challenges after systemic administration, including safety, stability, and effective delivery of siRNA (224). Therefore, the key issue to solve these challenges and improve therapeutic outcomes to siRNA application lies on the development of safe and effective siRNA-delivery systems.

Biocompatible and biodegradable cationic liposomes formed by phospholipids are considered excellent vehicles for siRNA delivery (245). This is attributed to their ability to form lipoplexes with negatively-charged siRNA via electrostatic interaction, additionally they enhance binding to negatively charged biological membrane components facilitating the uptake of the liposomes by endocytosis (230, 246, 247). In the present study we developed vitamin A-coupled liposomes to specifically target HSC with BMP4-siRNA and they were tested in an *in vitro* cell culture model. Utilizing vitamin A as a specific ligand is based on the remarkable capacity of HSC for vitamin A uptake and storage via the RBP receptor. Vitamin A-coupled liposomes have previously been shown to provide specific HSC targeting and enhance cellular uptake of siRNA (259).

The particle size was recorded to evaluate the effectiveness of size reduction and liposomes stability following lyophilization. Particle size is also an important parameter for entry across cellular membrane by endocytosis. Zeta potential is another important parameter that indicates stability because it reflects the degree of aggregation or repulsion between particles. It is also a critical factor that helps to predict permeability across biological membranes. The change in particle size and zeta potential of particles could cause changes in transfection efficiency (298).

In order to achieve successful delivery to the hepatic cells, previous studies suggested that the size of nano-therapeutic particles should not exceed 150 nm (304, 305). This is because the endothelial fenestrations, which regulate the passage of specific molecules from the blood through the perisinusoidal space to the liver cells, possess small pores (50-170 nm in size) (5). In addition, it has been also reported that nanoparticles between 50 and 200 nm are not only easily taken up by target cells via passive delivery, but also avoid rapid renal clearance as well as provide a large surface area that can improve drug release, extend bioavailability, bio-distribution and efficacy of drugs (236-238).

In the current study, liposomes with small particles size (~110 nm) and uniform size distribution (PDI~ 0.20) were obtained after brief sonication of the formulation for 80 sec. When liposomes were conjugated with siRNA to form lipoplexes, the average size was considerably increased to be around and below 200 nm with a narrow size distribution less than 0.2. The small PDI of liposomes indicates narrow size distribution (Table 3).

Data show that the average particle size and zeta potential of VA-coupled liposomes and lipoplexes were barely altered in comparison with their respective VA-free liposomes. The zeta potential values of all liposomes and lipoplexes are positive with a significant decrease after conjugation with siRNA. This decrease in the zeta potential could be due to the neutralization of the cationic lipid head groups (a quaternary amine head group) with anionic phosphate groups of siRNA.

The loading efficiency depends on strategies used for lipoplexes preparation, lipid/siRNA ratio, and the cationic lipids/neutral lipid ratio (306). In this study, lipoplexes were prepared by a simple adsorption method (external addition). To achieve this, liposomes were first prepared. After that, siRNA was added to the preformed liposomes. The siRNA binding efficiency was calculated by subtracting the free faction measured in the sample from the initially added amount of siRNA. Our results show that siRNA was efficiently associated with the cationic liposomes. The siRNA binding efficiency using fixed concentration of liposomes (30 µg/mL) at different siRNA concentration of siRNA (1, 3, 5, 9 µg/mL) was found to be in the range of 90-95 %. This may be because of a charge interaction between negatively charged siRNA and positively charged lipids (230, 246, 247). The data also indicate that siRNA BE% of lipoplexes prepared with VA-free liposomes and VA-coupled liposomes remained almost constant, suggesting that the modification of DOPE/DOTAP liposomes with Vit A has little impact on siRNA BE.

An essential step for siRNAs to achieve their silencing function is their internalization to the target cells. In the present study, the cellular uptake of lipoplexes has been studied using flow cytometry and spectrofluorimetry. The latter determined the greatest degree of cellular uptake by LX-2 cells based on measuring the fluorescence intensities of lysed cells that have previously been treated with FAM-siRNA. Therefore, this technique does not distinguish between siRNA associated with cells or the culture plate and those that are internalized. However, flow cytometry offers the advantage of counting only FAM-positive cells per 1 X 10^4 cells. Results from both spectrofluorimetry and flow cytometry revealed that VA-coupled liposomes achieved significantly higher cellular uptake in comparison with VA-free liposomes.

Hence, we can conclude that the significant differences in cellular uptake between VA-coupled liposomes and VA-free liposomes that are of similar composition and of nearly similar size but possess different outer layers, suggest that surface properties may strongly affect interactions with LX-2 cells. The data may also suggest that the cellular uptake of VA-coupled liposomes was mediated by RBP receptor-dependent pathway. The enhanced cellular uptake and transfection efficiency of VA-coupled liposomes into HSC render them promising carriers for targeting liver fibrosis. Further studies using fluorescence microscopy need to be considered to observe the release of siRNA to the cytosol.

In the present *in vitro* study, there was no significant change in viability of LX-2 cells transfected with VA-coupled liposomes or with VA-free liposomes at lower lipid concentrations (up to 100 µg/mL). However, at lipid concentration ≥ 150 µg/mL, the cell viability was significantly reduced. These findings suggest that the optimum safe concentration for both VA-coupled liposomes and VA-free liposomes is at 100 µg/mL, which shows no toxicity to LX-2 cells (~ 100

% cell viability) (Fig 7). The cytotoxicity result also led to the conclusion that the amount of vitamin A added to the liposomes did not enhance the cytotoxicity of liposomes.

BMP4 is a member of the TGF-β family that is widely involved in regulation of cellular behavior, such as cell growth, migration, differentiation, apoptosis and angiogenesis (93). For example, treatment with BMP4 resulted in inhibition of hepatocyte regeneration (122). Fan *et al* reported that BMP4 affects the differentiation of hepatic progenitors towards the hepatocyte lineage (124, 125). BMP4 is a potent regulator of HSC trans-differentiation and transformation into a myofibroblast-like phenotype (63). Our lab has reported that BMP2 and BMP4 can increase the expression of α-SMA in cultured HSC (63, 126). The expression of α-SMA is a marker of HSC trans-differentiation and transformation into their myofibroblast-like phenotype (44). Further supporting studies of the crucial role of BMP4 in liver diseases have shown that BMP4 itself is overexpressed in other liver diseases, *e.g* bile duct ligated liver (126) and in liver cancer tissue (104, 117).

In the present study, the *in vitro* gene silencing of BMP4 using different formulations carrying BMP4-siRNA was explored using real time PCR. The results of RT-PCR showed that BMP-siRNA delivered with VA-coupled liposomes caused ~75% decrease of BMP4 mRNA compared with untreated control, while treatment with BMP4-siRNA/ VA-free liposomes resulted in ~ 55 % knockdown of BMP4 mRNA. Since BMP4 regulates HSC trans-differentiation and transformation into myofibroblast-like phenotype through controlling the activity of α-SMA, we decided to examine α-SMA after treatment with BMP4-siRNA. Surprisingly, BMP4-siRNA inhibited α-SMA expression at the same level as it did for BMP4 (Figure.12). This result is consistent with previously published data implicating that the expression of α-SMA is increased

in HSC after treatment with BMP4 (63). Consequently, inhibition of BMP4 leads to inhibition of α-SMA.

Following confirmation of the effect of BMP4 gene silencing on reduction of α-SMA mRNA expression *in vitro,* we proceeded to evaluate BMP4-siRNA-mediated silencing on BMP4 and α-SMA protein expression *in vitro* using ELISA. Our result showed that there was nearly no effect on both BMP4 and α-SMA protein expression after 24 h post treatment with BMP4-siRNA. However at 48 h and 72 h post transfection, there was a significant reduction reaching ~ 50 % of both BMP4 and α-SMA protein expression.

Generally, the duration and level of gene silencing resulting from siRNA are dependent on cell type, concentration of siRNA and size of protein. This effect usually last from five to seven days (221, 222). Therefore, transfections may be repeated to maintain knockdown.

Because siRNA only suppresses the expression of new transcribed mRNA, it is possible that the observed level may be either due to the residual protein expressed by cell prior to siRNA treatment or due to the mRNA that was not successfully transfected (307). The unsuccessful or incomplete capacity to silence the target gene expression could result from a liposomal failure to deliver siRNA, or siRNA degradation. These reasons might explain why BMP4-siRNA could not downregulate protein expression after 24 h and why we did not obtain 100 % protein knockdown 48 and 72 h post treatment.

These results may indicate that the anti-fibrotic properties of BMP4-siRNA occur significantly via inhibition of the α-SMA.

Chapter 5: Conclusion

Recently, several anti-fibrotic therapies developed for targeting liver fibrosis were shown to be ineffective for clinical use. The key solution to address this issue lies on understanding the mechanism governing fibrosis pathogenesis and fibrosis regression, as well as developing new therapeutic approaches that specifically target HSC. Therefore, the current study focused on targeting HSC through inhibiting BMP4 using siRNA. RNA interference is a new therapeutic approach that can be a useful tool for studying gene function by knocking down its expression; it may provide a solution to manage multiple diseases through modulation of specific gene expression in diseased cells. The key challenge to utilize siRNA-based therapeutics lies on the development of a biocompatible and efficient delivery system to the target cells. In the present study, we developed cationic VA-coupled liposomes for the targeted delivery of siRNA directed against BMP4 to cultured HSC.

The efficacy of the formulation was tested in an *in vitro* cell culture model. Liposomes were optimized to result in a favorable particle size (~110 nm) and to maximize siRNA loading efficiency. Inclusion of vitamin A in the cationic liposomes significantly improved the cellular uptake without affecting the cytotoxicity.

We also evaluated *in vitro* gene silencing using real time PCR, which showed significant reduction in BMP4 mRNA level. Targeting HSC with BMP4-siRNA was associated with suppression of α-SMA mRNA expression. Our experimental evidence suggests that targeting BMP4 mRNA using BMP4-siRNA is paralleled by the suppression of the potent fibrinogenic α-SMA at both the mRNA and protein level. This finding provides a better understanding of the

role of BMP4 that plays in the development of liver fibrosis, and how inhibition of BMP4 could revert fibrosis.

BMP4-siRNA delivery to the liver might have the potential to restore liver homeostasis by inhibiting the α-SMA activation pathway. Further studies in different liver fibrosis models are required to demonstrate that BMP4 as a potentially new therapeutic target in the management of liver fibrosis and provide a new perspective for the development of formulations for the treatment of liver fibrosis.

Chapter 6: References

1. Adrian JE, Poelstra K, Kamps JA. Addressing liver fibrosis with liposomes targeted to hepatic stellate cells. Journal of liposome research. 2007;17(3-4):205-18.
2. Ye Z, Houssein HS, Mahato RI. Bioconjugation of oligonucleotides for treating liver fibrosis. Oligonucleotides. 2007;17(4):349-404.
3. Meijer DK, Molema G. Targeting of drugs to the liver. Seminars in liver disease. 1995;15(3):202-56.
4. Bian Z, Ma X. Liver fibrogenesis in non-alcoholic steatohepatitis. Frontiers in physiology. 2012;3:248.
5. Wisse E, De Zanger RB, Charels K, Van Der Smissen P, McCuskey RS. The liver sieve: considerations concerning the structure and function of endothelial fenestrae, the sinusoidal wall and the space of Disse. Hepatology (Baltimore, Md). 1985;5(4):683-92.
6. Maher JJ, McGuire RF. Extracellular matrix gene expression increases preferentially in rat lipocytes and sinusoidal endothelial cells during hepatic fibrosis in vivo. The Journal of clinical investigation. 1990;86(5):1641-8.
7. Irving MG, Roll FJ, Huang S, Bissell DM. Characterization and culture of sinusoidal endothelium from normal rat liver: lipoprotein uptake and collagen phenotype. Gastroenterology. 1984;87(6):1233-47.
8. Luster MI, Germolec DR, Yoshida T, Kayama F, Thompson M. Endotoxin-induced cytokine gene expression and excretion in the liver. Hepatology (Baltimore, Md). 1994;19(2):480-8.
9. Alcolado R, Arthur MJ, Iredale JP. Pathogenesis of liver fibrosis. Clinical science (London, England : 1979). 1997;92(2):103-12.
10. Hui AY, Friedman SL. Molecular basis of hepatic fibrosis. Expert reviews in molecular medicine. 2003;5(5):1-23.
11. Blaner WS, O'Byrne SM, Wongsiriroj N, Kluwe J, D'Ambrosio DM, Jiang H, et al. Hepatic stellate cell lipid droplets: a specialized lipid droplet for retinoid storage. Biochimica et biophysica acta. 2009;1791(6):467-73.
12. Blomhoff R, Green MH, Green JB, Berg T, Norum KR. Vitamin A metabolism: new perspectives on absorption, transport, and storage. Physiological reviews. 1991;71(4):951-90.
13. Goldberg IJ. Lipoprotein lipase and lipolysis: central roles in lipoprotein metabolism and atherogenesis. Journal of lipid research. 1996;37(4):693-707.
14. Blomhoff R, Helgerud P, Rasmussen M, Berg T, Norum KR. In vivo uptake of chylomicron [3H]retinyl ester by rat liver: evidence for retinol transfer from parenchymal to nonparenchymal cells. Proceedings of the National Academy of Sciences of the United States of America. 1982;79(23):7326-30.
15. Blomhoff R, Berg T, Norum KR. Transfer of retinol from parenchymal to stellate cells in liver is mediated by retinol-binding protein. Proceedings of the National Academy of Sciences of the United States of America. 1988;85(10):3455-8.
16. Andersen KB, Nilsson A, Blomhoff HK, Oyen TB, Gabrielsen OS, Norum KR, et al. Direct mobilization of retinol from hepatic perisinusoidal stellate cells to plasma. The Journal of biological chemistry. 1992;267(2):1340-4.
17. Friedman SL. Hepatic stellate cells: protean, multifunctional, and enigmatic cells of the liver. Physiological reviews. 2008;88(1):125-72.

18. Batres RO, Olson JA. A marginal vitamin A status alters the distribution of vitamin A among parenchymal and stellate cells in rat liver. The Journal of nutrition. 1987;117(5):874-9.
19. Knittel T, Mehde M, Kobold D, Saile B, Dinter C, Ramadori G. Expression patterns of matrix metalloproteinases and their inhibitors in parenchymal and non-parenchymal cells of rat liver: regulation by TNF-alpha and TGF-beta1. Journal of hepatology. 1999;30(1):48-60.
20. Tacke F, Weiskirchen R. Update on hepatic stellate cells: pathogenic role in liver fibrosis and novel isolation techniques. Expert review of gastroenterology & hepatology. 2012;6(1):67-80.
21. Geerts A. History, heterogeneity, developmental biology, and functions of quiescent hepatic stellate cells. Seminars in liver disease. 2001;21(3):311-35.
22. Ramadori G, Neubauer K, Odenthal M, Nakamura T, Knittel T, Schwogler S, et al. The gene of hepatocyte growth factor is expressed in fat-storing cells of rat liver and is downregulated during cell growth and by transforming growth factor-beta. Biochemical and biophysical research communications. 1992;183(2):739-42.
23. Asahina K, Sato H, Yamasaki C, Kataoka M, Shiokawa M, Katayama S, et al. Pleiotrophin/heparin-binding growth-associated molecule as a mitogen of rat hepatocytes and its role in regeneration and development of liver. The American journal of pathology. 2002;160(6):2191-205.
24. Ishikawa K, Mochida S, Mashiba S, Inao M, Matsui A, Ikeda H, et al. Expressions of vascular endothelial growth factor in nonparenchymal as well as parenchymal cells in rat liver after necrosis. Biochemical and biophysical research communications. 1999;254(3):587-93.
25. Shao R, Yan W, Rockey DC. Regulation of endothelin-1 synthesis by endothelin-converting enzyme-1 during wound healing. The Journal of biological chemistry. 1999;274(5):3228-34.
26. De Bleser PJ, Niki T, Rogiers V, Geerts A. Transforming growth factor-beta gene expression in normal and fibrotic rat liver. Journal of hepatology. 1997;26(4):886-93.
27. Maxwell PH, Ferguson DJ, Osmond MK, Pugh CW, Heryet A, Doe BG, et al. Expression of a homologously recombined erythopoietin-SV40 T antigen fusion gene in mouse liver: evidence for erythropoietin production by Ito cells. Blood. 1994;84(6):1823-30.
28. Pinzani M, Gesualdo L, Sabbah GM, Abboud HE. Effects of platelet-derived growth factor and other polypeptide mitogens on DNA synthesis and growth of cultured rat liver fat-storing cells. The Journal of clinical investigation. 1989;84(6):1786-93.
29. Brun P, Castagliuolo I, Pinzani M, Palu G, Martines D. Exposure to bacterial cell wall products triggers an inflammatory phenotype in hepatic stellate cells. American journal of physiology Gastrointestinal and liver physiology. 2005;289(3):G571-8.
30. Marra F, Pinzani M. Role of hepatic stellate cells in the pathogenesis of portal hypertension. Nefrologia : publicacion oficial de la Sociedad Espanola Nefrologia. 2002;22 Suppl 5:34-40.
31. Schwabe RF, Bataller R, Brenner DA. Human hepatic stellate cells express CCR5 and RANTES to induce proliferation and migration. American journal of physiology Gastrointestinal and liver physiology. 2003;285(5):G949-58.
32. Paik YH, Schwabe RF, Bataller R, Russo MP, Jobin C, Brenner DA. Toll-like receptor 4 mediates inflammatory signaling by bacterial lipopolysaccharide in human hepatic stellate cells. Hepatology (Baltimore, Md). 2003;37(5):1043-55.
33. Yi HS, Jeong WI. Interaction of hepatic stellate cells with diverse types of immune cells: foe or friend? Journal of gastroenterology and hepatology. 2013;28 Suppl 1:99-104.

34. Hernandez-Gea V, Friedman SL. Pathogenesis of liver fibrosis. Annual review of pathology. 2011;6:425-56.
35. Marra F, Valente AJ, Pinzani M, Abboud HE. Cultured human liver fat-storing cells produce monocyte chemotactic protein-1. Regulation by proinflammatory cytokines. The Journal of clinical investigation. 1993;92(4):1674-80.
36. Maher JJ, Lozier JS, Scott MK. Rat hepatic stellate cells produce cytokine-induced neutrophil chemoattractant in culture and in vivo. The American journal of physiology. 1998;275(4 Pt 1):G847-53.
37. Fimmel CJ, Brown KE, O'Neill R, Kladney RD. Complement C4 protein expression by rat hepatic stellate cells. Journal of immunology (Baltimore, Md : 1950). 1996;157(6):2601-9.
38. Pinzani M, Abboud HE, Gesualdo L, Abboud SL. Regulation of macrophage colony-stimulating factor in liver fat-storing cells by peptide growth factors. The American journal of physiology. 1992;262(4 Pt 1):C876-81.
39. Czaja MJ, Geerts A, Xu J, Schmiedeberg P, Ju Y. Monocyte chemoattractant protein 1 (MCP-1) expression occurs in toxic rat liver injury and human liver disease. Journal of leukocyte biology. 1994;55(1):120-6.
40. Muhanna N, Doron S, Wald O, Horani A, Eid A, Pappo O, et al. Activation of hepatic stellate cells after phagocytosis of lymphocytes: A novel pathway of fibrogenesis. Hepatology (Baltimore, Md). 2008;48(3):963-77.
41. Winau F, Hegasy G, Weiskirchen R, Weber S, Cassan C, Sieling PA, et al. Ito cells are liver-resident antigen-presenting cells for activating T cell responses. Immunity. 2007;26(1):117-29.
42. Vinas O, Bataller R, Sancho-Bru P, Gines P, Berenguer C, Enrich C, et al. Human hepatic stellate cells show features of antigen-presenting cells and stimulate lymphocyte proliferation. Hepatology (Baltimore, Md). 2003;38(4):919-29.
43. Roger PM, Chaillou S, Breittmayer JP, Dahman M, St Paul MC, Chevallier P, et al. Intrahepatic CD4 T-Cell apoptosis is related to METAVIR score in patients with chronic hepatitis C virus. Scandinavian journal of immunology. 2005;62(2):168-75.
44. Lee UE, Friedman SL. Mechanisms of hepatic fibrogenesis. Best practice & research Clinical gastroenterology. 2011;25(2):195-206.
45. Li JT, Liao ZX, Ping J, Xu D, Wang H. Molecular mechanism of hepatic stellate cell activation and antifibrotic therapeutic strategies. Journal of gastroenterology. 2008;43(6):419-28.
46. Lee UE, Friedman SL. Mechanisms of hepatic fibrogenesis. Best Practice & Research Clinical Gastroenterology. 2011;25(2):195-206.
47. Arthur MJ. Fibrogenesis II. Metalloproteinases and their inhibitors in liver fibrosis. American journal of physiology Gastrointestinal and liver physiology. 2000;279(2):G245-9.
48. Bataller R, Brenner DA. Liver fibrosis. The Journal of clinical investigation. 2005;115(2):209-18.
49. Friedman SL. Liver fibrosis -- from bench to bedside. Journal of hepatology. 2003;38 Suppl 1:S38-53.
50. Wu J, Zern MA. Hepatic stellate cells: a target for the treatment of liver fibrosis. Journal of gastroenterology. 2000;35(9):665-72.
51. Friedman SL. Mechanisms of disease: Mechanisms of hepatic fibrosis and therapeutic implications. Nature clinical practice Gastroenterology & hepatology. 2004;1(2):98-105.
52. Friedman SL. Hepatic fibrosis -- overview. Toxicology. 2008;254(3):120-9.

53. Davis BH, Kramer RT, Davidson NO. Retinoic acid modulates rat Ito cell proliferation, collagen, and transforming growth factor beta production. The Journal of clinical investigation. 1990;86(6):2062-70.
54. Davis BH, Coll D, Beno DW. Retinoic acid suppresses the response to platelet-derived growth factor in human hepatic Ito-cell-like myofibroblasts: a post-receptor mechanism independent of raf/fos/jun/egr activation. The Biochemical journal. 1993;294 (Pt 3):785-91.
55. Geubel AP, De Galocsy C, Alves N, Rahier J, Dive C. Liver damage caused by therapeutic vitamin A administration: estimate of dose-related toxicity in 41 cases. Gastroenterology. 1991;100(6):1701-9.
56. Hellemans K, Verbuyst P, Quartier E, Schuit F, Rombouts K, Chandraratna RA, et al. Differential modulation of rat hepatic stellate phenotype by natural and synthetic retinoids. Hepatology (Baltimore, Md). 2004;39(1):97-108.
57. Mizobuchi Y, Shimizu I, Yasuda M, Hori H, Shono M, Ito S. Retinyl palmitate reduces hepatic fibrosis in rats induced by dimethylnitrosamine or pig serum. Journal of hepatology. 1998;29(6):933-43.
58. Okuno M, Moriwaki H, Imai S, Muto Y, Kawada N, Suzuki Y, et al. Retinoids exacerbate rat liver fibrosis by inducing the activation of latent TGF-beta in liver stellate cells. Hepatology (Baltimore, Md). 1997;26(4):913-21.
59. Okuno M, Sato T, Kitamoto T, Imai S, Kawada N, Suzuki Y, et al. Increased 9,13-di-cis-retinoic acid in rat hepatic fibrosis: implication for a potential link between retinoid loss and TGF-beta mediated fibrogenesis in vivo. Journal of hepatology. 1999;30(6):1073-80.
60. Sauvant P, Abergel A, Partier A, Alexandre-Gouabau MC, Rock E, Sion B, et al. Treatment of the rat hepatic stellate cell line, PAV-1, by retinol and palmitic acid leads to a convenient model to study retinoids metabolism. Biology of the cell / under the auspices of the European Cell Biology Organization. 2002;94(6):401-8.
61. Seifert WF, Bosma A, Brouwer A, Hendriks HF, Roholl PJ, van Leeuwen RE, et al. Vitamin A deficiency potentiates carbon tetrachloride-induced liver fibrosis in rats. Hepatology (Baltimore, Md). 1994;19(1):193-201.
62. Senoo H, Wake K. Suppression of experimental hepatic fibrosis by administration of vitamin A. Laboratory investigation; a journal of technical methods and pathology. 1985;52(2):182-94.
63. Shen H, Huang GJ, Gong YW. Effect of transforming growth factor beta and bone morphogenetic proteins on rat hepatic stellate cell proliferation and trans-differentiation. World journal of gastroenterology : WJG. 2003;9(4):784-7.
64. Pinzani M, Marra F. Cytokine receptors and signaling in hepatic stellate cells. Seminars in liver disease. 2001;21(3):397-416.
65. Pinzani M, Gentilini A, Caligiuri A, De Franco R, Pellegrini G, Milani S, et al. Transforming growth factor-beta 1 regulates platelet-derived growth factor receptor beta subunit in human liver fat-storing cells. Hepatology (Baltimore, Md). 1995;21(1):232-9.
66. Pinzani M, Knauss TC, Pierce GF, Hsieh P, Kenney W, Dubyak GR, et al. Mitogenic signals for platelet-derived growth factor isoforms in liver fat-storing cells. The American journal of physiology. 1991;260(3 Pt 1):C485-91.
67. Pinzani M, Milani S, Grappone C, Weber FL, Jr., Gentilini P, Abboud HE. Expression of platelet-derived growth factor in a model of acute liver injury. Hepatology (Baltimore, Md). 1994;19(3):701-7.

68. Wong L, Yamasaki G, Johnson RJ, Friedman SL. Induction of beta-platelet-derived growth factor receptor in rat hepatic lipocytes during cellular activation in vivo and in culture. The Journal of clinical investigation. 1994;94(4):1563-9.
69. Czochra P, Klopcic B, Meyer E, Herkel J, Garcia-Lazaro JF, Thieringer F, et al. Liver fibrosis induced by hepatic overexpression of PDGF-B in transgenic mice. Journal of hepatology. 2006;45(3):419-28.
70. Zeisberg M, Hanai J, Sugimoto H, Mammoto T, Charytan D, Strutz F, et al. BMP-7 counteracts TGF-beta1-induced epithelial-to-mesenchymal transition and reverses chronic renal injury. Nature medicine. 2003;9(7):964-8.
71. Wang S, Hirschberg R. BMP7 antagonizes TGF-beta -dependent fibrogenesis in mesangial cells. American journal of physiology Renal physiology. 2003;284(5):F1006-13.
72. Tacke F, Gabele E, Bataille F, Schwabe RF, Hellerbrand C, Klebl F, et al. Bone morphogenetic protein 7 is elevated in patients with chronic liver disease and exerts fibrogenic effects on human hepatic stellate cells. Digestive diseases and sciences. 2007;52(12):3404-15.
73. Herrera B, Sanchez A, Fabregat I. BMPS and liver: more questions than answers. Current pharmaceutical design. 2012;18(27):4114-25.
74. Zhong L, Wang X, Wang S, Yang L, Gao H, Yang C. The anti-fibrotic effect of bone morphogenic protein-7(BMP-7) on liver fibrosis. International journal of medical sciences. 2013;10(4):441-50.
75. Marra F, Romanelli RG, Giannini C, Failli P, Pastacaldi S, Arrighi MC, et al. Monocyte chemotactic protein-1 as a chemoattractant for human hepatic stellate cells. Hepatology (Baltimore, Md). 1999;29(1):140-8.
76. Kinnman N, Hultcrantz R, Barbu V, Rey C, Wendum D, Poupon R, et al. PDGF-mediated chemoattraction of hepatic stellate cells by bile duct segments in cholestatic liver injury. Laboratory investigation; a journal of technical methods and pathology. 2000;80(5):697-707.
77. Ikeda K, Wakahara T, Wang YQ, Kadoya H, Kawada N, Kaneda K. In vitro migratory potential of rat quiescent hepatic stellate cells and its augmentation by cell activation. Hepatology (Baltimore, Md). 1999;29(6):1760-7.
78. Knittel T, Dinter C, Kobold D, Neubauer K, Mehde M, Eichhorst S, et al. Expression and regulation of cell adhesion molecules by hepatic stellate cells (HSC) of rat liver: involvement of HSC in recruitment of inflammatory cells during hepatic tissue repair. The American journal of pathology. 1999;154(1):153-67.
79. Thimgan MS, Yee HF, Jr. Quantitation of rat hepatic stellate cell contraction: stellate cells' contribution to sinusoidal resistance. The American journal of physiology. 1999;277(1 Pt 1):G137-43.
80. Reynaert H, Thompson MG, Thomas T, Geerts A. Hepatic stellate cells: role in microcirculation and pathophysiology of portal hypertension. Gut. 2002;50(4):571-81.
81. Rockey DC. Hepatic blood flow regulation by stellate cells in normal and injured liver. Seminars in liver disease. 2001;21(3):337-49.
82. Shao R, Rockey DC. Effects of endothelins on hepatic stellate cell synthesis of endothelin-1 during hepatic wound healing. Journal of cellular physiology. 2002;191(3):342-50.
83. Rockey DC, Weisiger RA. Endothelin induced contractility of stellate cells from normal and cirrhotic rat liver: implications for regulation of portal pressure and resistance. Hepatology (Baltimore, Md). 1996;24(1):233-40.

84. Rockey DC, Chung JJ. Inducible nitric oxide synthase in rat hepatic lipocytes and the effect of nitric oxide on lipocyte contractility. The Journal of clinical investigation. 1995;95(3):1199-206.
85. Rockey DC, Boyles JK, Gabbiani G, Friedman SL. Rat hepatic lipocytes express smooth muscle actin upon activation in vivo and in culture. Journal of submicroscopic cytology and pathology. 1992;24(2):193-203.
86. Rombouts K, Knittel T, Machesky L, Braet F, Wielant A, Hellemans K, et al. Actin filament formation, reorganization and migration are impaired in hepatic stellate cells under influence of trichostatin A, a histone deacetylase inhibitor. Journal of hepatology. 2002;37(6):788-96.
87. Aldinger G, Herr G, Kusswetter W, Reis HJ, Thielemann FW, Holz U. Bone morphogenetic protein: a review. International orthopaedics. 1991;15(2):169-77.
88. Yamashita H, Ten Dijke P, Heldin CH, Miyazono K. Bone morphogenetic protein receptors. Bone. 1996;19(6):569-74.
89. Wozney JM, Rosen V. Bone morphogenetic protein and bone morphogenetic protein gene family in bone formation and repair. Clinical orthopaedics and related research. 1998(346):26-37.
90. Fan J, Shen H, Dai Q, Minuk GY, Burzynski FJ, Gong Y. Bone morphogenetic protein-4 induced Rat hepatic progenitor cell (WB-F344 cell) differentiation toward hepatocyte lineage. Journal of cellular physiology. 2009;220(1):72-81.
91. Bragdon B, Moseychuk O, Saldanha S, King D, Julian J, Nohe A. Bone morphogenetic proteins: a critical review. Cellular signalling. 2011;23(4):609-20.
92. Griffith DL, Keck PC, Sampath TK, Rueger DC, Carlson WD. Three-dimensional structure of recombinant human osteogenic protein 1: structural paradigm for the transforming growth factor beta superfamily. Proceedings of the National Academy of Sciences of the United States of America. 1996;93(2):878-83.
93. Kallioniemi A. Bone morphogenetic protein 4-a fascinating regulator of cancer cell behavior. Cancer genetics. 2012;205(6):267-77.
94. Reddi AH. Bone morphogenetic proteins: an unconventional approach to isolation of first mammalian morphogens. Cytokine & growth factor reviews. 1997;8(1):11-20.
95. Hogan BL. Bone morphogenetic proteins: multifunctional regulators of vertebrate development. Genes & development. 1996;10(13):1580-94.
96. Zhao GQ. Consequences of knocking out BMP signaling in the mouse. Genesis (New York, NY : 2000). 2003;35(1):43-56.
97. Gazzerro E, Minetti C. Potential drug targets within bone morphogenetic protein signaling pathways. Current opinion in pharmacology. 2007;7(3):325-33.
98. Gupta MC, Khan SN. Application of bone morphogenetic proteins in spinal fusion. Cytokine & growth factor reviews. 2005;16(3):347-55.
99. Wozney JM. Overview of bone morphogenetic proteins. Spine. 2002;27(16 Suppl 1):S2-8.
100. Winnier G, Blessing M, Labosky PA, Hogan BL. Bone morphogenetic protein-4 is required for mesoderm formation and patterning in the mouse. Genes & development. 1995;9(17):2105-16.
101. Sadlon TJ, Lewis ID, D'Andrea RJ. BMP4: its role in development of the hematopoietic system and potential as a hematopoietic growth factor. Stem cells (Dayton, Ohio). 2004;22(4):457-74.

102. Weber S, Taylor JC, Winyard P, Baker KF, Sullivan-Brown J, Schild R, et al. SIX2 and BMP4 mutations associate with anomalous kidney development. Journal of the American Society of Nephrology : JASN. 2008;19(5):891-903.
103. Kim SG, Park HR, Min SK, Choi JY, Koh SH, Kim JW, et al. Expression of bone morphogenic protein-4 is inversely related to prevalence of lymph node metastasis in gastric adenocarcinoma. Surgery today. 2011;41(5):688-92.
104. Chiu CY, Kuo KK, Kuo TL, Lee KT, Cheng KH. The activation of MEK/ERK signaling pathway by bone morphogenetic protein 4 to increase hepatocellular carcinoma cell proliferation and migration. Molecular cancer research : MCR. 2012;10(3):415-27.
105. Rothhammer T, Poser I, Soncin F, Bataille F, Moser M, Bosserhoff AK. Bone morphogenic proteins are overexpressed in malignant melanoma and promote cell invasion and migration. Cancer research. 2005;65(2):448-56.
106. Deng H, Makizumi R, Ravikumar TS, Dong H, Yang W, Yang WL. Bone morphogenetic protein-4 is overexpressed in colonic adenocarcinomas and promotes migration and invasion of HCT116 cells. Experimental cell research. 2007;313(5):1033-44.
107. Laatio L, Myllynen P, Serpi R, Rysa J, Ilves M, Lappi-Blanco E, et al. BMP-4 expression has prognostic significance in advanced serous ovarian carcinoma and is affected by cisplatin in OVCAR-3 cells. Tumour biology : the journal of the International Society for Oncodevelopmental Biology and Medicine. 2011;32(5):985-95.
108. Kwak C, Park YH, Kim IY, Moon KC, Ku JH. Expression of bone morphogenetic proteins, the subfamily of the transforming growth factor-beta superfamily, in renal cell carcinoma. The Journal of urology. 2007;178(3 Pt 1):1062-7.
109. Hjertner O, Hjorth-Hansen H, Borset M, Seidel C, Waage A, Sundan A. Bone morphogenetic protein-4 inhibits proliferation and induces apoptosis of multiple myeloma cells. Blood. 2001;97(2):516-22.
110. Guo D, Huang J, Gong J. Bone morphogenetic protein 4 (BMP4) is required for migration and invasion of breast cancer. Molecular and cellular biochemistry. 2012;363(1-2):179-90.
111. Shirai YT, Ehata S, Yashiro M, Yanagihara K, Hirakawa K, Miyazono K. Bone morphogenetic protein-2 and -4 play tumor suppressive roles in human diffuse-type gastric carcinoma. The American journal of pathology. 2011;179(6):2920-30.
112. Buckley S, Shi W, Driscoll B, Ferrario A, Anderson K, Warburton D. BMP4 signaling induces senescence and modulates the oncogenic phenotype of A549 lung adenocarcinoma cells. American journal of physiology Lung cellular and molecular physiology. 2004;286(1):L81-6.
113. Virtanen S, Alarmo EL, Sandstrom S, Ampuja M, Kallioniemi A. Bone morphogenetic protein -4 and -5 in pancreatic cancer--novel bidirectional players. Experimental cell research. 2011;317(15):2136-46.
114. Nishanian TG, Kim JS, Foxworth A, Waldman T. Suppression of tumorigenesis and activation of Wnt signaling by bone morphogenetic protein 4 in human cancer cells. Cancer biology & therapy. 2004;3(7):667-75.
115. Shepherd TG, Nachtigal MW. Identification of a putative autocrine bone morphogenetic protein-signaling pathway in human ovarian surface epithelium and ovarian cancer cells. Endocrinology. 2003;144(8):3306-14.
116. Haubold M, Weise A, Stephan H, Dunker N. Bone morphogenetic protein 4 (BMP4) signaling in retinoblastoma cells. International journal of biological sciences. 2010;6(7):700-15.

117. Maegdefrau U, Amann T, Winklmeier A, Braig S, Schubert T, Weiss TS, et al. Bone morphogenetic protein 4 is induced in hepatocellular carcinoma by hypoxia and promotes tumour progression. The Journal of pathology. 2009;218(4):520-9.
118. Gordon KJ, Kirkbride KC, How T, Blobe GC. Bone morphogenetic proteins induce pancreatic cancer cell invasiveness through a Smad1-dependent mechanism that involves matrix metalloproteinase-2. Carcinogenesis. 2009;30(2):238-48.
119. Theriault BL, Shepherd TG, Mujoomdar ML, Nachtigal MW. BMP4 induces EMT and Rho GTPase activation in human ovarian cancer cells. Carcinogenesis. 2007;28(6):1153-62.
120. Holien T, Vatsveen TK, Hella H, Rampa C, Brede G, Groseth LA, et al. Bone morphogenetic proteins induce apoptosis in multiple myeloma cells by Smad-dependent repression of MYC. Leukemia. 2012;26(5):1073-80.
121. Zhou Z, Sun L, Wang Y, Wu Z, Geng J, Miu W, et al. Bone morphogenetic protein 4 inhibits cell proliferation and induces apoptosis in glioma stem cells. Cancer biotherapy & radiopharmaceuticals. 2011;26(1):77-83.
122. Do N, Zhao R, Ray K, Ho K, Dib M, Ren X, et al. BMP4 is a novel paracrine inhibitor of liver regeneration. American journal of physiology Gastrointestinal and liver physiology. 2012;303(11):G1220-7.
123. Heng BC, Yu H, Yin Y, Lim SG, Cao T. Factors influencing stem cell differentiation into the hepatic lineage in vitro. Journal of gastroenterology and hepatology. 2005;20(7):975-87.
124. Fan J, Shen H, Dai Q, Minuk GY, Burzynski FJ, Gong Y. Bone morphogenetic protein-4 induced rat hepatic progenitor cell (WB-F344 cell) differentiation toward hepatocyte lineage. Journal of cellular physiology. 2009;220(1):72-81.
125. Dong J, Zeng S, Ouyang M, Huang Z, Gong Y, Shen H. [Effect of bone morphogenetic protein-4 on the proliferation and differentiation of rat hepatic precursor cells]. Zhong nan da xue xue bao Yi xue ban = Journal of Central South University Medical sciences. 2011;36(6):539-45.
126. Fan J, Shen H, Sun Y, Li P, Burczynski F, Namaka M, et al. Bone morphogenetic protein 4 mediates bile duct ligation induced liver fibrosis through activation of Smad1 and ERK1/2 in rat hepatic stellate cells. Journal of cellular physiology. 2006;207(2):499-505.
127. Gaca MD, Zhou X, Issa R, Kiriella K, Iredale JP, Benyon RC. Basement membrane-like matrix inhibits proliferation and collagen synthesis by activated rat hepatic stellate cells: evidence for matrix-dependent deactivation of stellate cells. Matrix biology : journal of the International Society for Matrix Biology. 2003;22(3):229-39.
128. Issa R, Williams E, Trim N, Kendall T, Arthur MJ, Reichen J, et al. Apoptosis of hepatic stellate cells: involvement in resolution of biliary fibrosis and regulation by soluble growth factors. Gut. 2001;48(4):548-57.
129. Shen H, Fan J, Minuk G, Gong Y. Apoptotic and survival signals in hepatic stellate cells. Zhong nan da xue xue bao Yi xue ban = Journal of Central South University Medical sciences. 2007;32(5):726-34.
130. Radaeva S, Sun R, Jaruga B, Nguyen VT, Tian Z, Gao B. Natural killer cells ameliorate liver fibrosis by killing activated stellate cells in NKG2D-dependent and tumor necrosis factor-related apoptosis-inducing ligand-dependent manners. Gastroenterology. 2006;130(2):435-52.
131. Saile B, Matthes N, Knittel T, Ramadori G. Transforming growth factor beta and tumor necrosis factor alpha inhibit both apoptosis and proliferation of activated rat hepatic stellate cells. Hepatology (Baltimore, Md). 1999;30(1):196-202.
132. Murphy FR, Issa R, Zhou X, Ratnarajah S, Nagase H, Arthur MJ, et al. Inhibition of apoptosis of activated hepatic stellate cells by tissue inhibitor of metalloproteinase-1 is mediated

via effects on matrix metalloproteinase inhibition: implications for reversibility of liver fibrosis. The Journal of biological chemistry. 2002;277(13):11069-76.
133. Iredale JP. Hepatic stellate cell behavior during resolution of liver injury. Seminars in liver disease. 2001;21(3):427-36.
134. Madge LA, Sierra-Honigmann MR, Pober JS. Apoptosis-inducing agents cause rapid shedding of tumor necrosis factor receptor 1 (TNFR1). A nonpharmacological explanation for inhibition of TNF-mediated activation. The Journal of biological chemistry. 1999;274(19):13643-9.
135. Mallet V, Gilgenkrantz H, Serpaggi J, Verkarre V, Vallet-Pichard A, Fontaine H, et al. Brief communication: the relationship of regression of cirrhosis to outcome in chronic hepatitis C. Annals of internal medicine. 2008;149(6):399-403.
136. Friedman SL, Bansal MB. Reversal of hepatic fibrosis -- fact or fantasy? Hepatology (Baltimore, Md). 2006;43(2 Suppl 1):S82-8.
137. Ramachandran P, Iredale JP. Reversibility of liver fibrosis. Annals of hepatology. 2009;8(4):283-91.
138. Henderson NC, Iredale JP. Liver fibrosis: cellular mechanisms of progression and resolution. Clinical science (London, England : 1979). 2007;112(5):265-80.
139. Powell LW, Kerr JF. Reversal of "cirrhosis" in idiopathic haemochromatosis following long-term intensive venesection therapy. Australasian annals of medicine. 1970;19(1):54-7.
140. Blumberg RS, Chopra S, Ibrahim R, Crawford J, Farraye FA, Zeldis JB, et al. Primary hepatocellular carcinoma in idiopathic hemochromatosis after reversal of cirrhosis. Gastroenterology. 1988;95(5):1399-402.
141. Rahoud SA, Mergani A, Khamis AH, Saeed OK, Mohamed-Ali Q, Dessein AJ, et al. Factors controlling the effect of praziquantel on liver fibrosis in Schistosoma mansoni-infected patients. FEMS immunology and medical microbiology. 2010;58(1):106-12.
142. Lai CL, Chien RN, Leung NW, Chang TT, Guan R, Tai DI, et al. A one-year trial of lamivudine for chronic hepatitis B. Asia Hepatitis Lamivudine Study Group. The New England journal of medicine. 1998;339(2):61-8.
143. Hadziyannis SJ, Tassopoulos NC, Heathcote EJ, Chang TT, Kitis G, Rizzetto M, et al. Adefovir dipivoxil for the treatment of hepatitis B e antigen-negative chronic hepatitis B. The New England journal of medicine. 2003;348(9):800-7.
144. Poynard T, McHutchison J, Manns M, Trepo C, Lindsay K, Goodman Z, et al. Impact of pegylated interferon alfa-2b and ribavirin on liver fibrosis in patients with chronic hepatitis C. Gastroenterology. 2002;122(5):1303-13.
145. Hammel P, Couvelard A, O'Toole D, Ratouis A, Sauvanet A, Flejou JF, et al. Regression of liver fibrosis after biliary drainage in patients with chronic pancreatitis and stenosis of the common bile duct. The New England journal of medicine. 2001;344(6):418-23.
146. Rockey DC. Antifibrotic therapy in chronic liver disease. Clinical gastroenterology and hepatology : the official clinical practice journal of the American Gastroenterological Association. 2005;3(2):95-107.
147. Heller J, Trebicka J, Shiozawa T, Schepke M, Neef M, Hennenberg M, et al. Vascular, hemodynamic and renal effects of low-dose losartan in rats with secondary biliary cirrhosis. Liver international : official journal of the International Association for the Study of the Liver. 2005;25(3):657-66.

148. Croquet V, Moal F, Veal N, Wang J, Oberti F, Roux J, et al. Hemodynamic and antifibrotic effects of losartan in rats with liver fibrosis and/or portal hypertension. Journal of hepatology. 2002;37(6):773-80.
149. Castano G, Viudez P, Riccitelli M, Sookoian S. A randomized study of losartan vs propranolol: Effects on hepatic and systemic hemodynamics in cirrhotic patients. Annals of hepatology. 2003;2(1):36-40.
150. De BK, Bandyopadhyay K, Das TK, Das D, Biswas PK, Majumdar D, et al. Portal pressure response to losartan compared with propranolol in patients with cirrhosis. The American journal of gastroenterology. 2003;98(6):1371-6.
151. Vial P, Riquelme A, Pizarro M, Solis N, Madariaga JA, Aguayo G, et al. Pentoxifylline does not prevent neither liver damage nor early profibrogenic events in a rat model of non-alcoholic steatohepatitis. Annals of hepatology. 2006;5(1):25-9.
152. Raetsch C, Jia JD, Boigk G, Bauer M, Hahn EG, Riecken EO, et al. Pentoxifylline downregulates profibrogenic cytokines and procollagen I expression in rat secondary biliary fibrosis. Gut. 2002;50(2):241-7.
153. Austin AS, Mahida YR, Clarke D, Ryder SD, Freeman JG. A pilot study to investigate the use of oxpentifylline (pentoxifylline) and thalidomide in portal hypertension secondary to alcoholic cirrhosis. Alimentary Pharmacology & Therapeutics. 2004;19(1):79-88.
154. Muriel P, Moreno MG, Hernández MdC, Chávez E, Alcantar LK. Resolution of Liver Fibrosis in Chronic CCl4 Administration in the Rat after Discontinuation of Treatment: Effect of Silymarin, Silibinin, Colchicine and Trimethylcolchicinic Acid. Basic & Clinical Pharmacology & Toxicology. 2005;96(5):375-80.
155. Nikolaidis N, Kountouras J, Giouleme O, Tzarou V, Chatzizisi O, Patsiaoura K, et al. Colchicine treatment of liver fibrosis. Hepato-gastroenterology. 2006;53(68):281-5.
156. Czaja MJ, Weiner FR, Eghbali M, Giambrone MA, Eghbali M, Zern MA. Differential effects of gamma-interferon on collagen and fibronectin gene expression. The Journal of biological chemistry. 1987;262(27):13348-51.
157. Baroni GS, D'Ambrosio L, Curto P, Casini A, Mancini R, Jezequel AM, et al. Interferon gamma decreases hepatic stellate cell activation and extracellular matrix deposition in rat liver fibrosis. Hepatology (Baltimore, Md). 1996;23(5):1189-99.
158. Muir AJ, Sylvestre PB, Rockey DC. Interferon gamma-1b for the treatment of fibrosis in chronic hepatitis C infection. Journal of viral hepatitis. 2006;13(5):322-8.
159. Miyahara T, Schrum L, Rippe R, Xiong S, Yee HF, Jr., Motomura K, et al. Peroxisome proliferator-activated receptors and hepatic stellate cell activation. The Journal of biological chemistry. 2000;275(46):35715-22.
160. Galli A, Crabb DW, Ceni E, Salzano R, Mello T, Svegliati-Baroni G, et al. Antidiabetic thiazolidinediones inhibit collagen synthesis and hepatic stellate cell activation in vivo and in vitro. Gastroenterology. 2002;122(7):1924-40.
161. Neuschwander-Tetri BA, Brunt EM, Wehmeier KR, Oliver D, Bacon BR. Improved nonalcoholic steatohepatitis after 48 weeks of treatment with the PPAR-gamma ligand rosiglitazone. Hepatology (Baltimore, Md). 2003;38(4):1008-17.
162. Lutchman G, Modi A, Kleiner DE, Promrat K, Heller T, Ghany M, et al. The effects of discontinuing pioglitazone in patients with nonalcoholic steatohepatitis. Hepatology (Baltimore, Md). 2007;46(2):424-9.

163. Belfort R, Harrison SA, Brown K, Darland C, Finch J, Hardies J, et al. A placebo-controlled trial of pioglitazone in subjects with nonalcoholic steatohepatitis. The New England journal of medicine. 2006;355(22):2297-307.
164. Jia JD, Bauer M, Cho JJ, Ruehl M, Milani S, Boigk G, et al. Antifibrotic effect of silymarin in rat secondary biliary fibrosis is mediated by downregulation of procollagen alpha1(I) and TIMP-1. Journal of hepatology. 2001;35(3):392-8.
165. Boigk G, Stroedter L, Herbst H, Waldschmidt J, Riecken EO, Schuppan D. Silymarin retards collagen accumulation in early and advanced biliary fibrosis secondary to complete bile duct obliteration in rats. Hepatology (Baltimore, Md). 1997;26(3):643-9.
166. Ferenci P, Dragosics B, Dittrich H, Frank H, Benda L, Lochs H, et al. Randomized controlled trial of silymarin treatment in patients with cirrhosis of the liver. Journal of hepatology. 1989;9(1):105-13.
167. Pares A, Planas R, Torres M, Caballeria J, Viver JM, Acero D, et al. Effects of silymarin in alcoholic patients with cirrhosis of the liver: results of a controlled, double-blind, randomized and multicenter trial. Journal of hepatology. 1998;28(4):615-21.
168. Aleynik SI, Leo MA, Ma X, Aleynik MK, Lieber CS. Polyenylphosphatidylcholine prevents carbon tetrachloride-induced lipid peroxidation while it attenuates liver fibrosis. Journal of hepatology. 1997;27(3):554-61.
169. Lieber CS, Weiss DG, Groszmann R, Paronetto F, Schenker S. II. Veterans Affairs Cooperative Study of polyenylphosphatidylcholine in alcoholic liver disease. Alcoholism, clinical and experimental research. 2003;27(11):1765-72.
170. Tuncyurek P, Sari M, Firat O, Mutaf I, Gulter C, Tunger A, et al. Does pharmaconutrition with L-arginine and/or alpha-tocopherol improve the gut barrier in bile duct ligated rats? European surgical research Europaische chirurgische Forschung Recherches chirurgicales europeennes. 2006;38(1):4-10.
171. Andiran F, Ayhan A, Tanyel FC, Abbasoglu O, Sayek I. Regenerative capacities of normal and cirrhotic livers following 70% hepatectomy in rats and the effect of alpha-tocopherol on cirrhotic regeneration. The Journal of surgical research. 2000;89(2):184-8.
172. Harrison SA, Torgerson S, Hayashi P, Ward J, Schenker S. Vitamin E and vitamin C treatment improves fibrosis in patients with nonalcoholic steatohepatitis. The American journal of gastroenterology. 2003;98(11):2485-90.
173. Hasegawa T, Yoneda M, Nakamura K, Makino I, Terano A. Plasma transforming growth factor-beta1 level and efficacy of alpha-tocopherol in patients with non-alcoholic steatohepatitis: a pilot study. Aliment Pharmacol Ther. 2001;15(10):1667-72.
174. Shimizu I, Ma YR, Mizobuchi Y, Liu F, Miura T, Nakai Y, et al. Effects of Sho-saiko-to, a Japanese herbal medicine, on hepatic fibrosis in rats. Hepatology (Baltimore, Md). 1999;29(1):149-60.
175. Sakaida I, Matsumura Y, Akiyama S, Hayashi K, Ishige A, Okita K. Herbal medicine Sho-saiko-to (TJ-9) prevents liver fibrosis and enzyme-altered lesions in rat liver cirrhosis induced by a choline-deficient L-amino acid-defined diet. Journal of hepatology. 1998;28(2):298-306.
176. Deng G, Kurtz RC, Vickers A, Lau N, Yeung KS, Shia J, et al. A single arm phase II study of a Far-Eastern traditional herbal formulation (sho-sai-ko-to or xiao-chai-hu-tang) in chronic hepatitis C patients. Journal of ethnopharmacology. 2011;136(1):83-7.

177. Nieto N, Cederbaum AI. S-adenosylmethionine blocks collagen I production by preventing transforming growth factor-beta induction of the COL1A2 promoter. The Journal of biological chemistry. 2005;280(35):30963-74.
178. Mato JM, Camara J, Fernandez de Paz J, Caballeria L, Coll S, Caballero A, et al. S-adenosylmethionine in alcoholic liver cirrhosis: a randomized, placebo-controlled, double-blind, multicenter clinical trial. Journal of hepatology. 1999;30(6):1081-9.
179. Thompson K, Maltby J, Fallowfield J, McAulay M, Millward-Sadler H, Sheron N. Interleukin-10 expression and function in experimental murine liver inflammation and fibrosis. Hepatology (Baltimore, Md). 1998;28(6):1597-606.
180. Nelson DR, Tu Z, Soldevila-Pico C, Abdelmalek M, Zhu H, Xu YL, et al. Long-term interleukin 10 therapy in chronic hepatitis C patients has a proviral and anti-inflammatory effect. Hepatology (Baltimore, Md). 2003;38(4):859-68.
181. Poo JL, Feldmann G, Moreau A, Gaudin C, Lebrec D. Early colchicine administration reduces hepatic fibrosis and portal hypertension in rats with bile duct ligation. Journal of hepatology. 1993;19(1):90-4.
182. Rodriguez L, Cerbon-Ambriz J, Munoz ML. Effects of colchicine and colchiceine in a biochemical model of liver injury and fibrosis. Archives of medical research. 1998;29(2):109-16.
183. Kaplan MM, Alling DW, Zimmerman HJ, Wolfe HJ, Sepersky RA, Hirsch GS, et al. A prospective trial of colchicine for primary biliary cirrhosis. The New England journal of medicine. 1986;315(23):1448-54.
184. Kershenobich D, Vargas F, Garcia-Tsao G, Perez Tamayo R, Gent M, Rojkind M. Colchicine in the treatment of cirrhosis of the liver. The New England journal of medicine. 1988;318(26):1709-13.
185. Rambaldi A, Gluud C. Colchicine for alcoholic and non-alcoholic liver fibrosis or cirrhosis. Liver. 2001;21(2):129-36.
186. Wright MC, Issa R, Smart DE, Trim N, Murray GI, Primrose JN, et al. Gliotoxin stimulates the apoptosis of human and rat hepatic stellate cells and enhances the resolution of liver fibrosis in rats. Gastroenterology. 2001;121(3):685-98.
187. Dekel R, Zvibel I, Brill S, Brazovsky E, Halpern Z, Oren R. Gliotoxin ameliorates development of fibrosis and cirrhosis in a thioacetamide rat model. Digestive diseases and sciences. 2003;48(8):1642-7.
188. Sandig V, Strauss M. Liver-directed gene transfer and application to therapy. Journal of molecular medicine (Berlin, Germany). 1996;74(4):205-12.
189. Beljaars L, Meijer DK, Poelstra K. Targeting hepatic stellate cells for cell-specific treatment of liver fibrosis. Frontiers in bioscience : a journal and virtual library. 2002;7:e214-22.
190. Grimm D, Lee JS, Wang L, Desai T, Akache B, Storm TA, et al. In vitro and in vivo gene therapy vector evolution via multispecies interbreeding and retargeting of adeno-associated viruses. Journal of virology. 2008;82(12):5887-911.
191. Yi Y, Noh MJ, Lee KH. Current advances in retroviral gene therapy. Current gene therapy. 2011;11(3):218-28.
192. Di Campli C, Wu J, Zern MA. Targeting of therapeutics to the liver: liposomes and viral vectors. Alcoholism, clinical and experimental research. 1999;23(5):950-4.
193. Nakamura T, Sakata R, Ueno T, Sata M, Ueno H. Inhibition of transforming growth factor beta prevents progression of liver fibrosis and enhances hepatocyte regeneration in dimethylnitrosamine-treated rats. Hepatology (Baltimore, Md). 2000;32(2):247-55.

194. Wells RG. Fibrogenesis. V. TGF-beta signaling pathways. American journal of physiology Gastrointestinal and liver physiology. 2000;279(5):G845-50.
195. Dooley S, Hamzavi J, Breitkopf K, Wiercinska E, Said HM, Lorenzen J, et al. Smad7 prevents activation of hepatic stellate cells and liver fibrosis in rats. Gastroenterology. 2003;125(1):178-91.
196. Fu R, Wu J, Ding J, Sheng J, Hong L, Sun Q, et al. Targeting transforming growth factor betaRII expression inhibits the activation of hepatic stellate cells and reduces collagen synthesis. Experimental biology and medicine (Maywood, NJ). 2011;236(3):291-7.
197. Ponnappa BC, Israel Y. Targeting Kupffer cells with antisense oligonucleotides. Frontiers in bioscience : a journal and virtual library. 2002;7:e223-33.
198. Li Q, Liu DW, Zhang LM, Zhu B, He YT, Xiao YH. Effects of augmentation of liver regeneration recombinant plasmid on rat hepatic fibrosis. World journal of gastroenterology : WJG. 2005;11(16):2438-43.
199. Inoue T, Okada H, Kobayashi T, Watanabe Y, Kanno Y, Kopp JB, et al. Hepatocyte growth factor counteracts transforming growth factor-beta1, through attenuation of connective tissue growth factor induction, and prevents renal fibrogenesis in 5/6 nephrectomized mice. FASEB journal : official publication of the Federation of American Societies for Experimental Biology. 2003;17(2):268-70.
200. Jiang D, Jiang Z, Han F, Zhang Y, Li Z. HGF suppresses the production of collagen type III and alpha-SMA induced by TGF-beta1 in healing fibroblasts. European journal of applied physiology. 2008;103(5):489-93.
201. Kanemura H, Iimuro Y, Takeuchi M, Ueki T, Hirano T, Horiguchi K, et al. Hepatocyte growth factor gene transfer with naked plasmid DNA ameliorates dimethylnitrosamine-induced liver fibrosis in rats. Hepatology research : the official journal of the Japan Society of Hepatology. 2008;38(9):930-9.
202. Hemmann S, Graf J, Roderfeld M, Roeb E. Expression of MMPs and TIMPs in liver fibrosis - a systematic review with special emphasis on anti-fibrotic strategies. Journal of hepatology. 2007;46(5):955-75.
203. Siller-Lopez F, Sandoval A, Salgado S, Salazar A, Bueno M, Garcia J, et al. Treatment with human metalloproteinase-8 gene delivery ameliorates experimental rat liver cirrhosis. Gastroenterology. 2004;126(4):1122-33; discussion 949.
204. Kim EJ, Cho HJ, Park D, Kim JY, Kim YB, Park TG, et al. Antifibrotic effect of MMP13-encoding plasmid DNA delivered using polyethylenimine shielded with hyaluronic acid. Molecular therapy : the journal of the American Society of Gene Therapy. 2011;19(2):355-61.
205. Iimuro Y, Nishio T, Morimoto T, Nitta T, Stefanovic B, Choi SK, et al. Delivery of matrix metalloproteinase-1 attenuates established liver fibrosis in the rat. Gastroenterology. 2003;124(2):445-58.
206. Arthur MJ, Mann DA, Iredale JP. Tissue inhibitors of metalloproteinases, hepatic stellate cells and liver fibrosis. Journal of gastroenterology and hepatology. 1998;13 Suppl:S33-8.
207. Roderfeld M, Weiskirchen R, Wagner S, Berres ML, Henkel C, Grotzinger J, et al. Inhibition of hepatic fibrogenesis by matrix metalloproteinase-9 mutants in mice. FASEB journal : official publication of the Federation of American Societies for Experimental Biology. 2006;20(3):444-54.

208. Chen M, Wang GJ, Diao Y, Xu RA, Xie HT, Li XY, et al. Adeno-associated virus mediated interferon-gamma inhibits the progression of hepatic fibrosis in vitro and in vivo. World journal of gastroenterology : WJG. 2005;11(26):4045-51.
209. Kim DH, Rossi JJ. Overview of gene silencing by RNA interference. Current protocols in nucleic acid chemistry / edited by Serge L Beaucage [et al]. 2009;Chapter 16:Unit 16.1.
210. de Fougerolles A, Vornlocher HP, Maraganore J, Lieberman J. Interfering with disease: a progress report on siRNA-based therapeutics. Nature reviews Drug discovery. 2007;6(6):443-53.
211. Fire A, Xu S, Montgomery MK, Kostas SA, Driver SE, Mello CC. Potent and specific genetic interference by double-stranded RNA in Caenorhabditis elegans. Nature. 1998;391(6669):806-11.
212. Elbashir SM, Harborth J, Lendeckel W, Yalcin A, Weber K, Tuschl T. Duplexes of 21-nucleotide RNAs mediate RNA interference in cultured mammalian cells. Nature. 2001;411(6836):494-8.
213. McCaffrey AP, Meuse L, Pham TT, Conklin DS, Hannon GJ, Kay MA. RNA interference in adult mice. Nature. 2002;418(6893):38-9.
214. Okumura A, Pitha PM, Harty RN. ISG15 inhibits Ebola VP40 VLP budding in an L-domain-dependent manner by blocking Nedd4 ligase activity. Proceedings of the National Academy of Sciences of the United States of America. 2008;105(10):3974-9.
215. Kim D, Rossi J. RNAi mechanisms and applications. BioTechniques. 2008;44(5):613-6.
216. Bernstein E, Caudy AA, Hammond SM, Hannon GJ. Role for a bidentate ribonuclease in the initiation step of RNA interference. Nature. 2001;409(6818):363-6.
217. Matranga C, Tomari Y, Shin C, Bartel DP, Zamore PD. Passenger-strand cleavage facilitates assembly of siRNA into Ago2-containing RNAi enzyme complexes. Cell. 2005;123(4):607-20.
218. Ameres SL, Martinez J, Schroeder R. Molecular basis for target RNA recognition and cleavage by human RISC. Cell. 2007;130(1):101-12.
219. Rand TA, Petersen S, Du F, Wang X. Argonaute2 cleaves the anti-guide strand of siRNA during RISC activation. Cell. 2005;123(4):621-9.
220. Hutvagner G, Zamore PD. A microRNA in a multiple-turnover RNAi enzyme complex. Science (New York, NY). 2002;297(5589):2056-60.
221. Bartlett DW, Davis ME. Insights into the kinetics of siRNA-mediated gene silencing from live-cell and live-animal bioluminescent imaging. Nucleic acids research. 2006;34(1):322-33.
222. Leng Q, Woodle MC, Lu PY, Mixson AJ. Advances in Systemic siRNA Delivery. Drugs of the future. 2009;34(9):721.
223. Hammond SM, Bernstein E, Beach D, Hannon GJ. An RNA-directed nuclease mediates post-transcriptional gene silencing in Drosophila cells. Nature. 2000;404(6775):293-6.
224. Whitehead KA, Langer R, Anderson DG. Knocking down barriers: advances in siRNA delivery. Nature reviews Drug discovery. 2009;8(2):129-38.
225. Peer D, Lieberman J. Special delivery: targeted therapy with small RNAs. Gene therapy. 2011;18(12):1127-33.
226. Burnett JC, Rossi JJ. RNA-based therapeutics: current progress and future prospects. Chemistry & biology. 2012;19(1):60-71.
227. Bumcrot D, Manoharan M, Koteliansky V, Sah DWY. RNAi therapeutics: a potential new class of pharmaceutical drugs. Nat Chem Biol. 2006;2(12):711-9.

228. Qi W, Ding D, Zhu H, Lu D, Wang Y, Ding J, et al. Efficient siRNA transfection to the inner ear through the intact round window by a novel proteidic delivery technology in the chinchilla. Gene therapy. 2014;21(1):10-8.
229. White PJ. Barriers to successful delivery of short interfering RNA after systemic administration. Clinical and experimental pharmacology & physiology. 2008;35(11):1371-6.
230. Kesharwani P, Gajbhiye V, Jain NK. A review of nanocarriers for the delivery of small interfering RNA. Biomaterials. 2012;33(29):7138-50.
231. Jackson AL, Burchard J, Leake D, Reynolds A, Schelter J, Guo J, et al. Position-specific chemical modification of siRNAs reduces "off-target" transcript silencing. RNA (New York, NY). 2006;12(7):1197-205.
232. Gavrilov K, Saltzman WM. Therapeutic siRNA: principles, challenges, and strategies. The Yale journal of biology and medicine. 2012;85(2):187-200.
233. Oh YK, Park TG. siRNA delivery systems for cancer treatment. Advanced drug delivery reviews. 2009;61(10):850-62.
234. Elmen J, Thonberg H, Ljungberg K, Frieden M, Westergaard M, Xu Y, et al. Locked nucleic acid (LNA) mediated improvements in siRNA stability and functionality. Nucleic acids research. 2005;33(1):439-47.
235. Kim DH, Rossi JJ. Strategies for silencing human disease using RNA interference. Nature reviews Genetics. 2007;8(3):173-84.
236. Tiram G, Scomparin A, Ofek P, Satchi-Fainaro R. Interfering cancer with polymeric siRNA nanomedicines. Journal of biomedical nanotechnology. 2014;10(1):50-66.
237. Zhang L, Gu FX, Chan JM, Wang AZ, Langer RS, Farokhzad OC. Nanoparticles in medicine: therapeutic applications and developments. Clinical pharmacology and therapeutics. 2008;83(5):761-9.
238. Petros RA, DeSimone JM. Strategies in the design of nanoparticles for therapeutic applications. Nature reviews Drug discovery. 2010;9(8):615-27.
239. Yang S, Chen Y, Gu K, Dash A, Sayre CL, Davies NM, et al. Novel intravaginal nanomedicine for the targeted delivery of saquinavir to CD4+ immune cells. International journal of nanomedicine. 2013;8:2847-58.
240. Fenske DB, Cullis PR. Liposomal nanomedicines. Expert opinion on drug delivery. 2008;5(1):25-44.
241. Balazs DA, Godbey W. Liposomes for Use in Gene Delivery. Journal of Drug Delivery. 2011;2011.
242. Montier T, Benvegnu T, Jaffres PA, Yaouanc JJ, Lehn P. Progress in cationic lipid-mediated gene transfection: a series of bio-inspired lipids as an example. Current gene therapy. 2008;8(5):296-312.
243. Tros de Ilarduya C, Sun Y, Duzgunes N. Gene delivery by lipoplexes and polyplexes. European journal of pharmaceutical sciences : official journal of the European Federation for Pharmaceutical Sciences. 2010;40(3):159-70.
244. Ozpolat B, Sood AK, Lopez-Berestein G. Liposomal siRNA nanocarriers for cancer therapy. Advanced drug delivery reviews. 2014;66:110-6.
245. de Fougerolles AR. Delivery vehicles for small interfering RNA in vivo. Human gene therapy. 2008;19(2):125-32.
246. Verma UN, Surabhi RM, Schmaltieg A, Becerra C, Gaynor RB. Small interfering RNAs directed against beta-catenin inhibit the in vitro and in vivo growth of colon cancer cells. Clinical

cancer research : an official journal of the American Association for Cancer Research. 2003;9(4):1291-300.
247. Gomes-da-Silva LC, Fonseca NA, Moura V, Pedroso de Lima MC, Simoes S, Moreira JN. Lipid-based nanoparticles for siRNA delivery in cancer therapy: paradigms and challenges. Accounts of chemical research. 2012;45(7):1163-71.
248. Manthorpe M, Hobart P, Hermanson G, Ferrari M, Geall A, Goff B, et al. Plasmid Vaccines and Therapeutics: From Design to Applications. In: Schaffer D, Zhou W, editors. Gene Therapy and Gene Delivery Systems. Advances in Biochemical Engineering/Biotechnology. 99: Springer Berlin Heidelberg; 2005. p. 41-92.
249. Knudsen KB, Northeved H, Kumar Ek P, Permin A, Gjetting T, Andresen TL, et al. In vivo toxicity of cationic micelles and liposomes. Nanomedicine : nanotechnology, biology, and medicine. 2014.
250. Harmon AM, Lash MH, Sparks SM, Uhrich KE. Preferential cellular uptake of amphiphilic macromolecule-lipid complexes with enhanced stability and biocompatibility. Journal of controlled release : official journal of the Controlled Release Society. 2011;153(3):233-9.
251. Simoes S, Filipe A, Faneca H, Mano M, Penacho N, Duzgunes N, et al. Cationic liposomes for gene delivery. Expert opinion on drug delivery. 2005;2(2):237-54.
252. Dokka S, Toledo D, Shi X, Castranova V, Rojanasakul Y. Oxygen radical-mediated pulmonary toxicity induced by some cationic liposomes. Pharmaceutical research. 2000;17(5):521-5.
253. Filion MC, Phillips NC. Toxicity and immunomodulatory activity of liposomal vectors formulated with cationic lipids toward immune effector cells. Biochimica et biophysica acta. 1997;1329(2):345-56.
254. Spagnou S, Miller AD, Keller M. Lipidic carriers of siRNA: differences in the formulation, cellular uptake, and delivery with plasmid DNA. Biochemistry. 2004;43(42):13348-56.
255. Narmada BC, Kang Y, Venkatraman L, Peng Q, Sakban RB, Nugraha B, et al. Hepatic stellate cell-targeted delivery of hepatocyte growth factor transgene via bile duct infusion enhances its expression at fibrotic foci to regress dimethylnitrosamine-induced liver fibrosis. Human gene therapy. 2013;24(5):508-19.
256. Wu J, Zern MA. Modification of liposomes for liver targeting. Journal of hepatology. 1996;24(6):757-63.
257. Wu J, Nantz MH, Zern MA. Targeting hepatocytes for drug and gene delivery: emerging novel approaches and applications. Frontiers in bioscience : a journal and virtual library. 2002;7:d717-25.
258. Fan Y, Wu J. Polylipid Nanoparticle, a Novel Lipid-Based Vector for Liver Gene Transfer2013 2013-02-27.
259. Sato Y, Murase K, Kato J, Kobune M, Sato T, Kawano Y, et al. Resolution of liver cirrhosis using vitamin A-coupled liposomes to deliver siRNA against a collagen-specific chaperone. Nature biotechnology. 2008;26(4):431-42.
260. Miller CR, Bondurant B, McLean SD, McGovern KA, O'Brien DF. Liposome-cell interactions in vitro: effect of liposome surface charge on the binding and endocytosis of conventional and sterically stabilized liposomes. Biochemistry. 1998;37(37):12875-83.
261. Jokerst JV, Lobovkina T, Zare RN, Gambhir SS. Nanoparticle PEGylation for imaging and therapy. Nanomedicine (London, England). 2011;6(4):715-28.

262. Balazs DA, Godbey W. Liposomes for use in gene delivery. J Drug Deliv. 2011;2011:326497.
263. Shi F, Wasungu L, Nomden A, Stuart MC, Polushkin E, Engberts JB, et al. Interference of poly(ethylene glycol)-lipid analogues with cationic-lipid-mediated delivery of oligonucleotides; role of lipid exchangeability and non-lamellar transitions. The Biochemical journal. 2002;366(Pt 1):333-41.
264. Gao J, Yu Y, Zhang Y, Song J, Chen H, Li W, et al. EGFR-specific PEGylated immunoliposomes for active siRNA delivery in hepatocellular carcinoma. Biomaterials. 2012;33(1):270-82.
265. Halder J, Kamat AA, Landen CN, Jr., Han LY, Lutgendorf SK, Lin YG, et al. Focal adhesion kinase targeting using in vivo short interfering RNA delivery in neutral liposomes for ovarian carcinoma therapy. Clinical cancer research : an official journal of the American Association for Cancer Research. 2006;12(16):4916-24.
266. Landen CN, Jr., Chavez-Reyes A, Bucana C, Schmandt R, Deavers MT, Lopez-Berestein G, et al. Therapeutic EphA2 gene targeting in vivo using neutral liposomal small interfering RNA delivery. Cancer research. 2005;65(15):6910-8.
267. Farhood H, Gao X, Son K, Yang YY, Lazo JS, Huang L, et al. Cationic liposomes for direct gene transfer in therapy of cancer and other diseases. Annals of the New York Academy of Sciences. 1994;716:23-34; discussion -5.
268. Simoes S, Slepushkin V, Gaspar R, de Lima MC, Duzgunes N. Gene delivery by negatively charged ternary complexes of DNA, cationic liposomes and transferrin or fusigenic peptides. Gene therapy. 1998;5(7):955-64.
269. Koltover I, Salditt T, Radler JO, Safinya CR. An inverted hexagonal phase of cationic liposome-DNA complexes related to DNA release and delivery. Science (New York, NY). 1998;281(5373):78-81.
270. Zuhorn IS, Bakowsky U, Polushkin E, Visser WH, Stuart MC, Engberts JB, et al. Nonbilayer phase of lipoplex-membrane mixture determines endosomal escape of genetic cargo and transfection efficiency. Molecular therapy : the journal of the American Society of Gene Therapy. 2005;11(5):801-10.
271. Davis ME, Zuckerman JE, Choi CH, Seligson D, Tolcher A, Alabi CA, et al. Evidence of RNAi in humans from systemically administered siRNA via targeted nanoparticles. Nature. 2010;464(7291):1067-70.
272. Lee JM, Yoon TJ, Cho YS. Recent developments in nanoparticle-based siRNA delivery for cancer therapy. BioMed research international. 2013;2013:782041.
273. Konishi M, Wu CH, Wu GY. Inhibition of HBV replication by siRNA in a stable HBV-producing cell line. Hepatology (Baltimore, Md). 2003;38(4):842-50.
274. Morrissey DV, Lockridge JA, Shaw L, Blanchard K, Jensen K, Breen W, et al. Potent and persistent in vivo anti-HBV activity of chemically modified siRNAs. Nature biotechnology. 2005;23(8):1002-7.
275. Lee H, Kim SI, Shin D, Yoon Y, Choi TH, Cheon GJ, et al. Hepatic siRNA delivery using recombinant human apolipoprotein A-I in mice. Biochemical and biophysical research communications. 2009;378(2):192-6.
276. Raskopf E, Vogt A, Sauerbruch T, Schmitz V. siRNA targeting VEGF inhibits hepatocellular carcinoma growth and tumor angiogenesis in vivo. Journal of hepatology. 2008;49(6):977-84.

277. Li H, Fu X, Chen Y, Hong Y, Tan Y, Cao H, et al. Use of adenovirus-delivered siRNA to target oncoprotein p28GANK in hepatocellular carcinoma. Gastroenterology. 2005;128(7):2029-41.
278. Kim KH, Kim HC, Hwang MY, Oh HK, Lee TS, Chang YC, et al. The antifibrotic effect of TGF-beta1 siRNAs in murine model of liver cirrhosis. Biochemical and biophysical research communications. 2006;343(4):1072-8.
279. Lang Q, Liu Q, Xu N, Qian KL, Qi JH, Sun YC, et al. The antifibrotic effects of TGF-beta1 siRNA on hepatic fibrosis in rats. Biochemical and biophysical research communications. 2011;409(3):448-53.
280. Li G, Xie Q, Shi Y, Li D, Zhang M, Jiang S, et al. Inhibition of connective tissue growth factor by siRNA prevents liver fibrosis in rats. The journal of gene medicine. 2006;8(7):889-900.
281. George J, Tsutsumi M. siRNA-mediated knockdown of connective tissue growth factor prevents N-nitrosodimethylamine-induced hepatic fibrosis in rats. Gene therapy. 2007;14(10):790-803.
282. Li GM, Li DG, Fan JG, Xie Q. [Effect of silencing connective tissue growth factor on the liver fibrosis in rats]. Zhonghua gan zang bing za zhi = Zhonghua ganzangbing zazhi = Chinese journal of hepatology. 2010;18(11):822-5.
283. Chen SW, Zhang XR, Wang CZ, Chen WZ, Xie WF, Chen YX. RNA interference targeting the platelet-derived growth factor receptor beta subunit ameliorates experimental hepatic fibrosis in rats. Liver international : official journal of the International Association for the Study of the Liver. 2008;28(10):1446-57.
284. Cheng K, Yang N, Mahato RI. TGF-beta1 gene silencing for treating liver fibrosis. Molecular pharmaceutics. 2009;6(3):772-9.
285. Park K, Hong SW, Hur W, Lee MY, Yang JA, Kim SW, et al. Target specific systemic delivery of TGF-beta siRNA/(PEI-SS)-g-HA complex for the treatment of liver cirrhosis. Biomaterials. 2011;32(21):4951-8.
286. Kang JH, Tachibana Y, Kamata W, Mahara A, Harada-Shiba M, Yamaoka T. Liver-targeted siRNA delivery by polyethylenimine (PEI)-pullulan carrier. Bioorganic & medicinal chemistry. 2010;18(11):3946-50.
287. Kim SJ, Ise H, Kim E, Goto M, Akaike T, Chung BH. Imaging and therapy of liver fibrosis using bioreducible polyethylenimine/siRNA complexes conjugated with N-acetylglucosamine as a targeting moiety. Biomaterials. 2013;34(27):6504-14.
288. Kanasty R, Dorkin JR, Vegas A, Anderson D. Delivery materials for siRNA therapeutics. Nature materials. 2013;12(11):967-77.
289. Bangham AD, De Gier J, Greville GD. Osmotic properties and water permeability of phospholipid liquid crystals. Chemistry and Physics of Lipids. 1967;1(3):225-46.
290. Chaudhury A, Das S, Lee RF, Tan KB, Ng WK, Tan RB, et al. Lyophilization of cholesterol-free PEGylated liposomes and its impact on drug loading by passive equilibration. International journal of pharmaceutics. 2012;430(1-2):167-75.
291. Kundu AK, Chandra PK, Hazari S, Ledet G, Pramar YV, Dash S, et al. Stability of lyophilized siRNA nanosome formulations. International journal of pharmaceutics. 2012;423(2):525-34.
292. Chen C, Han D, Cai C, Tang X. An overview of liposome lyophilization and its future potential. Journal of controlled release : official journal of the Controlled Release Society. 2010;142(3):299-311.

293. Allison SD, Anchordoquy TJ. Mechanisms of protection of cationic lipid-DNA complexes during lyophilization. Journal of pharmaceutical sciences. 2000;89(5):682-91.
294. Allison SD, Molina MC, Anchordoquy TJ. Stabilization of lipid/DNA complexes during the freezing step of the lyophilization process: the particle isolation hypothesis. Biochimica et biophysica acta. 2000;1468(1-2):127-38.
295. Ozaki K, Hayashi M. The effects of glucose oligomers (maltodextrins) on freeze-drying liposomes. Chemical & pharmaceutical bulletin. 1997;45(1):165-70.
296. Taetz S, Bochot A, Surace C, Arpicco S, Renoir JM, Schaefer UF, et al. Hyaluronic acid-modified DOTAP/DOPE liposomes for the targeted delivery of anti-telomerase siRNA to CD44-expressing lung cancer cells. Oligonucleotides. 2009;19(2):103-16.
297. Ciani L, Ristori S, Salvati A, Calamai L, Martini G. DOTAP/DOPE and DC-Chol/DOPE lipoplexes for gene delivery: zeta potential measurements and electron spin resonance spectra. Biochimica et Biophysica Acta (BBA) - Biomembranes. 2004;1664(1):70-9.
298. Romoren K, Aaberge A, Smistad G, Thu BJ, Evensen O. Long-term stability of chitosan-based polyplexes. Pharmaceutical research. 2004;21(12):2340-6.
299. Gilleron J, Querbes W, Zeigerer A, Borodovsky A, Marsico G, Schubert U, et al. Image-based analysis of lipid nanoparticle-mediated siRNA delivery, intracellular trafficking and endosomal escape. Nature biotechnology. 2013;31(7):638-46.
300. Genestar C, Grases F. Determination of vitamin A in pharmaceutical preparations by high-performance liquid chromatography with diode-array detection. Chromatographia. 1995;40(3-4):143-6.
301. Tian Q, Zhang CN, Wang XH, Wang W, Huang W, Cha RT, et al. Glycyrrhetinic acid-modified chitosan/poly(ethylene glycol) nanoparticles for liver-targeted delivery. Biomaterials. 2010;31(17):4748-56.
302. Li SD, Huang L. Targeted delivery of antisense oligodeoxynucleotide and small interference RNA into lung cancer cells. Molecular pharmaceutics. 2006;3(5):579-88.
303. Bhala N, Jouness RI, Bugianesi E. Epidemiology and natural history of patients with NAFLD. Current pharmaceutical design. 2013;19(29):5169-76.
304. Fumoto S, Nakadori F, Kawakami S, Nishikawa M, Yamashita F, Hashida M. Analysis of hepatic disposition of galactosylated cationic liposome/plasmid DNA complexes in perfused rat liver. Pharmaceutical research. 2003;20(9):1452-9.
305. Higuchi Y, Kawakami S, Fumoto S, Yamashita F, Hashida M. Effect of the particle size of galactosylated lipoplex on hepatocyte-selective gene transfection after intraportal administration. Biological & pharmaceutical bulletin. 2006;29(7):1521-3.
306. Maitani Y. Lipoplex formation using liposomes prepared by ethanol injection. Methods in molecular biology (Clifton, NJ). 2010;605:393-403.
307. Zhou D, He QS, Wang C, Zhang J, Wong-Staal F. RNA interference and potential applications. Current topics in medicinal chemistry. 2006;6(9):901-11.